# DYNAMIC SUPRAMOLECULAR HYDROGELS WITH ADAPTIVE BIOLOGICAL FUNCTIONALITY

**By**

**Yousef Mustafa Yousef Abul-Haija**

A thesis submitted to the Department of Pure and Applied Chemistry, University of Strathclyde, in fulfilment of the requirements for the degree of Doctor of Philosophy

**2015**

## Declaration

‘This thesis is the result of the author’s original research. It has been composed by the author and has not been previously submitted for examination which has led to the award of a degree.’

## Copyright



Signed:

Date:

## Contents

# Acknowledgments

I would like to thank my supervisor, Prof. Rein Ulijn, for giving me the opportunity to undertake my PhD in such an interesting and stimulating field and for his continuous support and encouragement.

Special thanks go to my colleagues and friends at the Ulijn group for their useful discussion and comments and for the nice time I spent with them in and out of the lab. Special thanks also go to the 3B's research group at University of Minho in Portugal for the collaboration that led to biology results reported in chapter 4 and 5 of the thesis.

I would like to thank Dr. Vineetha Jayawarna for the cell culture training, Dr. Nadeem Javid for his help in light scattering measurements, Dr. Pim Frederix for FTIR measurements, Dr. Margaret Mullin from University of Glasgow for TEM imaging and finally Dr. Jugal Sahoo and Charalampos Pappas (Babis) for always being there.

I owe my loving thanks to my wife, Eman Hussien; thanks Eman for patiently bearing up with me and giving me the unlimited support to undertake this research; to my daughter Taleen and to my son Jad. My special gratitude is also due to my brothers: Ashraf, Akram, Hussein, Ghassan, Ahmad, Mohammad and their families; to my sisters Dareen, Eman, Aseel and their families for their loving support. Above all, it is my loving father, Mustafa Abul-Haija; my loving mother, Samiha Asad, who deserve most of what I have achieved in my life. I have no words to thank them for their assistance, moral support and more than anything for their love. Thank you for always believing in me.

I would like also to thank the European Research Council for the financial support *via* the initial training network (READ), contract no. 289723.

# Abstract

Molecular self-assembly coupled with (bio)catalysis underlie dynamic processes in biology and are considered as powerful tools for fabricating adaptive materials. In nature, the extracellular matrix (ECM) - the complex yet dynamic environment surrounding cells, provides cell support and ultimately determines cell fate. Cell behaviour depends on three main ECM properties; (i) its biochemistry presented by the chemical functionality exposed to the cells, (ii) its (nanoscale) topography and (iii) its mechanical properties (*i.e.* stiffness). The ultimate goal of this research is to develop materials that could mimic the ECM properties and function with minimal complexity by combining self-assembly and biocatalysis. Aromatic peptide amphiphiles and aromatic sugar amphiphiles are particularly interesting building blocks in this context and were mainly utilised in this work.

For the development of applications and novel uses for peptide nanostructures, robust routes for their surface functionalization, that ideally do not interfere with their self-assembly properties, are required. Many existing methods rely on covalent functionalization, where building blocks are appended with functional groups, either pre- or post-assembly. In the first part of this thesis, we demonstrate a facile supramolecular approach for the formation of functionalized nanofibers by combining the advantages of biocatalytic self-assembly and surfactant/gelator co-assembly. This is achieved by enzymatically triggered reconfiguration of free flowing micellar aggregates of pre-gelators and functional surfactants to form nanofibers that incorporate and display the surfactants' functionality at the surface.

Furthermore, by varying enzyme concentration, the gel stiffness and supramolecular organization of building blocks can be varied.

Then, a non-enzymatically triggered peptide-based hydrogelator was co-assembled with different amino acid and simple sugar based surfactant-like functionality. We aimed to study the effect of chemical functionality of co-assembled two-components on the differentiation of adipose stem cells. Different surfactant-based functionalities (simple amino acid and sugar derivatives) were co-assembled with Fmoc-FF, a well-established hydrogelator. The co-assembled structures were characterised by various techniques including FTIR, fluorescence spectroscopy, circular dichroism, zeta potential, TEM and rheology. Depending on the components chemistry, co-assembly mode can be affected by the chemical functionality presented on the surface of the nanofibres. Moreover, the mechanical properties of the formed hydrogels could be tuned by varying the total concentration of the co-assembled components.

After that the ability of simple sugar amphiphiles to self-assemble into nanofibers upon enzymatic dephosphorylation was investigated. The self-assembly process can be triggered by alkaline phosphatase (ALP) in solution or *in situ* by the ALP produced by osteosarcoma cell line, SaOs2. In the former case, self-assembly rate, mechanical properties (stiffness) and the supramolecular organisation could be controlled. In the latter case, assembly and localized gelation occurs mainly on the cell surface. The gelation of the pericellular environment induces a reduction of the SaOs2 metabolic activity at an initial stage (≤7 h) that results in cell death at longer exposure periods (≥24 h). We show that this effect depends on the phosphatase concentration and thus, it is cell-selective with prechondrocytes ATDC5 (that express ~15-20 times lower ALP activity compared to SaOs2) not being affected at

concentrations ≤ 1 mM. These results demonstrate that simple carbohydrate derivatives can be used in an anti-osteosarcoma strategy with limited impact on the surrounding healthy cells/tissues.

Biological systems are exceptionally able to respond to new situations. This is achieved through dynamically interacting molecules that assemble, compete and selectively decompose, enabled by biological catalysis. In the final part of this thesis, we describe a synthetic mimic by combining (i) peptide self-assembly, (ii) catalytic sequence exchange, (iii) peptide/polymer co-assembly in one system. Thus, we use coupled biocatalytic peptide condensation and self-assembly to achieve reversible and continuous exchange of peptide sequences and by incorporating charged residues, achieve selective amplification in the presence of cationic (chitosan) or anionic (heparin) biomacromolecules. We show that morphologically different peptide/polymer structures (nanotubes *or* nanosheets) can be competitively or sequentially accessed at physiological conditions.

# The Author

## Academic training

1. PhD in Physical Chemistry; supramolecular self-assembly for biomedical applications, The University of Strathclyde, Glasgow, UK. (leading to this thesis).

2. MSc degree in Applied Chemistry, Jordan University of science and Technology, Irbid, Jordan. Thesis title: "[Pectin-co-(N-vinylpyrrolidone)] and [Pectin-co-(N-isopropylacrylamide)] Hydrogel Copolymers for Sustained Drug Release: Synthesis and Control".

3. BSc degree in Applied Chemistry, Jordan University of science and Technology, Irbid, Jordan.

## Publications during candidature

**1.** C. G. Pappas, P. W. J. M.; T. Mutasa, S. Fleming, **Y. M. Abul-Haija**, S. Kelly, A. Gachagan, D. Kalafatovic, J. Trevino, R. V. Ulijn, S. Bai, Alignment of Nanostructured Tripeptide Gels by Directional Ultrasonication. *Chemical Communications* **2015**, 51, 8465-8468.

**2.** R. A. Pires[#], **Y. M. Abul-Haija**[#], D. S. Costa, R. Novoa-Carballal, R. L. Reis, R. V. Ulijn, I. Pashkuleva, Controlling Cancer Cell Fate Using Localized Biocatalytic Self-Assembly of an Aromatic Carbohydrate Amphiphile. *J. Am. Chem. Soc.* **2015**, 137, 576-579. (#: equally contributed authors). Highlighted in *Spotlights on Recent JACS Publications* and in *Chemical & Engineering News*.

**3.** P. W. J. M. Frederix, G. Scott, **Y. M. Abul-Haija**, D. Kalafatovic, C. G. Pappas, N. Javid, N. Hunt, R. V. Ulijn, Exploring The Sequence Space for (Tri-) Peptide Self-Assembly to Design and Discover New Hydrogels. *Nature Chemistry* **2015**, 7, 30–37. Front cover.

**4. Y. M. Abul-Haija**, S. Roy, P. W. J. M. Frederix, N. Javid, V. Jayawarna, R. V. Ulijn, Biocatalytically Triggered Co-Assembly of Two-Component Core/Shell Nanofibers. *Small* **2014**, 10, 973-979. Back cover and featured online on *Advances in Engineering* (https://advanceseng.com).

**5.** C. G. Pappas[#], **Y. M. Abul-Haija**[#], A. Flack, P. W. J. M. Frederix, R. V. Ulijn, Tuneable Fmoc–Phe–(4-X)–Phe–$NH_2$ Nanostructures by Variable Electronic Substitution. *Chemical Communications* **2014**, 50, 10630-10633. (¥: equally contributed authors).

**6.** K. Thornton, **Y. M. Abul-Haija**, N. Hodson, R. V. Ulijn, Mechanistic Insights into Phosphatase Triggered Self-Assembly Including Enhancement of Biocatalytic Conversion Rate. *Soft Matter* **2013**, 9, 9430-9439.

**7.** G. Scott, S. Roy, **Y. M. Abul-Haija**, S. Fleming, S. Bai, R. V. Ulijn, Pickering Stabilized Peptide Gel Particles as Tunable Microenvironments for Biocatalysis. *Langmuir* **2013**, 29, 14321-14327.

**8. Y. M. Abul-Haija**, R. V. Ulijn, Enzyme-Responsive Hydrogels for Biomedical Applications. In: Hydrogels in Cell-Based Therapies. The Royal Society of Chemistry: Cambridge, U.K. **2014**, 2, p. 112.

**Conferences and workshops**

- Nanopeptide 2015, University of Strathclyde, Glasgow, UK, 2-4 March 2015: poster presentation.
- Chemical Complexity and Biology Symposium, University of Strasbourg, France, 19-20 January 2015: poster presentation.
- MRS Fall Meeting 2014, The Hynes Convention Centre and Sheraton Boston Hotel in Boston, Massachusetts, USA, 30$^{th}$ November-5$^{th}$ December 2014: oral presentation.
- RSC Biomaterials Conference 2014, The University of Manchester, UK. 7-8$^{th}$ January 2014: oral presentation.
- RSC Macrocyclic and Supramolecular Chemistry Meeting 2013, University of Glasgow, UK. 16-17$^{th}$ December 2013: poster presentation.
- Term Stem 2013, Porto Palácio Congress Hotel Spa, Porto, Portugal. 10-12$^{th}$ October 2013: oral presentation.
- 1$^{st}$ POLARIS Workshop, Porto Palácio Congress Hotel Spa, Porto, Portugal. 07-09$^{th}$ October 2013: oral presentation.
- The European-Winter School on Physical Organic Chemistry (E-WISPOC) [Supramolecular Chemistry], Bressanone, Italy. 27$^{th}$ January – 1$^{st}$ February 2013: poster presentation.
- ERC Grantees Conference 2012 "Frontier Research in Chemistry", Strasbourg, France. 22$^{nd}$-24$^{th}$ November 2012: poster presentation.
- Polymeric and Self-Assembled Hydrogels meeting "From fundamental understanding to Applications", London, UK. 4-5th September 2012: poster presentation.

- Postgraduate Conference on Biomedical Engineering and Medical Physics (PGBiomed-2011), Glasgow, UK. 14-16th August 2011: Attendance.

**Existing IP**

1. Rein Ulijn, Tell Tuttle, Pim Frederix, Gary Scott, Yousef Abul-Haija, "Tripeptides", UK patent application no. 1417885.9 (09/10/2014).

# 1. Introduction

## 1.1Introduction to thesis

Dynamic processes in biological systems are commonly controlled by spatially confined molecular mechanisms such as catalysis and molecular recognition. This is in contrast to traditional laboratory-based approaches to controlling supramolecular synthesis, which usually involve changing one or more of the environmental conditions such as pH,[1] temperature,[2] solvent polarity[3] and/or ionic strength.[4] In the last decade or so, the use of enzymes has become more popular to direct laboratory based supramolecular assembly.[5-7] Biocatalysis is increasingly of interest in this context because it (i) allows responsive assembly under constant, physiological conditions;[8] (ii) allows exploitation of biocatalytic reactions which are specifically associated with certain cell types or diseased states;[9-11] (iii) catalysis inherently involves molecular amplification (turnover numbers of $10^3$-$10^7$ are common), which may give rise to fast response times; (iv) provides new tools for bottom-up nanofabrication by taking advantage of the ability to spatially and kinetically control the self-assembly process;[12] (v) thermodynamically controlled systems provide routes towards discovery of peptide based nanostructures by exploiting reversible exchange of amino acid sequences in dynamic peptide libraries.[13-15]

Supramolecular hydrogels based on peptidic building blocks are of particular interest because of (i) their rich chemistry in non-covalent (hydrogen bonding, electrostatic, π-stacking, hydrophobic) interactions; (ii) ease of synthesis and (iii) biological compatibility. As peptides are biology's expression language, there is potential for them to be used as instructive biomaterials, *i.e.* containing peptide sequences found in the natural extracellular matrix, which will be the focus of the following chapters.

## 1.2Thesis outline

This thesis is divided into seven chapters. The chapters follow an organised sequence starting from the literature review (**Chapter 2**) which discusses enzyme-responsive hydrogels (particularly peptide-based hydrogels) for biomedical applications. The following four chapters (**chapters 3, 4, 5 and 6**) are structured in such a way that each chapter covers one area of the overall research presented in publication format. Each chapter defines its own objectives and carries an abstract and an introduction before presenting the materials and methods, results and discussion and finally conclusion and list of references.

Enzymatically triggered functionalisation of peptide-based nanofibres is described in **Chapter 3**. The system is composed of an enzyme-responsive peptide-based hydrogelator and a surfactant-like amino acids/peptide derivative designed to form core-shell functionalised nanostructures, which may be used for cell culture applications. Although the design was successful (*i.e.* fibres functionalisation was successfully achieved), the fabricated scaffolds failed to maintain the culture of human dermal fibroblasts. This might be attributed to a number of possible reasons such as intracellular self-assembly, cytotoxicity of the hydrogelators or the high concentration of enzyme used to trigger the self-assembly process. In order to avoid the high concentration of the used enzyme and to test a wider range of gelators/surfactant functionalities, non-enzymatically triggered peptide-based hydrogelators with different amino acid and simple sugar based surfactant-like functionality were studied (**Chapter 4**). In collaboration with the 3B's research group at University of Minho, Portugal, the functionalised scaffolds with different chemical functionality were used for adipose stem cell culture and to check for

possible cell differentiation. In **Chapter 5**, the first example of enzymatically triggered sugar-based hydrogelator was found. Mechanical properties were tuned depending on the concentration of enzyme. In collaboration with the 3B's research group, this material was used for controlling cancer cell fate. **Chapter 6** describes the design of a new class of synthetic adaptive materials which are able to change their molecular composition and nanoscale structure by combining biocatalytic peptide exchange (using peptide dynamic combinatorial chemistry), sequence selective peptide self-assembly (forming nanotubes versus nanosheets) and peptide/polymer co-assembly. Finally, **Chapter 7** summarises the key findings from the previous chapters, discusses the study limitations and provides directions for future research.

## 1.3References


1. C. Tang, A. M. Smith, R. F. Collins, R. V. Ulijn and A. Saiani, *Langmuir*, 2009, **25**, 9447-9453.
2. H. Hong, Y. Mai, Y. Zhou, D. Yan and Y. Chen, *Journal of Polymer Science Part A: Polymer Chemistry*, 2007, **46**, 668-681.
3. M. Reches and E. Gazit, *Science*, 2003, **300**, 625-627.
4. B. Ozbas, J. Kretsinger, K. Rajagopal, J. P. Schneider and D. J. Pochan, *Macromolecules*, 2004, **37**, 7331-7337.
5. M. Zelzer, S. J. Todd, A. R. Hirst, T. O. McDonald and R. V. Ulijn, *Biomaterials Science*, 2013, **1**, 11-39.
6. Z. Yang, H. Gu, D. Fu, P. Gao, J. K. Lam and B. Xu, *Advanced Materials*, 2004, **16**, 1440-1444.
7. Z. Yang, G. Liang and B. Xu, *Accounts of chemical research*, 2008, **41**, 315-326.
8. B. Xu, *Langmuir*, 2009, **25**, 8375-8377.
9. Z. Yang, G. Liang, Z. Guo and B. Xu, *Angewandte Chemie International Edition*, 2007, **46**, 8216-8219.
10. Z. Yang, K. Xu, Z. Guo, Z. Guo and B. Xu, *Advanced Materials*, 2007, **19**, 3152-3156.
11. A. Tanaka, Y. Fukuoka, Y. Morimoto, T. Honjo, D. Koda, M. Goto and T. Maruyama, *Journal of the American Chemical Society*, 2015, **137**, 770-775.
12. A. R. Hirst, S. Roy, M. Arora, A. K. Das, N. Hodson, P. Murray, S. Marshall, N. Javid, J. Sefcik, J. Boekhoven, J. H. van Esch, S. Santabarbara, N. T. Hunt and R. V. Ulijn, *Nature Chemistry*, 2010, **2**, 1089-1094.

13. R. J. Williams, A. M. Smith, R. Collins, N. Hodson, A. K. Das and R. V. Ulijn, *Nature Nanotechnology*, 2008, **4**, 19-24.

14. A. K. Das, A. R. Hirst and R. V. Ulijn, *Faraday discussions*, 2009, **143**, 293-303.

15. S. K. M. Nalluri and R. V. Ulijn, *Chemical Science*, 2013, **4**, 3699-3705.

# 2. Literature Review: Enzyme-Responsive Hydrogels for Biomedical Applications*

* This chapter was published in part as: Y. M. Abul-Haija, R. V. Ulijn, Enzyme-Responsive Hydrogels for Biomedical Applications. In *Hydrogels in Cell-Based Therapies*, The Royal Society of Chemistry: 2014; pp 112-134.

Declaration of contribution to publication: Any reproduced work from the aforementioned publication I was solely responsible for unless otherwise stated.

## 2.1Introduction

Hydrogels are critically important components in biology as both the intracellular cytoskeleton and extracellular matrix are gel phase materials. Biological gels are highly responsive to changes in their environment, with enzymatic processes involved in adaption and reorganisation of gel structures. This adaption and reorganisation is key to processes such as differentiation and cell division. Given these observations, it is clear why an increasing number of researchers are focusing on the production of synthetic mimics of these biological hydrogels that may find applications in the measuring and directing of biological processes. In addition to the interest in enzyme-responsive systems in mimicking biological matrices, enzymatic processes are also useful in fabrication (enzyme assisted assembly) of gels with precisely defined properties.[1] This chapter focuses on recent developments in these areas as well as the application of enzyme-responsive hydrogels in biomedicine, with a focus on supramolecular gels based on small molecular weight gelators (LMWG).

### 2.1.1 Polymeric and self-assembling hydrogels

Synthetic hydrogels have been considered in biomedical applications from 1960 when Wichterle and Lim demonstrated biocompatible hydrogels composed of cross-linked poly(hydroxyethylmethacrylic)acid [poly(HEMA)] that were later used in contact lenses.[2] Naturally derived hydrogels (alginates) were reported in the 1980s for encapsulation of pancreatic cells,[3] followed by the use of shark collagen as burn dressings.[4] Clearly, both synthetic and natural materials can be used effectively, with well-documented advantages and disadvantages for each of these. Hybrid systems, incorporating aspects of both are increasingly considered.[5] Early reports focused on the structural properties of hydrogels, which can match those of natural tissues. This focus has shifted to production of materials that do not just structurally, but also

chemically, mimic aspects of biological gels, for example, by inclusion of short peptides, sugars or other biomolecules, to encourage 'active' interaction with biological systems. More recently, controlled degradation through enzyme action has become an additional feature of designed biomaterials.[1] The use of enzymes in the fabrication of materials has also become increasingly popular due to their selectivity and synthetic capability under mild conditions.[1]

Two types of synthetic gels can be distinguished, depending on the chemical nature of their networks **(Figure 1)**. Polymeric hydrogels are covalently cross-linked networks that can swell due to the absorption and ability to trap water.[2] Supramolecular hydrogels are associated with reversible, non-covalent molecular interactions (hydrogen bonding, π-stacking, electrostatic, hydrophobic interactions, van der Waals forces) between self-assembling molecules (known as hydrogelators) to form nanofibres. These nanofibres then entangle into 3D networks that, depending on their surface chemistry, are able to trap water and form hydrogels. The design of polymeric hydrogels for biomedical applications is informed by substantial knowledge and literature on polymer synthesis and functionalisation strategies. This is now a relatively mature field with many excellent contributions reported.[5, 6] For supramolecular systems, the design rules are less well established and still emerging, with natural systems providing guidance and inspiration for their synthesis.

### 2.1.2 Use of enzymes in fabrication of next generation biomaterials

One area where functionalised hydrogels have shown enormous potential is in gel phase biomaterials for cell culture[7-10] and biosensing[11] platforms. In particular, there have been major developments in the application of hydrogels as instructive matrices for stem cell growth. The emphasis has been on the inclusion of biochemical signals,

usually comprising matrix protein specific peptidic motifs, such as the well-known fibronectin derived arginine-glycine-aspartic acid (RGD) motif that encourages cellular adhesion. A number of breakthroughs in recent years have shown that stem cell growth and differentiation, in addition to biochemical signals, are highly sensitive to physical stimuli presented by their immediate environment.[12, 13] Specifically, mechanical[14] (*i.e.* gel stiffness) and structural/topographical factors[15] of the cell-contacting matrix play crucial roles that have, in some cases, been shown to be more powerful than soluble biochemical signals. These approaches pave the way towards hydrogels that allow for the control of cell fate. Producing gels with specific requirements on physical properties and chemical composition will require new synthetic protocols that enable control of stiffness, gel network structure and chemical functionalisation. It will be demonstrated that enzymatic fabrication methods provide useful tools to achieve this.[1, 16]

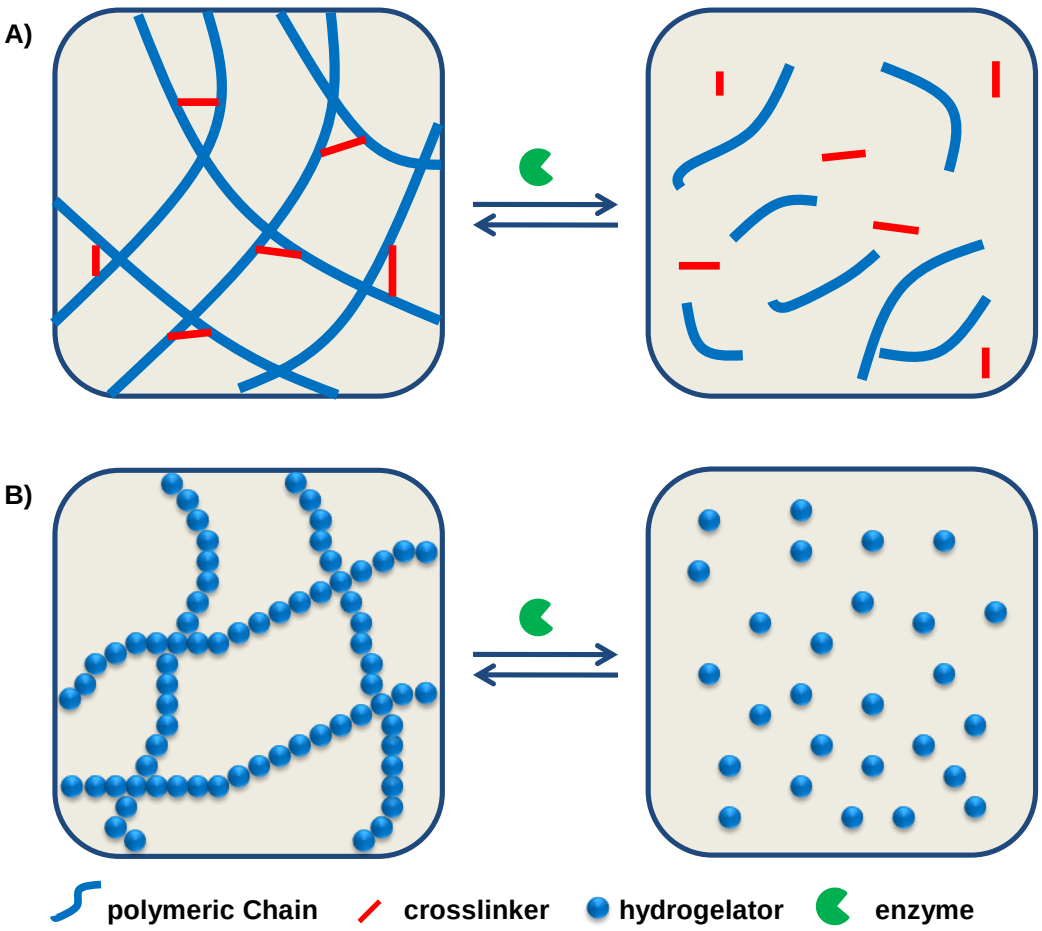


**Figure 2.1** Schematic presentation of enzyme responsive materials based on A) polymeric and B) supramolecular hydrogels. Enzymatic processes may be exploited both in the degradation and controlled assembly of hydrogel materials.

### 2.1.3 Use of enzymes as 'stimuli' in smart materials

Since the early days of hydrogel research, efforts have been devoted towards the development of stimuli-responsive hydrogels as they potentially enable external control of cell encapsulation or release of actives. Stimuli-responsive, smart or intelligent hydrogels are those gels which may display property or functionality changes in response to variations in the external environment. Typically, these changes in their surroundings involve solvent polarity, temperature, pH, supply of

electric field, light etc.[17-20] More generally, materials based on stimuli-responsive technologies are increasingly attracting attention due their potential applications in every-day life, offering improvements in many technologies.[1, 21-25] There are excellent reviews on this topic that discuss the design, advantages and challenges of stimuli-responsive hydrogels.[19, 26-29] In cellular environments, most stimuli-responsive mechanisms take place under the control of enzymes.[30] Compared with physical or conventional chemical stimuli (e.g., pH, temperature, ionic strength, ligand-receptor interactions, etc.), enzymatic regulation of materials properties shows much promise because it enables responsiveness to biology's own signals, that are highly selective and involve catalytic amplification to enable fast response times.[31, 32] Examples have been reported on both polymeric[33, 34] and supramolecular hydrogels in this context.

Controlled degradation of matrices is a particularly important focus area for enzyme-responsive materials. Hydrogels may be designed to render them degradable, which may involve breaking of chemical crosslinks (polymeric hydrogels) or controlled dis-assembly (supramolecular hydrogels) **(Figure 2.1)**. Enzymatic degradation is selective and can, in principle, be tightly regulated and is therefore highly attractive as will be discussed below.

## 2.2Biocatalytic Assembly of Supramolecular Hydrogels

Dynamic processes in biological systems are commonly controlled by spatially confined molecular mechanisms such as catalysis and molecular recognition. This is in contrast to traditional laboratory-based approaches to controlling supramolecular synthesis, which usually involves changing one or more of the environmental conditions such as pH,[35] temperature,[36] solvent polarity[37] and/or ionic strength.[38] In

the last decade or so, the use of enzymes has become more popular to direct supramolecular assembly.[1, 39-43] Biocatalysis is increasingly of interest in this context because it (i) allows responsive assembly under constant, physiological conditions;[44] (ii) allows exploitation of biocatalytic reactions which are specifically associated with certain cell types or diseased states;[31, 45] (iii) catalysis inherently involves molecular amplification (turnover numbers of $10^3$-$10^7$ are common), which may give rise to fast response times; (iv) provides new tools for bottom-up nanofabrication by taking advantage of the ability to spatially and kinetically control the self-assembly process;[46] (v) thermodynamically controlled systems provide routes towards discovery of peptide based nanostructures by exploiting reversible exchange of amino acid sequences in dynamic peptide libraries.[47-49]

Biocatalytic self-assembly involves the formation of gelators by the action of enzymes (either through hydrolysis or condensation of precursors), which is followed by the self-assembly of these molecules to form supramolecular structures. These assemblies in turn entangle to form one, two or three dimensional nanostructures **(Figure 2.2)** through non-covalent interactions such as π-π interactions, hydrogen bonding and electrostatic interactions.[50, 51]

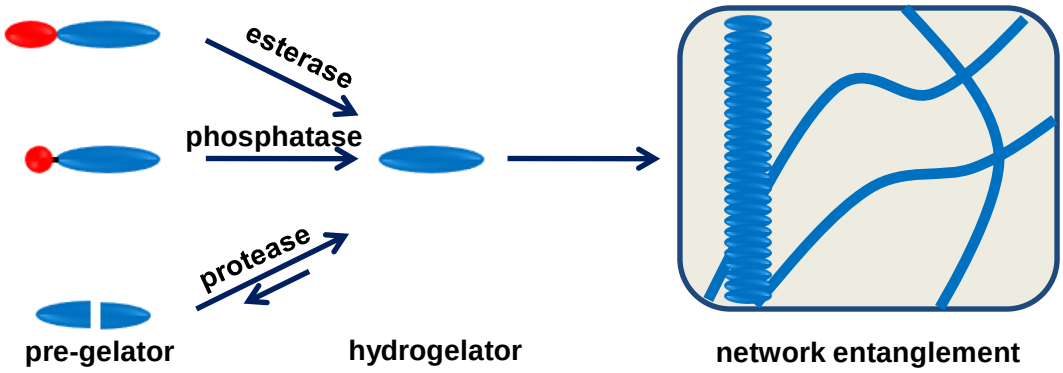

**Figure 2.2** Schematic illustration of enzyme assisted self-assembly. The enzyme action results in hydrogelators formation which are able to self-assemble to form supramolecular structures and then entangle to form a network.

### 2.2.1 Peptide-based hydrogels

The majority of biocatalytic self-assembly systems reported to date are based on peptidic building blocks so a brief introduction in this area is appropriate. Supramolecular hydrogels based on peptidic building blocks are of particular interest because of (i) their rich chemistry in non-covalent (hydrogen bonding, electrostatic, π-stacking, hydrophobic) interactions; (ii) ease of synthesis and (iii) biological compatibility. As peptides are biology's expression language, there is potential for them to be used as instructive biomaterials, *i.e.* containing peptide sequences found in the natural extracellular matrix.

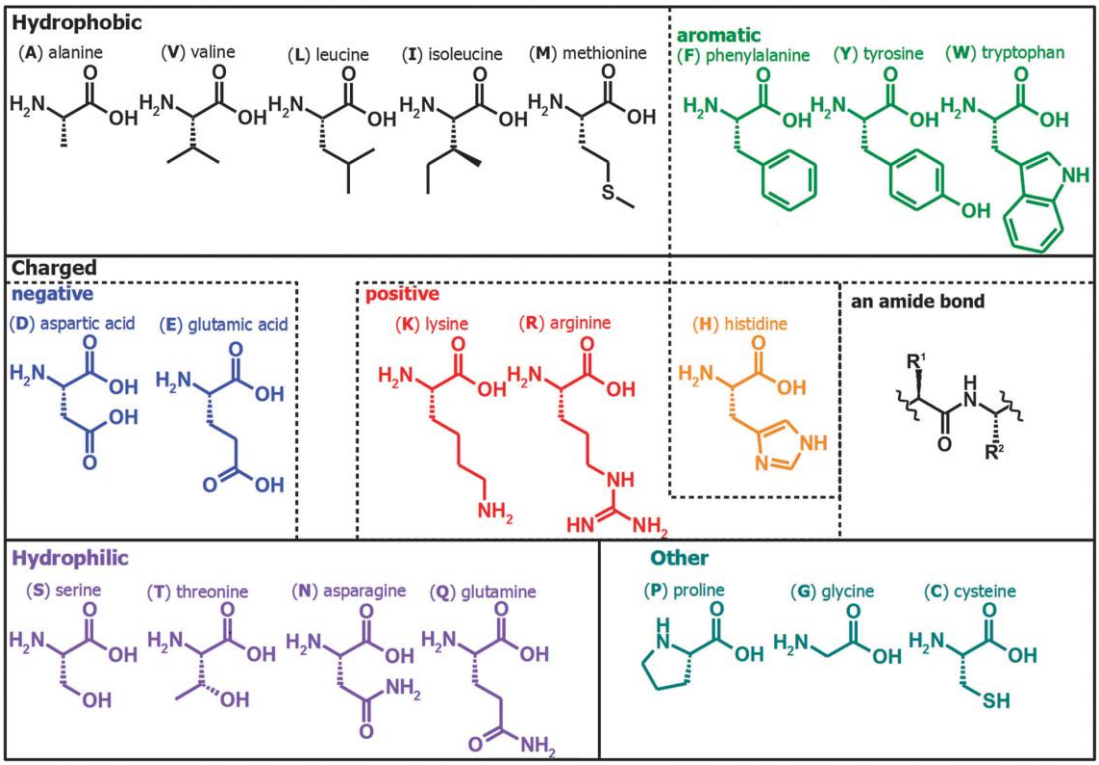


**Figure 2.3** The twenty gene-coded amino acids commonly found in nature. Adapted from ref. 62.

There are 20 gene-encoded amino acids commonly found in nature (**Figure 2.3**).[62] Depending on the nature of their side chains, non-covalent interactions can be incorporated at specific locations and the propensity for self-assembly thus varied. Considerable efforts have been made towards elucidating design rules for peptide-based supramolecular materials.[52-54] The design rules are either derived by copying nature (α-helix, β-sheet)[55, 56] or are entirely new designs that exploit peptide derivatives such as aliphatic[57, 58] or aromatic peptide amphiphiles.[22, 40, 59-62] While systems based on naturally occurring sequences typically use oligopeptides of ten or more residues, the latter systems allow for the use of the minimalistic approach where much simpler and shorter peptides (as short as dipeptides) may be used. Aromatic peptide amphiphiles have been the basis of many biocatalytically triggered gels and are the focus of this chapter.

### 2.2.2 Biocatalytic peptide self-assembly for biomaterials fabrication

The key point in enzyme assisted self-assembly approaches is using an enzymatic bond making/breaking reaction to regulate the balance between hydrophobicity and hydrophilicity to convert soluble precursor molecules into self-assembling hydrogelators, or *vice versa*. This can be achieved by two main methods: catalytic formation of a covalent bond to link two non-assembling components together to form a gelator, or catalytic cleavage of a covalent bond to transform a non-assembling precursor to a self-assembly building block. The first approach is achieved by catalysing the condensation reaction between two amino acid derivatives or peptide fragments. The second approach involves removing a functional group through a hydrolysis reaction, which might affect the molecular packing ability due to its bulky size or by causing electrostatic repulsion between monomeric units.[63]

Most commonly, phosphatases, esterases and proteases have been exploited as triggers for self-assembly of peptide derivatives (**Figure 2.2**). Enzymatic dephosphorylation is used in biological systems to modify the structural features and biological activity of proteins. Self-assembly can be controlled using this method, driven by changes in electrostatic interactions as a result of the addition or removal of negatively charged phosphate groups. For example, Xu and Yang presented the first examples, where 9-fluorenylmethoxycarbonyl (Fmoc)-tyrosine modified with phosphate group (Fmoc-Y*p*) dissolves in phosphate buffer solution. The electrostatic repulsion between phosphate groups of neighbouring molecules is known to prevent molecular self-assembly. Upon the addition of alkaline phosphatase enzyme to the peptide solution, Fmoc-Y*p* will be converted into Fmoc-Y**,** a more hydrophobic compound, which is a hydrogelator able to self-assemble to form fibres.[64] It was demonstrated that by extending the amino acid to a phenylalanine -tyrosine (FY) dipeptide, thus enabling beta sheet interactions to contribute to the assembly, enzymatic dephosphorylation of Fmoc-FY*p* gives rise to a transformation of micelles to chiral, unidirectional fibres.[65] By exchanging phenylalanine (F) with other amino acids with different side chain properties, it becomes possible to form a range of different supramolecular structures[66-68] (*i.e.* different morphologies) which will be discussed further in the next section.

In order to provide a further step in understanding the mechanism of biocatalytic self-assembly, the mechanism and kinetics of the phosphatase triggered self-assembly of Fmoc-Y*p*, as a model system, was investigated.[69] The biocatalytic conversion, changes in supramolecular interactions and chirality, nanostructure formation and gelation at varying enzyme concentrations gave rise to new

mechanistic insights into the multi-stage self-assembly process. Furthermore, a remarkable enhancement of catalytic activity during the early stages of the self-assembly process was observed, providing evidence for enhancement of enzymatic activation by the supramolecular structures formed.

Esterases may be used to catalyse ester hydrolysis of ester terminated peptides to form self-assembling peptides. Ulijn et al demonstrated that methyl esters of Fmoc-dipeptides could be converted into gelators by subtilisin, a common protease with esterase activity, resulting in formation of networks of nanotubes and fibres, depending on the peptide sequence.[46] Similarly, proteases can hydrolyse an amide bond to cleave a group associated with blocking.[70] Koda *et al.* have produced a hydrogelating species by hydrolysis of an amide bond, removing a fragment of the peptide chain which hinders self-assembly. The reaction was catalysed by matrix metalloproteinase-7 (MMP-7), an enzyme associated with degradation of extracellular matrix components by cells.[71] Additionally, β-lactamases were also used to catalyse the formation of hydrogelators in the context of antibiotic resistant bacteria that are known to express this type of enzyme. Here, the precursors were designed with a specific target for β-lactamase (*i.e.* β-lactam ring), with the resulting cleaved molecule acting as a hydrogelator, with molecular self-assembly resulting in a nanofibrillar network structure.[72] The use of condensation reactions (*i.e.* the direct reversal of hydrolysis of amides) to produce gelators is a special case and will be discussed in the next section.

#### 2.2.2.1 Morphology control

Controlling the morphology of self-assembling peptide nanostructures continues to be an important challenge. As outlined in section 2.2, fibre morphology (nano-

topography) is an important variable in the design of supramolecular biomaterials, as it can impact dramatically on cellular response. Considerable research efforts have been devoted to develop the design rules for peptide building blocks to achieve morphological control which depends on two main principles (i) self-assembly pathway (ii) peptide sequence.

2.2.2.1.1 Morphology control by pathway: Thermodynamic *vs* Kinetic

It is increasingly recognised that the chosen self-assembly pathway dictates the structure of the final gel-phase material.[46,73] Biocatalytic self-assembly may proceed under kinetic control or thermodynamic control, depending on the reversibility of the enzyme reaction. Kinetic control gives rise to pathway dependant properties, while thermodynamic control gives rise to reversible/self-healing materials that represent a free energy minimum stage. Both approaches are of interest in different contexts.

***Biocatalytic Assembly under Kinetic Control***

Due to the restricted molecular dynamics in the gel-phase, it is possible to trap molecular assemblies that do not represent the thermodynamically preferred structure. As a consequence, biocatalytic self-assembly may be used to form diverse materials from a single gelator structure, regulated by the kinetics (enzyme concentration) of the reaction. Kinetic control is achieved when both the enzymatic reaction and the self-assembly process are independently favoured as illustrated in **Figure 2.4A**, as observed for phosphatase[39] and subtilisin[74] responsive systems that operate by ester or phosphate ester hydrolysis, which readily proceeds in aqueous conditions. The rate of self-assembly in this case has substantial effect on the final structure, which is locked in the gel-state. So, different supramolecular structures can

be obtained by having control over the rate which can be controlled by changing the amount of the catalyst with stiffer gels generally resulting at higher rates of catalysis.[75] Upon gelation, systems become fixed in this arrangement, a process referred to as 'kinetic locking', as it is energetically unfavourable to reorganise the self-assembled monomers in combination with the extremely slow molecular dynamics associated with the gel phase. Consequently, the structures observed may not represent the global thermodynamic minimum.[74, 76] Theoretically, by using a low concentration of enzyme molecules to control assembly, it would be possible to access the thermodynamically favoured structure to achieve thermodynamic control in these systems.

Utilising a kinetically controlled system can be advantageous. It could be possible to control the properties of the produced hydrogels and allow tailoring materials for specific purposes while keeping the overall gelator concentration and chemical composition the same. For example, it was shown that the mechanical properties of the hydrogels (*i.e.* stiffness) have been directly linked to the enzyme concentration. Higher enzyme concentration, leading to faster gel formation, could result in stiffer gels when directly compared with similar systems with lower enzyme concentration.[77, 78]

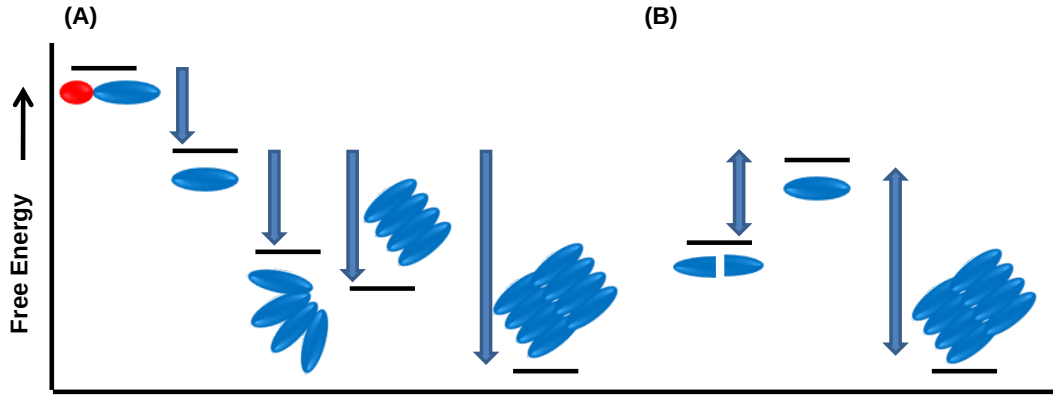


**Figure 2.4** Free energy diagram of **(A)** kinetically controlled enzymatic self-assembly, where both the enzymatic reaction and the self-assembly processes are thermodynamically favoured. **(B)** Thermodynamically controlled enzymatic self-assembly, where the enzymatic reaction is thermodynamically unfavoured while the self-assembly process is energetically favoured.

***Biocatalytic Assembly under Thermodynamic Control***

An enzymatically triggered system is said to operate under thermodynamic control when the enzymatic reaction producing self-assembling molecules is fully reversible. This is achieved when the enzymatic reaction is in itself energetically unfavourable (*e.g.* amide condensation, instead of hydrolysis) but is enabled by the favourable (small) free energy contribution of molecular self-assembly of the reaction product (**Figure 2.4B**). This was demonstrated by the formation of a self-assembling peptide produced from non-assembling precursors, *via* amide condensation.[43] This approach gives rise to dynamic and fully reversible assemblies, which in turn, allow for defect correction and molecular reorganisation, ultimately, reproducibly achieving a homogenous assembly of a structure representing the thermodynamic minimum.

Utilising a thermodynamically driven approach introduces a means to directly compare the relative stabilities of each molecular building block and non-assembling

precursor. Interestingly, when mixtures of precursors are supplied, these components would compete and finally self-select the most thermodynamically stable structure from dynamic mixtures. This type of system, where building blocks are continuously substituted until equilibrium is reached, is known as a dynamic combinatorial library (DCL).[79, 80] This approach has been utilized in the discovery of stable supramolecular assemblies from mixtures. Due to the large possible peptide sequences that can be synthesised, the DCL approach is interesting for the identification of supramolecular peptide interactions.

Utilising the enzymatic DCL approach, a range of dipeptide sequences in Fmoc-dipeptide methyl ester gelators was screened.[48] Two DCLs based on Fmoc-S or Fmoc-T with the amino-acid methyl esters (leucine (L), phenylalanine (F), tyrosine (Y), valine (V) glycine (G) and alanine (A)) were investigated in the presence of thermolysin to produce Fmoc–dipeptide esters.. Fmoc-SF-OMe and Fmoc-TF-OMe were found to be the most thermodynamically stable dipeptide derivatives. Thus, the most stable self-assembled structures can be identified from a mixture of several components. This opens up the potential of exploiting the versatility of peptides for the discovery of functional nanostructures for various applications.

The use of enzyme-driven DCL approach was taken one step further with an unprecedented discovery of functional gels (rather than just structural) from component mixtures.[81] As shown in **Figure 2.5**, the DCL was generated by mixing Nap-Y donor, various amino acid amide nucleophiles (F, L, V, Y, A and G) and thermolysin in the absence and presence of dansyl-β-alanine acceptor (DA). In the absence of the acceptor, reversed-phase HPLC results showed that only a single component (Nap-YF-$NH_2$) was preferentially produced. Remarkably, similar

experiments in the presence of DA (1:1 donor/acceptor ratio) showed that the formation of the major component Nap-YF-$NH_2$ was significantly amplified to 82% (instead of 52%), while the abundance of the second preferred compound, Nap-YL-$NH_2$ was reduced to 8% (instead of 23%). Furthermore, transmission electron microscopy showed the presence of entangled nanofibres of up to several micrometres in length **(Figure 2.5/D)**. The presence of both donors and acceptors in the nanofibres was resulted an efficient energy transfer observation between naphthalene donors and dansyl acceptors. Thus, the presence of suitable donors and acceptors in DCL greatly enhances its potential ability not just for self-selection but also for the amplification of most stable energy transfer nanostructures at the expense of less stable self-assembling nanostructures. These energy transfer nanostructures may pave the way towards the development of gels for interfacing electronics with biology, e.g. interfacing materials with neurons.

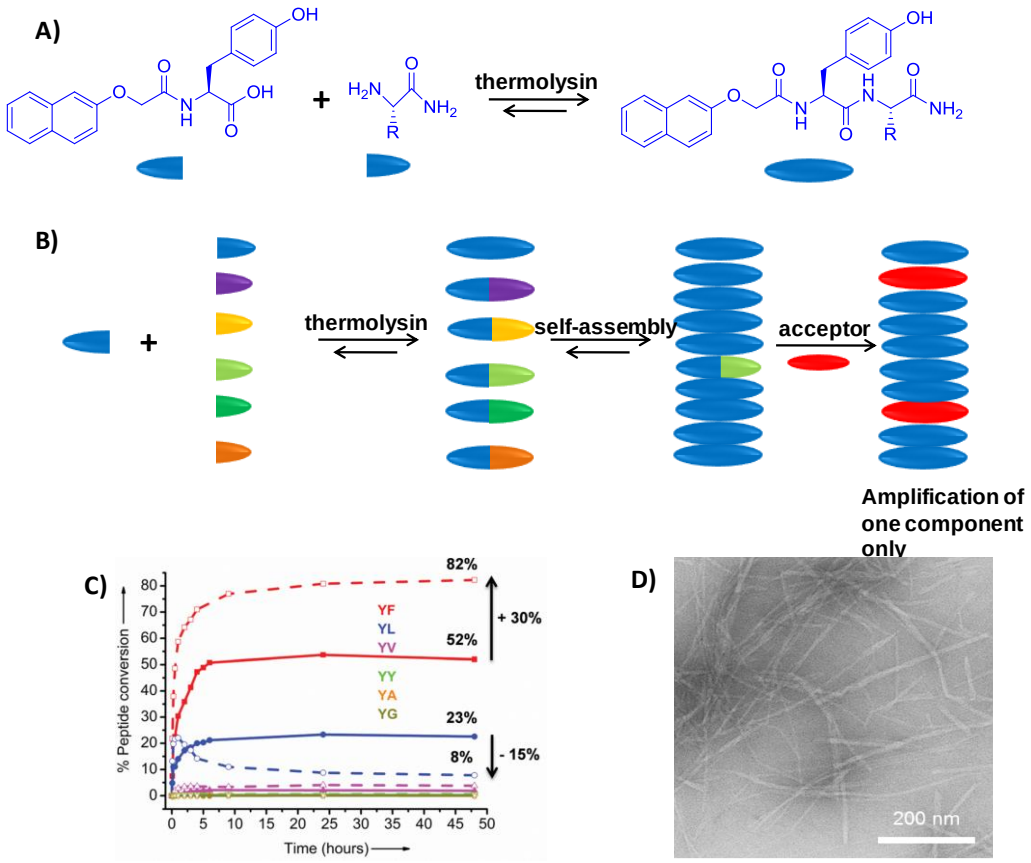


**Figure 2.5 (A)** Thermolysin catalysed condensation reaction. **(B)** Schematic presentation of peptide library where the most stable product is preferentially amplified by acceptor molecule. **(C)** Time course of the percentage conversion in DCL system by HPLC as measured in the absence (solid traces) and presence (dashed traces) of DA library. (**D)** TEM image in presence of the acceptor molecules in DCL system. Reproduced from ref. 81.

2.2.2.1.2 Morphology control by sequence

The second, perhaps more conventional, method to gain control over morphology is by changing the peptide sequence. For aromatic peptide amphiphiles, it is known that self-assembly can be controlled by the combination of weak interactions. For these systems, directional control of self-assembly can be achieved through the aromatic π-π stacking. For example, it was found that protecting the N-terminus of short peptides with an aromatic group (fluorenylmethoxycarbonyl (Fmoc), naphthalene

(Nap), carbobenzyloxy) may enhance the formation of stable hydrogels. Fmoc-dipeptide gelators where first described in 1995 by Vegners *et al.*[82] It was found that systematic variation of the side chains of the amino acids (*i.e.* peptide sequence) has a remarkable effect on the formed structures (spheres, fibres, tubes and sheets)[61, 83] which is believed to have a significant impact on materials design for different purposes.

Recently, supramolecular structures were produced by *in situ* enzymatic condensation of Fmoc-Phe-(4-X), where X denotes electron withdrawing or donating groups, with Phe-$NH_2$ **(Figure 2.6)**. Analysis by a range of complementary spectroscopic techniques shows that is possible to regulate the π-stacking and H-bonding interactions by the *para* substituent on a phenylalanine (Phe) residue, resulting in enzymatic formation of tuneable nanoscale morphologies depending on the balance between hydrophobic and hydrogen bonding interactions.[84]

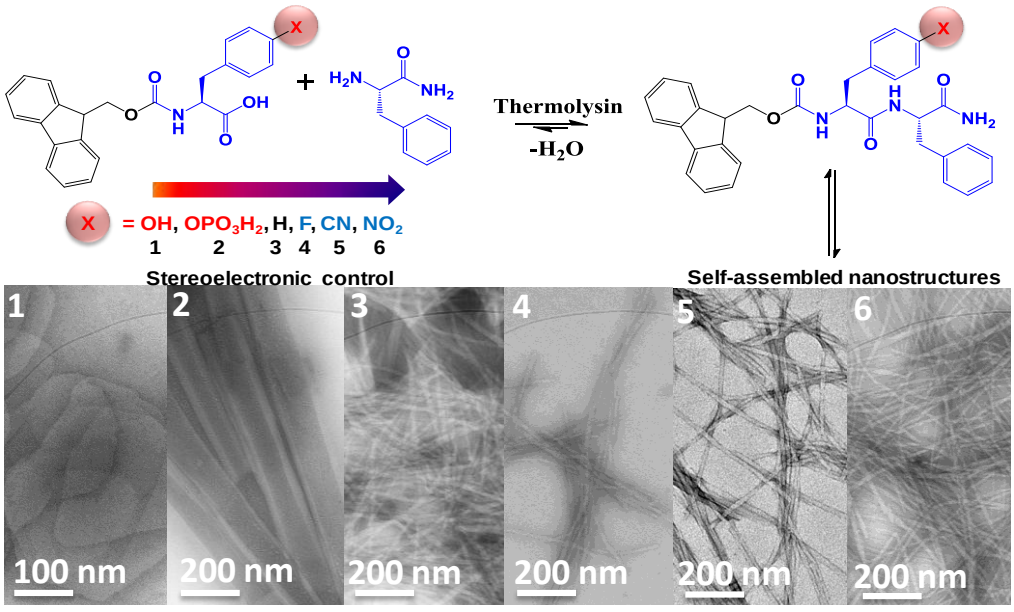

**Figure 2.6** Thermolysin catalysed amide bond formation of Fmoc-dipeptide derivatives containing groups with different electronic density. Adapted from ref. 84.

Ulijn group studied the sequence/structure relationship in an enzyme-responsive aromatic dipeptides hydrogels under thermodynamic control, which ensures that the final self-assembled systems represent a thermodynamic minimum, rather than a trapped state. Systems studied were based on Fmoc-protected dipeptide methyl esters which produced using thermolysin. It was found that by varying the peptidic sequence, different morphologies could be accessed[85] as shown in **Figure 2.7/A-B**. This system remarkably led to the discovery of new, extended two dimensional self-assembled structures.[86]

Using a kinetically controlled reaction, Hughes *et al* reported on subtilisin catalysed formation of a range of peptide gelators with polar peptide functional groups, **Figure 2.7/C-D**. The results demonstrated dramatic differences in morphology for four closely related Fmoc-dipeptide amphiphiles, including formation of spherical structures from Fmoc-YQ, while the closely related Fmoc-YN formed fibres. It was demonstrated that the molecular packing abilities and hence the supramolecular structure are directly affected by changing amino acid in position two.[87] Recently, hydrogelators were produced from phosphatase-responsive precursors, confirming that all peptide derivatives resulted in nanostructures with similar morphologies, independent of the enzymatic route used to produce them.[88]

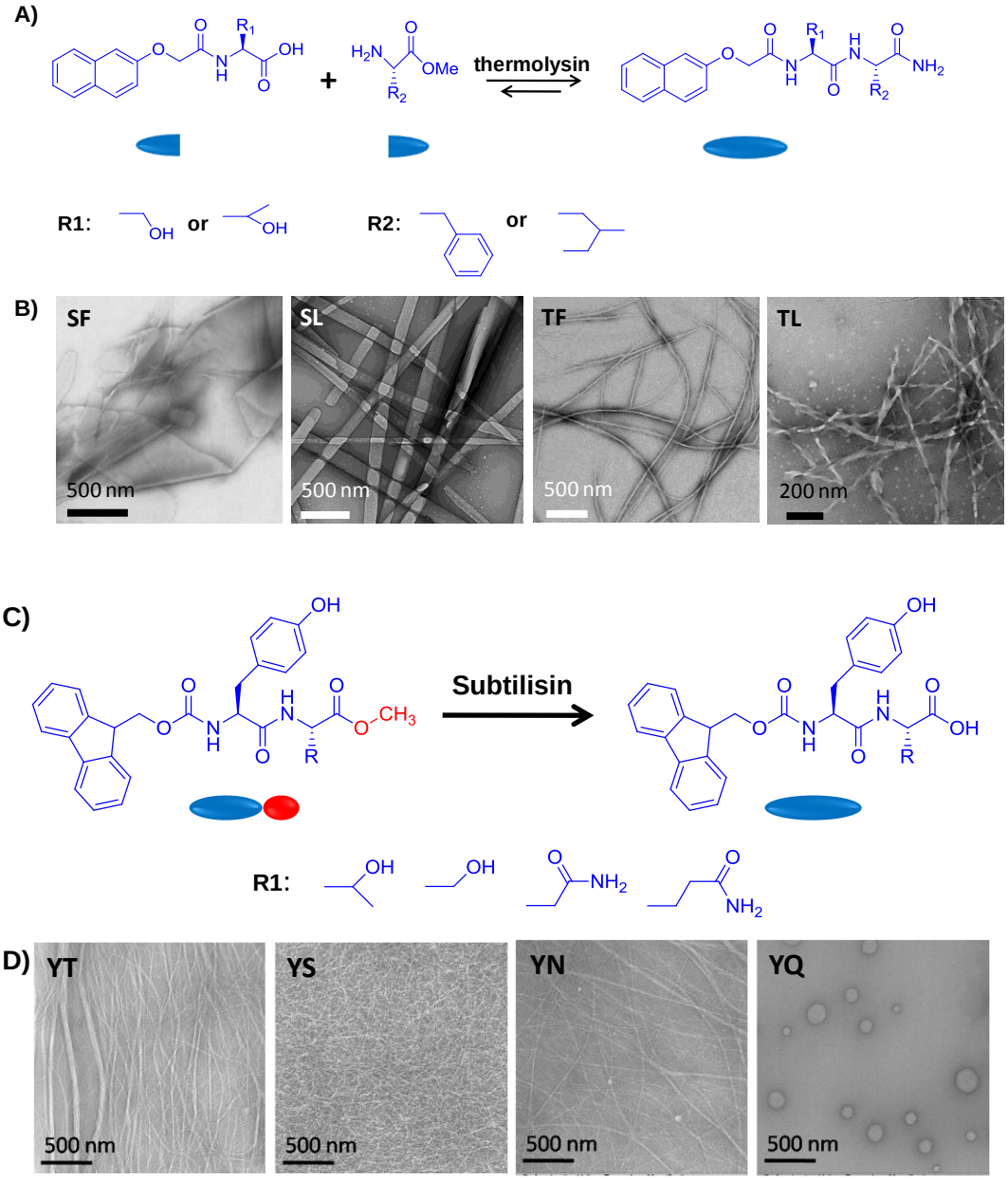


**Figure 2.7** Controlling the morphology of enzyme-responsive hydrogels by changing the peptidic sequence. A) Chemical structures of precursors and hydrogelators. B) TEM images of Fmoc protected dipeptides methyl esters produced by thermolysin. Reproduced from ref. 86. C) Chemical Structures of hydrogels produced by subtilisin triggered hydrolysis of Fmoc-dipeptide esters. D) TEM images of self-assembled structures. Reproduced from ref. 87.

It is clear that the combination of enzymatic reactions and peptide design provides access to a range of different structures. Using a combination of spectroscopy, microscopy techniques and molecular dynamics simulations progress is made with the elucidation of the 'design rules' for these systems. Ultimately, it should be possible to control the nanoscale topography and stiffness quite precisely, and in an on-demand fashion which might be useful for future biomaterials design. In addition to structure, there is a need to control the chemical functionality of these systems, which will be described next.

## 2.3Biomedical Applications

It is clear from the above that enzyme-responsive hydrogels, based on peptide self-assembly, are gaining increasing interest as biomaterials. The main application areas that are envisaged are cell culture, drug delivery, biosensing and, increasingly, the ability to control and direct cell fate in a dynamic manner using systems that operate intra- or extracellularly. In this section, details on some recent highlights that pave the way towards potential biomedical applications of enzyme-responsive hydrogels are provided.

### 2.3.1 Controlling and directing cell fate

As molecular self-assembly and catalysis are two of the key molecular mechanisms that drive dynamic processes in cells, it makes sense to harness these mechanisms and produce systems that allow researchers to interfere with these cellular processes. The first example that utilised enzyme-responsive hydrogels intracellularly was published by Xu and his co-workers.[31] They designed a peptide-based precursor which could be triggered by an esterase enzyme to form self-assembled nanostructures to induce gelation inside the cell. When exposed to cells, the

precursor enters into the cell by diffusion and undergoes hydrolysis by an endogenous esterase enzyme to form a hydrogelator which self-assembles into nanostructures **(Figure 2.8).**[31, 45] This gelation induced an abrupt change in the viscosity of the cell cytoplasm and caused cell death. At a certain concentration, the majority of cells derived from human cervical cancer tumours died within 3 days, whereas fibroblast cells remained alive under the same conditions. Moreover, it also found that the formation kinetics of the intracellular nanofibres was specific to different types of cells because of different esterase expression levels,[45] which may open up new ways to treat tumour with high selectivity (*e.g.* tumour cells usually have higher esterase expression levels than normal cells).

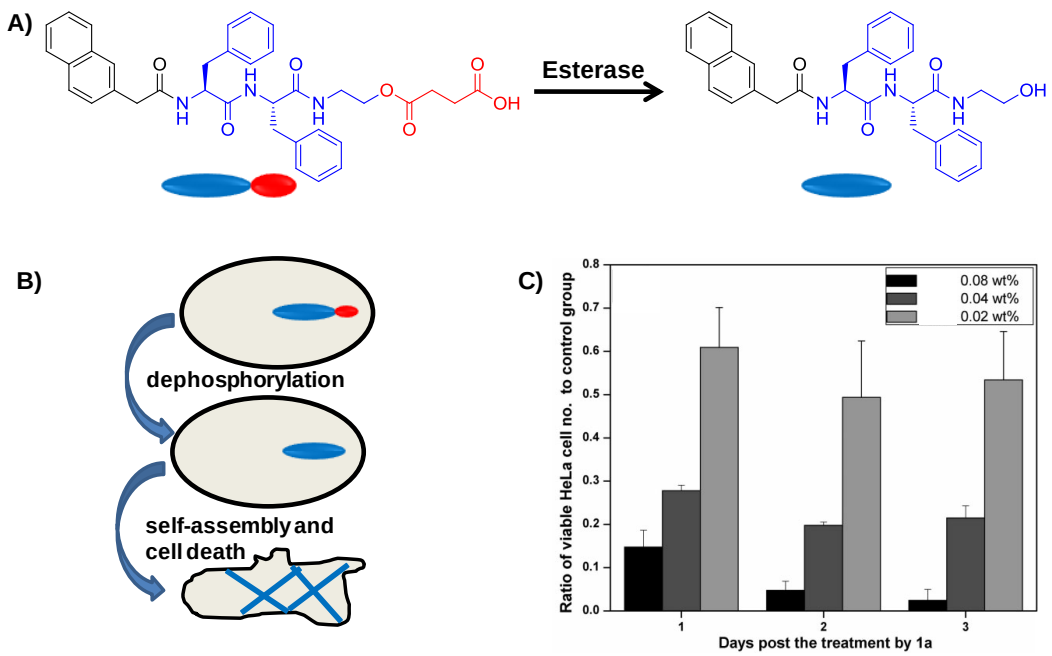


**Figure 2.8 A)** Chemical structures of intracellular cleavage of an esterase responsive precursor by an endogenous esterase to a hydrogelator B) corresponding schematic representation for the formation of supramolecular assembly within the cells C) MTT

assay results of HeLa cells treated with different concentrations (0.2%, 0.4% and 0.8%) of the precursor. Reproduced from ref. 31.

Using a similar approach, Tanaka *et al.* designed an MMP-7 sensitive pregelator which can be cleaved upon enzymatic action to self-assemble into nanofibres and finally gel. MMP-7 is overexpressed in various cancer cells. The precursor was cleaved by the enzyme and once inside the cell it starts to form supramolecular structures (*i.e.* fibres) leading to cell death. The gelator was found to be cytotoxic for five different cancer cell lines compared to the precursor which showed low toxicity for normal cells, **Figure 2.9** .[89]

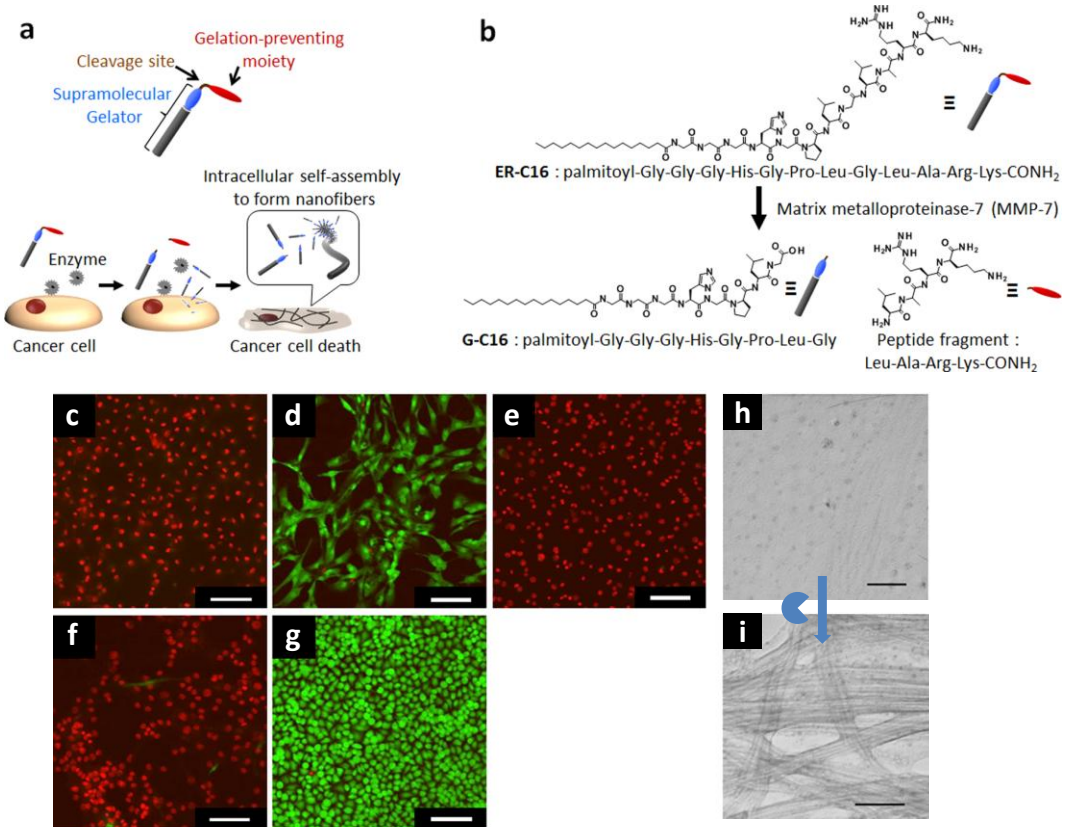


**Figure 2.9** (a) Illustration of cancer cell death induced by intracellular self-assembly of MMP-7 responsive pregelator, (b) chemical structures of N-palmitoyl-Gly-Gly-Gly-His-Gly-Pro-Leu-Gly-Leu-Ala-Arg-Lys-$CONH_2$ (ER-C16), N-palmitoyl-Gly-

Gly-Gly-His-Gly-Pro-Leu-Gly (G-C16), and Leu-Ala-Arg-Lys-$CONH_2$ (Peptide Fragment), (c-g) Live/dead assays of HeLa cells (c, e, g) and MvE cells (b, f) after incubation for 18 h with ER-C16 and its derivatives. (a, b) The pregelator (ER-C16, 0.02 wt %), (c, d) the hydrogelator (G-C16, 0.02 wt %), and (e) the peptide fragment (Leu-Ala-Arg-Lys-$CONH_2$, 0.02 wt %). Scale bars represent 100 μm. (h, i) TEM images 0.2 wt % ER-C16 solution (a) and hydrogel (b) obtained after adding MMP-7 (2 μg/mL) to the solution. Scale bars represent 50 and 100 nm, respectively. Reproduced from ref. 89.

Xu and co-workers exploited enzymatic hydrogelation to control bacterial cells. They designed a phosphatase-responsive precursor that remains in solution (*i.e.* soluble) in absence of enzyme. *E. coli* is known to overexpress phosphatase enzymes in the periplasmic space.[31] By using the overexpressed alkaline phosphatase in *E. coli* bacteria, this precursor is converted to the corresponding hydrogelator inside the bacterial cell. The subsequent intracellular hydrogelation inhibited the bacterial growth. Experiments showed that intracellular enzymatic formation of supramolecular nanostructures can be used for the development of antimicrobial biomaterials.

In order to investigate whether nanostructural morphology could impact on *E. coli* cell fate,[31] Hughes *et al* used a range of different aromatic peptide amphiphiles which are known to form different supramolecular structures. They investigated whether the enzymatic formation of nanostructures within the periplasmic space (where phosphatases reside) may provide a powerful means to achieve antimicrobial activity.[88] First, the self-assembly of a number of designed phosphatase-responsive precursors based on Fmoc protected amphiphiles; namely, FY*p*, Y*p*T, Y*p*S, Y*p*N and

Y*p*Q was studied. Then, it was investigated whether the antimicrobial activity can be differentially controlled by the introduction of these aromatic peptide amphiphiles. While there was a substantial difference in uptake of the gelators by cells, no significant difference in the antimicrobial response was observed for different treatments, all showing modest antimicrobial activity **(Figure 2.10)**.

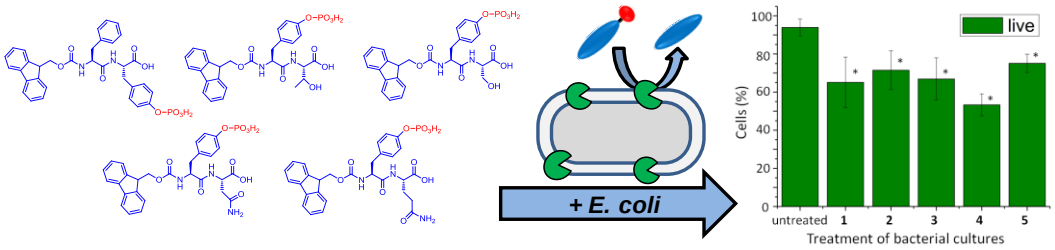


**Figure 2.10** Chemical structures of alkaline phosphatase-responsive amphiphilic precursors and the percentage of viable (live) cells in bacterial cultures after treatment with the phosphorylated precursors of self-assembling aromatic peptide amphiphiles. Reproduced from ref. 88.

Another approach to control cancer cell fate is by using enzyme-responsive supramolecular systems that operate extracellularly. The first examples were provided by the Xu group.[90, 91] They reported that enzymatic formation of nanofibers of self-assembled aromatic tripeptide amphiphiles (Nap-FFY*p*) in the pericellular space of cancer cells leads to selective inhibition of the cellular metabolic activity, which depends on the concentration of phosphatases in the biological medium **(Figure 2.11)**.

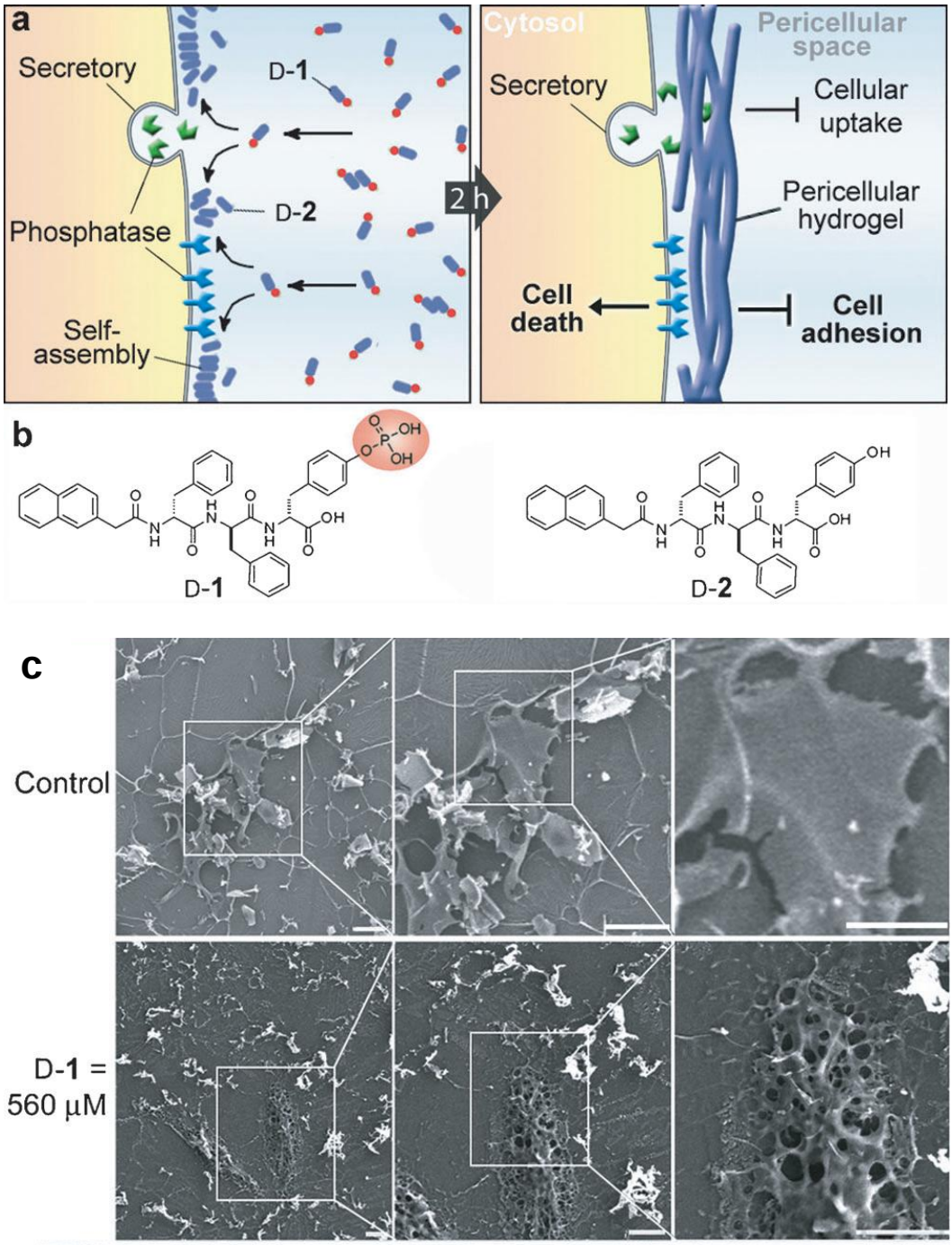


**Figure 2.11** a) Enzyme-catalysed formation of pericellular hydrogel/nanonets to induce cell death. b) Molecular structures of the precursor (D-1) and the hydrogelator (D-2). c) SEM images of freeze-dried HeLa cells treated with D-1 at 0 (control) or 560 µM for 2 h. Scale bar=10 mm. Adapted from ref. 90.

### 2.3.2 Imaging and biosensing

An approach was developed for fluorescent intracellular imaging by Xu and co-workers by using gelators with an incorporated fluorophore, which intensifies upon self-assembly.[92] After an enzymatic conversion inside the cell, the precursor turns to the corresponding hydrogelator, a more hydrophobic molecule that able to self-assemble to form nanofibres. When the precursors are outside cells or the concentration of hydrogelator is too low to form nanofibres, those precursors or hydrogelators diffuse, distribute homogeneously, fluoresce identically within each pixel and thus show little contrast. Once the concentration of hydrogelator reaches high enough to form nanofibres, these nanofibres have more fluorophores within each pixel than the rest of the solution, and the fluorophores within nanofibres are localized within the cell, therefore the nanofibres fluoresce more brightly and generate the contrast and in principle allow for the assessment of the locale of enzyme action within the cell **(Figure 2.12)**. The approach is potentially very powerful in visualising different enzyme activities (protease, phosphatase, esterase, etc.) within different cellular compartments.

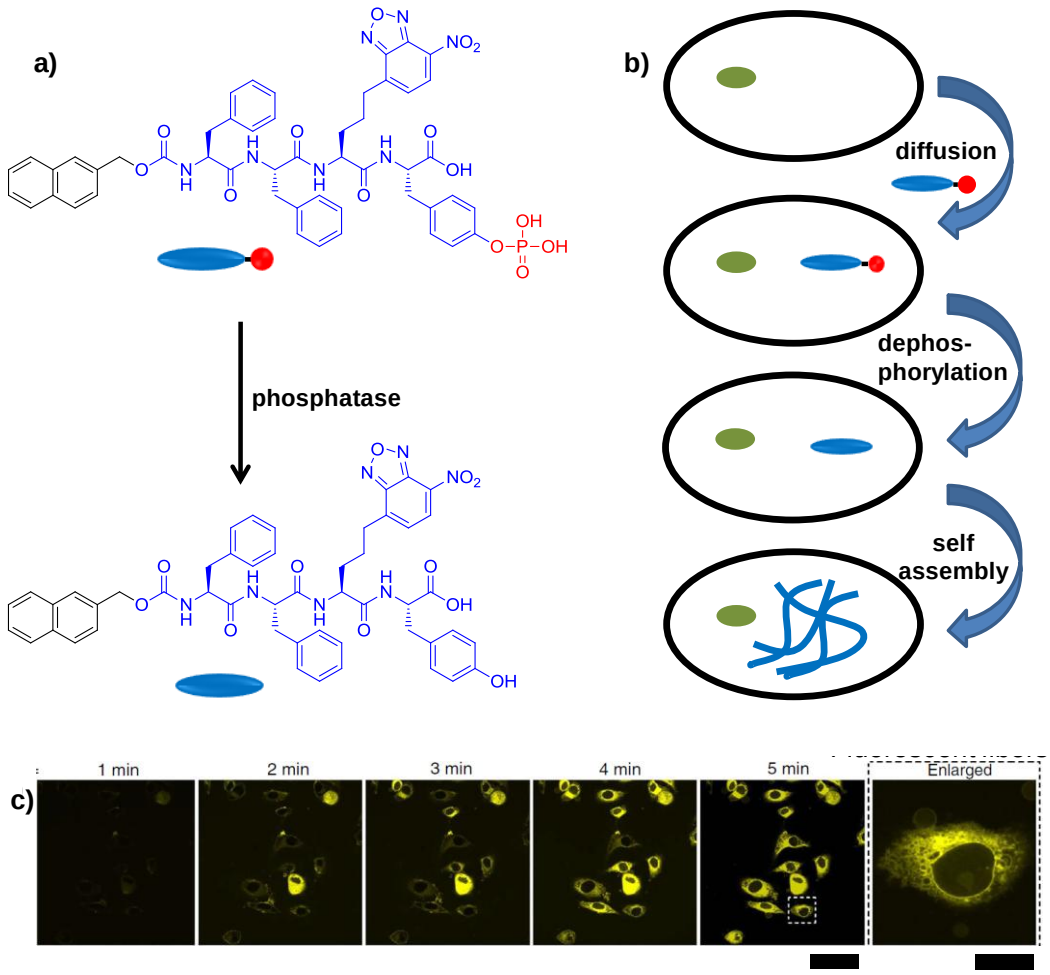


**Figure 2.12 a**) Chemical structure of phosphatase-responsive compound which forms a hydrogel under the action of enzyme, **b**) Schematic representation of the precursor diffusion into the cell and subsequent dephosphorylation and self-assembly, and **c**) Time course of fluorescent confocal microscope images inside the HeLa cells (scale bar = 50 μm for time course images and 10 μm for the enlarged image.). Reproduced from ref. 92.

Inspired by reports by the Abbott group,[93] who showed that enzyme activity could be directly visualised using liquid crystals (LCs), Lin *et al* developed an optical sensor for enzyme activity by interfacing an enzyme-responsive hydrogel with a liquid crystal (LC) display. In proof of concept work, they made use of a two stage process, involving Fmoc-TL-OMe produced by thermolysin catalysed condensation. The

OMe group can be subsequently hydrolysed by subtilisin, which results in disassembly. A dual layer design was developed, where a phospholipid-loaded upper gel layer (Fmoc-TL-OMe) was separated from the LC display by a phospholipid free lower Fmoc-TL-OMe layer. When subtilisin was applied, it was shown to digest both layers, releasing the phospholipids to give a gel-to-sol transition after several hours that liberated the phospholipid and produced a light-to-dark optical change in the LC display.[94] In future, it may be possible to use similar designs to achieve sensing of other biologically relevant events, including digestion of extracellular matrix by cell secreted enzymes.

### 2.3.3 Controlled drug release

An interesting supramolecular design approach towards a drug delivery application was reported by Gao *et al*. In this work, taxol (an anti-cancer drug) was modified to form nanofibres which were found to be able to entangle to form a supramolecular hydrogel. The drug was covalently attached to a precursor which bears a cleavable part by phosphatase.[95] Hydrolysis of phosphate group occurs upon exposure to alkaline phosphatase leading to hydrogel formation with a subsequent release of taxol derivative. This derivative showed similar activity to taxol in toxicology studies.

In another report, they exploited a tyrosinase enzyme to control a supramolecular disassembly process which was considered to be potentially useful for controlled drug release in exploiting elevated tyrosinase activity in malignant melanoma. Congo red (as a model drug) was incorporated within hydrogel matrix assembled from aromatic tetrapeptide methyl esters, Ac-YYYY-OMe and Ac-FYYY-OMe.[68] Upon treatment with tyrosinase, tyrosine residues were converted to quinone. This

oxidation process results in the loss of π-π interactions between phenol rings and ultimately a gel-to-sol transition which interns results in release of drug molecules. The incorporated model drug could be released in a controllable manner by using different enzyme concentrations.

Most recently, Kalavatovic *et al* designed a MMP-9 responsive peptide amphiphile to control the release of doxorubicin (an anticancer drug).[96] MMP-9 cleaves the peptide and triggers micelle to fibre structural transformation. Fibres formation allows for encapsulating the drug within these fibres and consequently slows its release **(Figure 2.13)**.

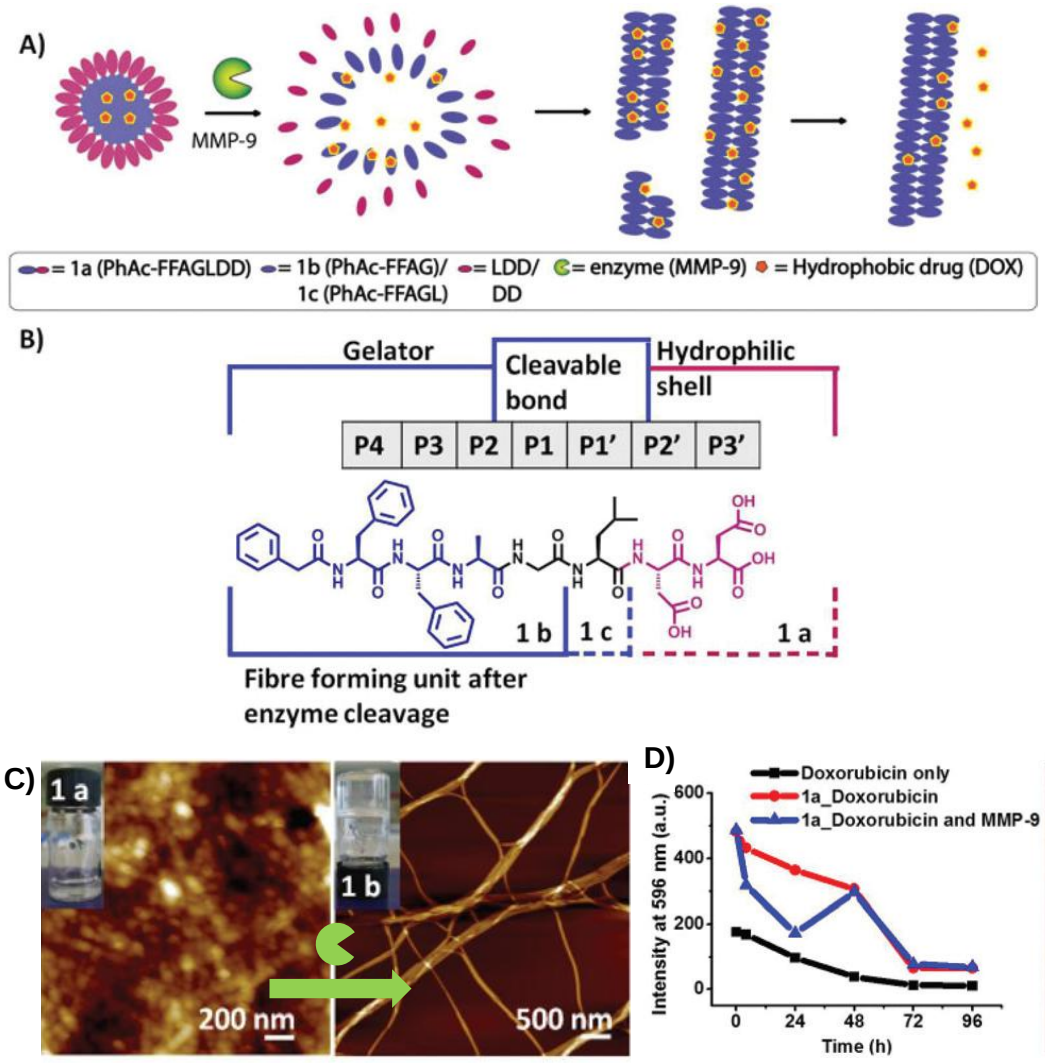

**Figure 2.13** (A) Schematic representation of micelle to fibre transition induced by MMP-9 cleavage showing disassembly of micelles and the re-assembly into fibres after the removal of the hydrophilic group enabling prolonged drug release. (B) Chemical structure of the biocatalytic gelation system and its components. (C) AFM showing the micellar aggregates (solution) for 1a and fibres (hydrogels at 20 mM) for 1b. (D) Fluorescence intensities of doxorubicin monitored over time for doxorubicin only, doxorubicin loaded into precursor peptide (1a) micelles and MMP-9 treated precursor peptide (1a) micelles loaded with doxorubicin. Reproduced from ref. 96.

### 2.3.4 Cell scaffolds and tissue engineering

A first cell culture example that makes use of biocatalytic self-assembly was published by Williams' group **(Figure 2.14)**.[97] In their work, they demonstrated the use of (immobilised) thermolysin catalysed condensation of Fmoc-L and $L_2$ to form a self-assembling tri-peptide derivative. It was demonstrated that laminin could be distributed throughout the network *via* non-covalent interactions. The stability and suitability of the material for *in vivo* use was tested utilising microinjection into a dystrophic zebrafish model organism. This organism lacks laminin as a result of a genetic mutation, instead laminin is provided by the self-assembled gel system. It could be confirmed that the biomaterial remained *in situ* at the site of injection.

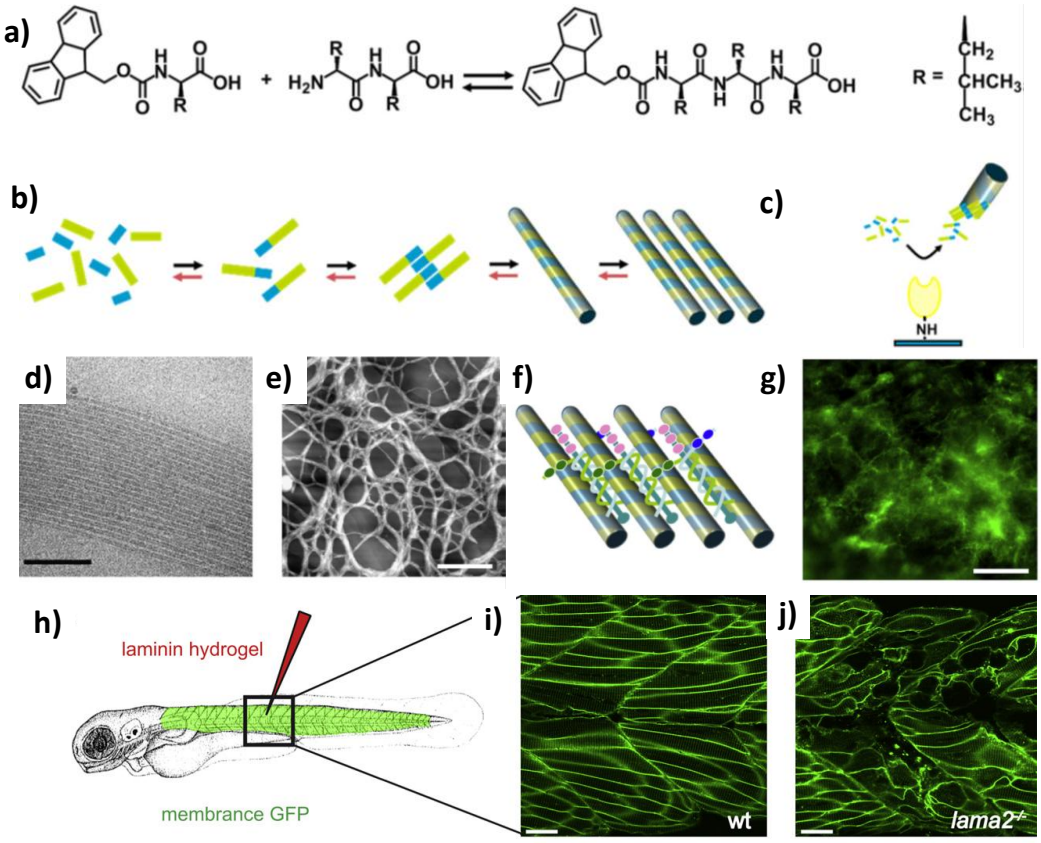


**Figure 2.14** *In vivo* performance of hydrogel produced by biocatalytic peptide self-assembly a) Fmoc-amino acid reacts with a dipeptide in the presence of the enzyme, to yield the hydrogelator Fmoc-trileucine; b) formation of self-assembling fibres *via* thermolysin catalysed condensation c) using an immobilised enzyme; d) TEM (scale bar 200 nm) and e) AFM of gel fibres (scale bar 2 mm). F) shows complexation with laminin as verified by (g) fluorescence microscopy (scale bar 2 mm). h) cartoon of the site of hydrogel injection in a 3 day old laminin deficient, zebrafish i) confocal microscope image of intact muscle in wild-type (*wt*) zebrafish (Scale bar 25 mm) (j) corresponding image of muscle from a laminin deficient (lama2$^{-/-}$), dystrophic zebrafish. (Scale bar 25 mm). Copyright (2011), with permission from Elsevier ref. 97.

## 2.4Conclusions and Outlook

There is an increasing interest to mimic biological systems in an effort to enhance the ability to have control over bottom-up fabrication process. Events in biological systems are often controlled by spatially confined molecular mechanisms such as catalysis and molecular recognition. Therefore, enzymes are identified as a useful handle to dictate such nanofabrication process towards developing complex and highly selective next generation biomaterials. Enzyme-assisted formation and de-formation of supramolecular structures have many advantages such as self-assembly under constant conditions, spatiotemporal control of nucleation and structure growth, controlling mechanical properties (*i.e.* stiffness). Moreover, systems which assemble under thermodynamic control have particular features such as defect correcting and component selecting abilities. Researchers have devoted their attention towards designing materials for particular applications in cell culture, drug delivery, imaging, biosensing and in controlling cell fate.

The dynamic processes in biological systems are usually controlled by enzymes. This has prompted research in order to understand these processes at the molecular level through enzymatic controlled self-assembly approach. Key challenges are related to (i) controlling nucleation and structure growth, (ii) accessing structures that represent non-equilibrium assemblies and (iii) producing asymmetric, dynamic and multi-component structures with desired functionalities.

It is becoming more obvious that studying systems based on enzyme-responsiveness will become of great interest not only for the formation of supramolecular structures but also to study the ability of these structures to recognize, adapt, correct, and interact in complex ways and give rise to evolving behaviours. This can be

demonstrated, for example, in the field of specific disease control where the development of molecular materials that respond to disease particular molecular event is highly desired.

## 2.5References


1. M. Zelzer, S. J. Todd, A. R. Hirst, T. O. McDonald and R. V. Ulijn, *Biomaterials Science*, 2013, **1**, 11-39.
2. O. Wichterle and D. Lim, *Nature*, 1960, **185**, 117-118.
3. F. Lim and A. M. Sun, *Science (New York, N.Y.)*, 1980, **210**, 908-910.
4. I. V. Yannas, E. Lee, D. P. Orgill, E. M. Skrabut and G. F. Murphy, *Proceedings of the National Academy of Sciences*, 1989, **86**, 933-937.
5. B. Ratner, A. S. Hoffman, F. Schoen and J. E. Lemons, *San Diego, California*, 2004, 162-164.
6. D. Seliktar, *Science*, 2012, **336**, 1124-1128.
7. G. A. Silva, C. Czeisler, K. L. Niece, E. Beniash, D. A. Harrington, J. A. Kessler and S. I. Stupp, *Science*, 2004, **303**, 1352-1355.
8. P. Y. Dankers, M. C. Harmsen, L. A. Brouwer, M. J. Van Luyn and E. Meijer, *Nature materials*, 2005, **4**, 568-574.
9. E. F. Banwell, E. S. Abelardo, D. J. Adams, M. A. Birchall, A. Corrigan, A. M. Donald, M. Kirkland, L. C. Serpell, M. F. Butler and D. N. Woolfson, *Nature materials*, 2009, **8**, 596-600.
10. F. Gelain, D. Bottai, A. Vescovi and S. Zhang, *PLoS One*, 2006, **1**, e119.
11. S. Kiyonaka, K. Sada, I. Yoshimura, S. Shinkai, N. Kato and I. Hamachi, *Nature materials*, 2003, **3**, 58-64.
12. D. E. Discher, D. J. Mooney and P. W. Zandstra, *Science*, 2009, **324**, 1673-1677.
13. M. Lutolf and J. Hubbell, *Nature biotechnology*, 2005, **23**, 47-55.
14. A. J. Engler, S. Sen, H. L. Sweeney and D. E. Discher, *Cell*, 2006, **126**, 677-689.

15. M. J. Dalby, N. Gadegaard, R. Tare, A. Andar, M. O. Riehle, P. Herzyk, C. D. Wilkinson and R. O. Oreffo, *Nature materials*, 2007, **6**, 997-1003.

16. M. Ehrbar, S. C. Rizzi, R. G. Schoenmakers, B. San Miguel, J. A. Hubbell, F. E. Weber and M. P. Lutolf, *Biomacromolecules*, 2007, **8**, 3000-3007.

17. B. D. Ratner, A. S. Hoffman, F. J. Schoen and J. E. Lemons, *Biomaterials science: an introduction to materials in medicine*, Academic press, 2004.

18. J. Kopecek, *European journal of pharmaceutical sciences: official journal of the European Federation for Pharmaceutical Sciences*, 2003, **20**, 1.

19. J. F. Mano, *Advanced Engineering Materials*, 2008, **10**, 515-527.

20. D. Schmaljohann, *Advanced drug delivery reviews*, 2006, **58**, 1655-1670.

21. S. Koutsopoulos, L. D. Unsworth, Y. Nagai and S. Zhang, *Proceedings of the National Academy of Sciences*, 2009, **106**, 4623-4628.

22. A. M. Smith, R. J. Williams, C. Tang, P. Coppo, R. F. Collins, M. L. Turner, A. Saiani and R. V. Ulijn, *Advanced Materials*, 2008, **20**, 37-41.

23. L. Chen, K. Morris, A. Laybourn, D. Elias, M. R. Hicks, A. Rodger, L. Serpell and D. J. Adams, *Langmuir*, 2009, **26**, 5232-5242.

24. M. Zhou, A. M. Smith, A. K. Das, N. W. Hodson, R. F. Collins, R. V. Ulijn and J. E. Gough, *Biomaterials*, 2009, **30**, 2523-2530.

25. Y. C. Jung, H. Muramatsu, K. Fujisawa, J. H. Kim, T. Hayashi, Y. A. Kim, M. Endo, M. Terrones and M. S. Dresselhaus, *Small*, 2011, **7**, 3292-3297.

26. C. de las Heras Alarcón, S. Pennadam and C. Alexander, *Chem. Soc. Rev.*, 2005, **34**, 276-285.

27. K. Soppimath, T. Aminabhavi, A. Dave, S. Kumbar and W. Rudzinski, *Drug development and industrial pharmacy*, 2002, **28**, 957-974.

28. M. Prabaharan and J. F. Mano, *Macromolecular bioscience*, 2006, **6**, 991-1008.

29. R. Kulkarni and S. Biswanath, *Journal of applied biomaterials & biomechanics: JABB*, 2007, **5**, 125.

30. C. Walsh, *Nature: London*, 2001, 226-231.

31. Z. Yang, G. Liang, Z. Guo and B. Xu, *Angewandte Chemie International Edition*, 2007, **46**, 8216-8219.

32. J. M. Spruell and C. J. Hawker, *Chemical Science*, 2011, **2**, 18-26.

33. J. L. West and J. A. Hubbell, *Macromolecules*, 1999, **32**, 241-244.

34. P. D. Thornton and A. Heise, *Chemical Communications*, 2011, **47**, 3108-3110.

35. C. Tang, A. M. Smith, R. F. Collins, R. V. Ulijn and A. Saiani, *Langmuir*, 2009, **25**, 9447-9453.

36. H. Hong, Y. Mai, Y. Zhou, D. Yan and Y. Chen, *Journal of Polymer Science Part A: Polymer Chemistry*, 2007, **46**, 668-681.

37. M. Reches and E. Gazit, *Science*, 2003, **300**, 625-627.

38. B. Ozbas, J. Kretsinger, K. Rajagopal, J. P. Schneider and D. J. Pochan, *Macromolecules*, 2004, **37**, 7331-7337.

39. Z. Yang, H. Gu, D. Fu, P. Gao, J. K. Lam and B. Xu, *Advanced Materials*, 2004, **16**, 1440-1444.

40. Z. Yang, G. Liang and B. Xu, *Accounts of chemical research*, 2008, **41**, 315-326.

41. J. H. Collier and P. B. Messersmith, *Bioconjugate chemistry*, 2003, **14**, 748-755.

42. S. Winkler, D. Wilson and D. Kaplan, *Biochemistry*, 2000, **39**, 12739-12746.

43. S. Toledano, R. J. Williams, V. Jayawarna and R. V. Ulijn, *Journal of the American Chemical Society*, 2006, **128**, 1070-1071.

44. B. Xu, *Langmuir*, 2009, **25**, 8375-8377.

45. Z. Yang, K. Xu, Z. Guo, Z. Guo and B. Xu, *Advanced Materials*, 2007, **19**, 3152-3156.

46. A. R. Hirst, S. Roy, M. Arora, A. K. Das, N. Hodson, P. Murray, S. Marshall, N. Javid, J. Sefcik, J. Boekhoven, J. H. van Esch, S. Santabarbara, N. T. Hunt and R. V. Ulijn, *Nature Chemistry*, 2010, **2**, 1089-1094.

47. R. J. Williams, A. M. Smith, R. Collins, N. Hodson, A. K. Das and R. V. Ulijn, *Nature Nanotechnology*, 2008, **4**, 19-24.

48. A. K. Das, A. R. Hirst and R. V. Ulijn, *Faraday discussions*, 2009, **143**, 293-303.

49. J. W. Sadownik and R. V. Ulijn, *Chemical Communications*, 2010, **46**, 3481-3483.

50. D. M. Ryan and B. L. Nilsson, *Polymer Chemistry*, 2012, **3**, 18-33.

51. D. J. Adams and P. D. Topham, *Soft Matter*, 2010, **6**, 3707-3721.

52. A. R. Hirst, I. A. Coates, T. R. Boucheteau, J. F. Miravet, B. Escuder, V. Castelletto, I. W. Hamley and D. K. Smith, *Journal of the American Chemical Society*, 2008, **130**, 9113-9121.

53. M. de Loos, B. L. Feringa and J. H. van Esch, *European journal of organic chemistry*, 2005, **2005**, 3615-3631.

54. H. Kobayashi, A. Friggeri, K. Koumoto, M. Amaike, S. Shinkai and D. N. Reinhoudt, *Organic letters*, 2002, **4**, 1423-1426.

55. D. N. Woolfson and M. G. Ryadnov, *Current opinion in chemical biology*, 2006, **10**, 559-567.

56. Y. Yanlian, K. Ulung, W. Xiumei, A. Horii, H. Yokoi and Z. Shuguang, *Nano Today*, 2009, **4**, 193-210.

57. R. V. Ulijn, *Journal of Materials Chemistry*, 2006, **16**, 2217-2225.

58. L. A. Estroff and A. D. Hamilton, *Chemical reviews*, 2004, **104**, 1201-1218.

59. M. Reches and E. Gazit, *Nature nanotechnology*, 2006, **1**, 195-200.

60. R. V. Ulijn and A. M. Smith, *Chemical Society Reviews*, 2008, **37**, 664-675.

61. D. J. Adams, M. F. Butler, W. J. Frith, M. Kirkland, L. Mullen and P. Sanderson, *Soft Matter*, 2009, **5**, 1856-1862.

62. S. Fleming and R. V. Ulijn, *Chemical Society Reviews*, 2014, **43**, 8150-8177.

63. M. Reches and E. Gazit, *Current Nanoscience*, 2006, **2**, 105-111.

64. Z. Yang and B. Xu, *Chemical Communications*, 2004, 2424-2425.

65. J. W. Sadownik, J. Leckie and R. V. Ulijn, *Chemical Communications*, 2011, **47**, 728-730.

66. H. Wang, C. Ren, Z. Song, L. Wang, X. Chen and Z. Yang, *Nanotechnology*, 2010, **21**, 225606.

67. Q. Wang, Z. Yang, Y. Gao, W. Ge, L. Wang and B. Xu, *Soft Matter*, 2008, **4**, 550-553.

68. J. Gao, W. Zheng, D. Kong and Z. Yang, *Soft Matter*, 2011, **7**, 10443-10448.

69. K. Thornton, Y. M. Abul-Haija, N. Hodson and R. V. Ulijn, *Soft Matter*, 2013, **9**, 9430-9439.

70. S. Dos Santos, A. Chandravarkar, B. Mandal, R. Mimna, K. Murat, L. Saucede, P. Tella, G. Tuchscherer and M. Mutter, *Journal of the American Chemical Society*, 2005, **127**, 11888-11889.

71. D. Koda, T. Maruyama, N. Minakuchi, K. Nakashima and M. Goto, *Chemical Communications*, 2010, **46**, 979-981.

72. Z. Yang, P.-L. Ho, G. Liang, K. H. Chow, Q. Wang, Y. Cao, Z. Guo and B. Xu, *Journal of the American Chemical Society*, 2007, **129**, 266-267.

73. H. Wang, Z. Yang and D. J. Adams, *Materials Today*, 2012, **15**, 500-507.

74. A. R. Hirst, S. Roy, M. Arora, A. K. Das, N. Hodson, P. Murray, S. Marshall, N. Javid, J. Sefcik, J. Boekhoven, J. H. van Esch, S. Santabarbara, N. T. Hunt and R. V. Ulijn, *Nature Chemistry*, 2010, **2**, 1089-1094.

75. R. J. Williams, R. J. Mart and R. V. Ulijn, *Biopolymers*, 2010, **94**, 107-117.

76. S. Roy and R. V. Ulijn, in *Enzymatic Polymerisation*, ed. A. R. A. H. A. Palmans, 2010, vol. 237, pp. 127-143.

77. K. Thornton, A. M. Smith, C. L. R. Merry and R. V. Ulijn, *Biochemical Society Transactions*, 2009, **37**, 660-664.

78. Z. Yang, G. Liang and B. Xu, *Soft Matter*, 2007, **3**, 515-520.

79. P. T. Corbett, J. Leclaire, L. Vial, K. R. West, J.-L. Wietor, J. K. M. Sanders and S. Otto, *Chemical Reviews*, 2006, **106**, 3652-3711.

80. S. J. Rowan, S. J. Cantrill, G. R. L. Cousins, J. K. M. Sanders and J. F. Stoddart, *Angewandte Chemie-International Edition*, 2002, **41**, 898-952.

81. S. K. M. Nalluri and R. V. Ulijn, *Chemical Science*, 2013, **4**, 3699-3705.

82. R. Vegners, I. Shestakova, I. Kalvinsh, R. M. Ezzell and P. A. Janmey, *Journal of Peptide Science*, 1995, **1**, 371-378.

83. Y. Zhang, H. Gu, Z. Yang and B. Xu, *Journal of the American Chemical Society*, 2003, **125**, 13680-13681.

84. C. G. Pappas, Y. M. Abul-Haija, A. Flack, P. W. J. M. Frederix and R. V. Ulijn, *Chemical Communications*, 2014, **50**, 10630-10633.

85. M. Hughes, P. W. J. M. Frederix, J. Raeburn, L. S. Birchall, J. Sadownik, F. C. Coomer, I. H. Lin, E. J. Cussen, N. T. Hunt, T. Tuttle, S. J. Webb, D. J. Adams and R. V. Ulijn, *Soft Matter*, 2012, **8**, 5595-5602.

86. M. Hughes, H. Xu, P. W. J. M. Frederix, A. M. Smith, N. T. Hunt, T. Tuttle, I. A. Kinloch and R. V. Ulijn, *Soft Matter*, 2011, **7**, 10032-10038.

87. M. Hughes, L. S. Birchall, K. Zuberi, L. A. Aitken, S. Debnath, N. Javid and R. V. Ulijn, *Soft Matter*, 2012, **8**, 11565-11574.

88. M. Hughes, S. Debnath, C. W. Knapp and R. V. Ulijn, *Biomaterials Science*, 2013, **1**, 1138-1142.

89. A. Tanaka, Y. Fukuoka, Y. Morimoto, T. Honjo, D. Koda, M. Goto and T. Maruyama, *Journal of the American Chemical Society*, 2015, **137**, 770-775.

90. Y. Kuang, J. Shi, J. Li, D. Yuan, K. A. Alberti, Q. Xu and B. Xu, *Angewandte Chemie International Edition*, 2014, **53**, 8104-8107.

91. J. Shi, X. Du, D. Yuan, J. Zhou, N. Zhou, Y. Huang and B. Xu, *Biomacromolecules*, 2014, **15**, 3559-3568.

92. Y. Gao, J. Shi, D. Yuan and B. Xu, *Nature Communications*, 2012, **3**, 1033.

93. J. M. Brake, M. K. Daschner, Y.-Y. Luk and N. L. Abbott, *Science*, 2003, **302**, 2094-2097.

94. I. H. Lin, L. S. Birchall, N. Hodson, R. V. Ulijn and S. J. Webb, *Soft Matter*, 2013, **9**, 1188-1193.

95. Y. Gao, Y. Kuang, Z.-F. Guo, Z. Guo, I. J. Krauss and B. Xu, *Journal of the American Chemical Society*, 2009, **131**, 13576-13577.

96. D. Kalafatovic, M. Nobis, N. Javid, P. W. J. M. Frederix, K. I. Anderson, B. R. Saunders and R. V. Ulijn, *Biomaterials Science*, 2015, **3**, 246-249.

97. R. J. Williams, T. E. Hall, V. Glattauer, J. White, P. J. Pasic, A. B. Sorensen, L. Waddington, K. M. McLean, P. D. Currie and P. G. Hartley, *Biomaterials*, 2011, **32**, 5304-5310.

# 3. Biocatalytically Triggered Co-Assembly of Two-Component Core/Shell Nanofibres*

## Objectives

The key research objectives of this chapter are to:

i. Develop a new approach for on-demand functionalisation of peptide-based hydrogels through biocatalytically triggered co-assembly.

ii. Investigate the possibility of tuning the physical and mechanical (*i.e.* stiffness) properties by changing the enzyme concentration.

iii. Study the compatibility of the functionalised fibres as scaffolds for cell culture.

* This work was published in part as: Y. M. Abul-Haija, S. Roy, P. W. J. M. Frederix, N. Javid, V. Jayawarna, R. V. Ulijn, *Small* 2014**, 10**, 973-979.

Declaration of contribution to published article: Any reproduced work from the aforementioned published article I was solely responsible for, including the written article itself, unless otherwise stated.

## 3.1Introduction

Supramolecular self-assembly[1] is an attractive, biologically inspired approach for the design of new materials with molecular precision.[2] There are in principle two possible routes for introducing functionality and molecular complexity in self-assembled materials.[3] One approach is to introduce functionality into building blocks, where care should be taken that these modifications do not substantially alter the self-assembly propensity. Peptide amphiphiles with aliphatic tails provide an excellent design approach for this purpose.[4] Beta sheet structures have also been appended successfully with functional short peptide sequences, as exemplified by covalent incorporation of RGD-based peptides.[5] Post-assembly functionalization provides an alternative approach where functionality can be introduced to previously formed self-assembled scaffolds. Successful examples include the use of click chemistry,[6] as well as non-covalent, co-assembly approaches using structural mimics that exploit molecular recognition[7] or hydrophobic interactions.[8] In this chapter, co-assembly of gelators and surfactants will be explored as a route to achieve functional nanofibres.

The ability to control and direct the self-assembly process provides a challenge in the production of co-assembled nanostructures from multiple building blocks. Self-assembly control usually involves the change of one or more of the environmental conditions such as pH,[9] temperature,[10] solvent polarity[11] and/or ionic strength[12] where nucleation and structure growth are difficult to control. Biocatalytic self-assembly provides an alternative approach, involving the formation of building blocks from precursors by the action of enzymes,[13] which enables directed assembly to occur under constant, physiological conditions, and offers a level of kinetic control

over the self-assembly process, which may be exploited to control the properties of the resulting material.[14]

The use of aromatic peptide amphiphiles provides an increasingly popular approach for the production of functional fibrous gels *via* (biocatalytic) self-assembly. [9, 10, 13a, 14] Previous co-assembly strategies for aromatic peptide amphiphiles include the use of a non-peptidic surfactant to coat nanoparticles of 9-fluorenylmethoxycarbonyl-phenylalanine-tyrosine (Fmoc-FY) self-assembled by enzymatic dephosphorylation[15] and formation of a core/shell structures through the self-assembly of two-component peptide mixtures.[16] We previously demonstrated that surfactant-like Fmoc-amino acids (upon enzymatic activation) can be used to functionalize the surface of carbon nanotubes and consequently enhance their dispersion.[17]

Herein, we study the co-assembly of gelator/surfactant peptide-based systems that can be triggered by biocatalytic action and offer the possibility of introducing functionality to the surface of the gelator's hydrophobic nanofibres in a one-step procedure. The investigated systems are composed of phosphatase responsive Fmoc-FY*p* pre-gelator and a surfactant-like amino acid (or peptide), Fmoc-X [X= S, T or RGD]. We previously demonstrated that Fmoc-FY*p* forms a micellar structure in aqueous environment which transforms into a nanofibrous network upon enzymatic dephosphorylation.[18] In this study, we show that combinations co-assembled to transform from micelle structures to fibrous structures which display functionality at the surface **(Scheme 3.1)**. Furthermore, by varying enzyme concentration, the gelation kinetics can be varied, resulting in varying gel stiffness and supramolecular organization of building blocks. These findings pave the way for on-demand

formation of peptide-based fibres functionalized for different biomedical applications e.g. as cell instructive scaffolds.

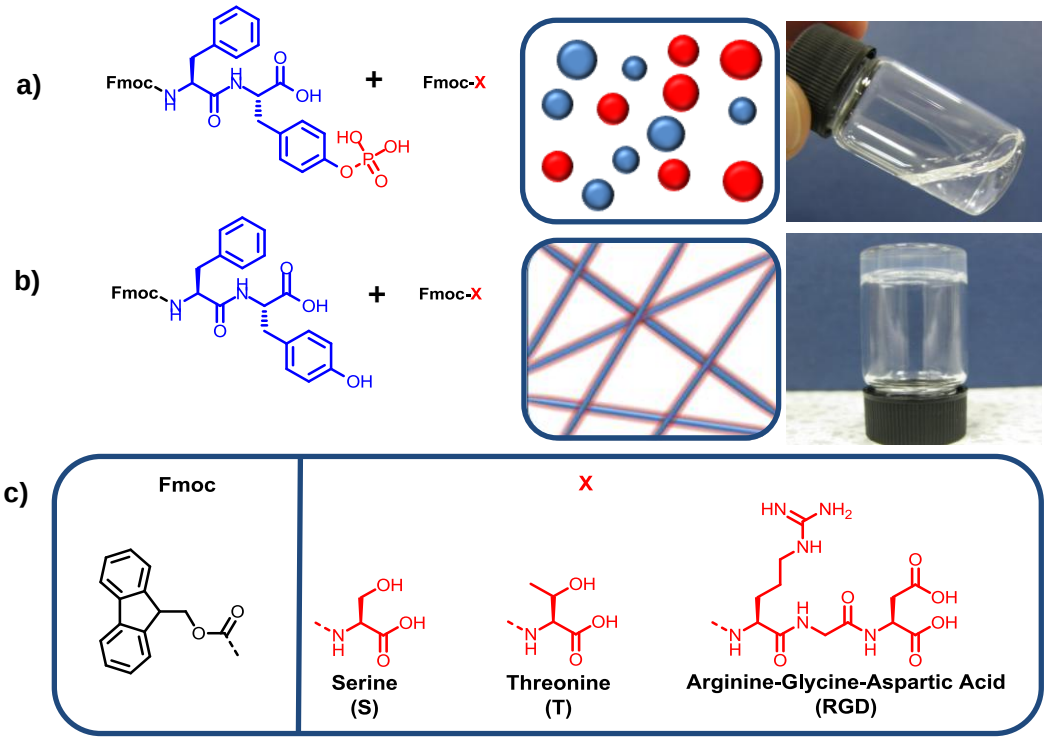


**Scheme 3.1** Illustration of surfactant-coated nanofibres formation. a) Both Fmoc-FY*p* and Fmoc-X [X=Serine (S), Threonine (T) or Arginine-Glycine-Aspartic Acid (RGD)] form spherical aggregates (blue and red spheres) in solution at physiological conditions which assemble into b) co-assembled functional nanofibrous gels when triggered by alkaline phosphatase c) chemical structures of Fmoc moiety and X peptide moieties.

## 3.2Materials and Methods

All commercial reagents were used as supplied from Sigma Aldrich, UK unless otherwise specified.

### 3.2.1 Gel preparation

Samples were prepared by mixing Fmoc-FY*p* (CS Bio Co.) and Fmoc-X [X= S (BACHEM), T (Aldrich) or RGD (Synthetech)] in 10 ml glass vials by suspending the powders to a total peptide concentration of 20 mM in pH 7.4 phosphate buffered solution. NaOH solution (0.5 M) was drop wise added to neutralize solution's acidity (pH 7.2-7.5) followed by vortex and sonication till full dissolution. Then, a predetermined volume of alkaline phosphatase (Sigma) was added. Immediately after that, solution was allowed to gel in an incubator at 37°C in 5% $CO_2$ atmosphere. All characterizations were performed after 24 hours unless otherwise mentioned.

### 3.2.2 Atomic force microscopy (AFM)

20 µl of gels prepared using the standard procedure described above (25U enzyme for all samples) were diluted to a total volume of 100 µl solution in deionized water. Then it was pipetted on a freshly cleaved mica sheet (G250-2 Mica sheets 1" x 1" x 0.006"; Agar Scientific Ltd, Essex, UK) attached to an AFM support stub and left to air-dry overnight in a dust-free environment, prior to imaging. The images were obtained by scanning the mica surface in air under ambient conditions using a Veeco diINNOVA Scanning Probe Microscope (VEECO/BRUKER, Santa Barbara, CA, USA) operated in tapping mode. The AFM scans were taken at 512 x 512 pixels resolution. Typical scanning parameters were as follows: tapping frequency 308 kHz, integral and proportional gains 0.3 and 0.5, respectively, set point 0.5–0.8 V and scanning speed 1.0 Hz. The images were analyzed using NanoScope Analysis software Version 1.40.

### 3.2.3 Transmission electron microscopy (TEM)

Carbon-coated copper grids (200 mesh) were glow discharged in air for 30 s. The support film was touched onto the gel surface for 3 s and blotted down using filter

paper. Negative stain (20 ml, 1% aqueous methylamine vanadate obtained from Nanovan; Nanoprobes) was applied and the mixture blotted again using filter paper to remove excess. The dried specimens were then imaged using a LEO 912 energy filtering transmission electron microscope operating at 120kV fitted with 14 bit/2 K Proscan CCD camera.

### 3.2.4 Fluorescence spectroscopy

1 ml samples were prepared in a 1 $cm^2$ quartz cuvette. Fluorescence emission spectra were measured on a Jasco FP-6500 spectrofluorometer at a scanning speed of 200 $nm.min^{-1}$. The emission spectra were recorded between 300 and 600 nm resulting from excitation at 295 nm, using a bandwidth of 3 nm with a medium response and a 1 nm data pitch.

### 3.2.5 Zeta potential

The zeta potential of micelles and fibers were measured by (Nano ZS, Malvern Instruments, Malvern, UK). The measurement was taken after 24 hours of sample preparation. The mobility of nanostructures was measured and was converted to zeta potential by the software.

### 3.2.6 FTIR spectroscopy

Spectra were acquired using a Bruker Vertex 70 spectrometer with a spectral resolution of 1 $cm^{-1}$. The spectra were obtained by averaging 25 scans per sample. Measurements were performed in a standard IR cuvette (Harrick Scientific), in which the sample was contained between two $CaF_2$ windows (thickness, 2 mm) separated by a 25 µm PTFE spacer. All sample manipulations were performed in a glove box to minimize interference from atmospheric water vapour. $D_2O$ (Sigma-Aldrich) was used as the solvent for all the infrared spectral measurements.

### 3.2.7 Rheology

To assess the mechanical properties of the hydrogels, dynamic frequency sweep experiments were carried out on a strain-controlled rheometer (Bohlin C-CVO) using a parallel-plate geometry (20 mm) with a 0.50 cm gap. An integrated temperature controller was used to maintain the temperature of the sample stage at 25°C. Precautions were taken to minimize solvent evaporation and to keep the sample hydrated: a solvent trap was used and the atmosphere within was kept saturated. To ensure the measurements were made in the linear viscoelastic regime, an amplitude sweep was performed and the results showed no variation in elastic modulus (G') and viscous modulus (G'') up to a strain of 1%. The dynamic modulus of the hydrogel was measured as a frequency function, where the frequency sweeps were carried out between 1 and 10 Hz. The measurements were repeated at least three times to ensure reproducibility.

### 3.2.8 High-performance liquid chromatography (HPLC)

A Dionex P680 high-performance liquid chromatography pump was used to quantify conversions of the enzymatic reaction. A 20 µl sample was injected onto a Macherey-Nagel C18 column with a length of 250 mm and an internal diameter of 4.6 mm and 5-mm fused silica particles at a flow rate of 1 $ml.min^{-1}$. The eluting solvent system had a linear gradient of 20% (v/v) acetonitrile in water for 4 min, gradually rising to 80% (v/v) acetonitrile in water at 35 min. This concentration was kept constant until 40 min when the gradient was decreased to 20% (v/v) acetonitrile in water at 42 min. Sample preparation involved mixing 30 µl of gel with acetonitrile–water (1300 µl, 50:50 mixture) containing 0.1% trifluoroacetic acid. The purity of each identified peak was determined by UV detection at 280 nm.

### 3.2.9 Biological methods

For cell culture experiments, the peptide solutions were prepared in glass vials using the procedure discussed in section 3.2.1. 300 µl of the prepared solutions was then transferred into 24 well plates (before the gel was formed) and left overnight to gel. After that, 300 µl cell suspension (1 x $10^5$) was then added on the top of the formed hydrogels. The cell media (α-MEM, from Sigma) was replaced after 24 hours and every other day, until the gel is used for further analysis.

A fluorescent live–dead staining assay (Invitrogen) was used to visualize live and dead cells present in the hydrogels. Gels were incubated at room temperature for 20 min in a solution of 4 µM ethidium homodimer-1 (EthD-1) and 2 µM calcein AM in PBS. The labelled cells were then viewed under a Nikon Eclipse E600 fluorescence microscope and images captured using Lucia software. Viable cells were stained with calcein (green), while non-viable cells were stained with EthD-1 (red).

## 3.3Results and Discussion

The self-assembled systems used in this study are based on mixing the pre-gelator, Fmoc-FY*p*, with a surfactant-like peptide derivative, Fmoc-X. Before enzyme addition, a transparent solution of the mixture was observed which transformed to gel upon enzyme addition. The time of gelation varied from 30 minutes to three hours depending on enzyme concentration and the surfactant-like peptide derivative, Fmoc-X. The morphology of pre-gelation components and self-assembled structures was initially investigated by AFM. We found that the combination of the pre-gelator Fmoc-FY*p* and one of the surfactant-like derivatives, Fmoc-X, form spherical aggregated structures in solution under physiological conditions **(see Figure 3.1/a-c)**. 24 hours after phosphatase addition, nanofibrous network formation was observed

with disappearance of the spherical aggregates of both Fmoc-X and Fmoc-FY*p*. These observations may suggest that the hydrophobic nanofibres of Fmoc-FY became coated with the surfactant-like peptide derivative forming a two-component core/shell structure as illustrated in **Figure 3.1/d-f**. The existence of these structures is further investigated by FTIR, fluorescence spectroscopy and zeta potential measurements, below.

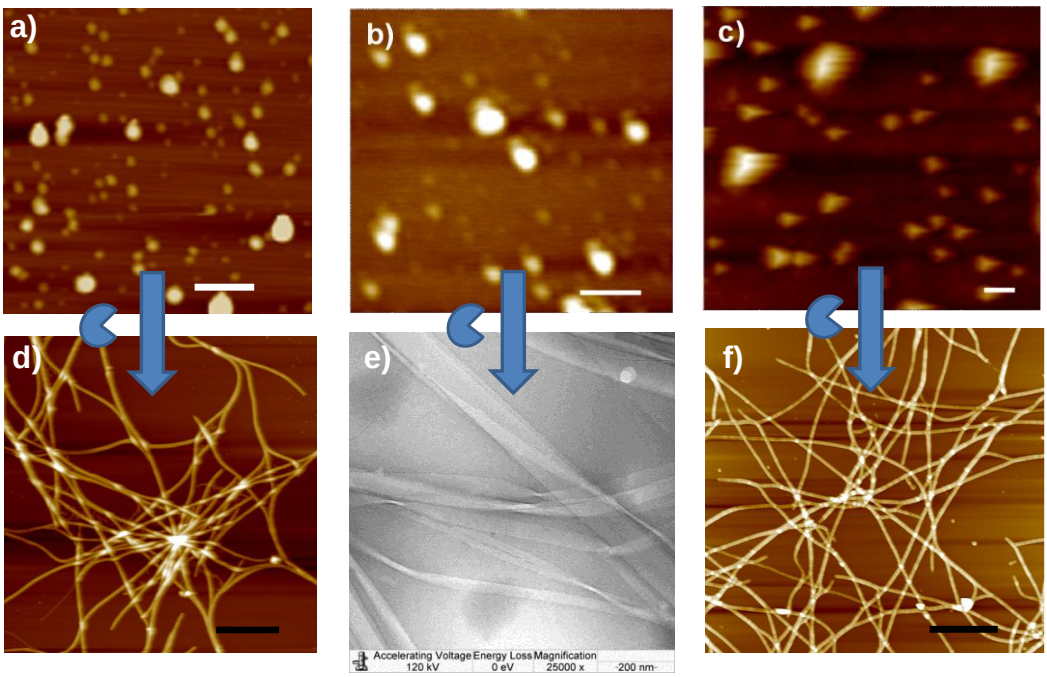


**Figure 3.1** Biocatalytic self-assembly of two-component nanofibres. Atomic force microscopy images showing the formation of spherical aggregates of the pre-gelation mixtures. a) Fmoc-FY*p*/S, b) Fmoc-FY*p*/T, c) Fmoc-FY*p*/RGD in solution. d-f) Surfactant coated nanofibres of Fmoc-FY/S, Fmoc-FY/T and Fmoc-FY/RGD in gel state, respectively. AFM image could not be produced for Fmoc-FY/T system (e) hence TEM was used instead.

All precursors' components formed a clear and transparent solution when dissolved at physiological conditions. The AFM shows spherical aggregates formation as illustrated in **Figure 3.2/a-d**.

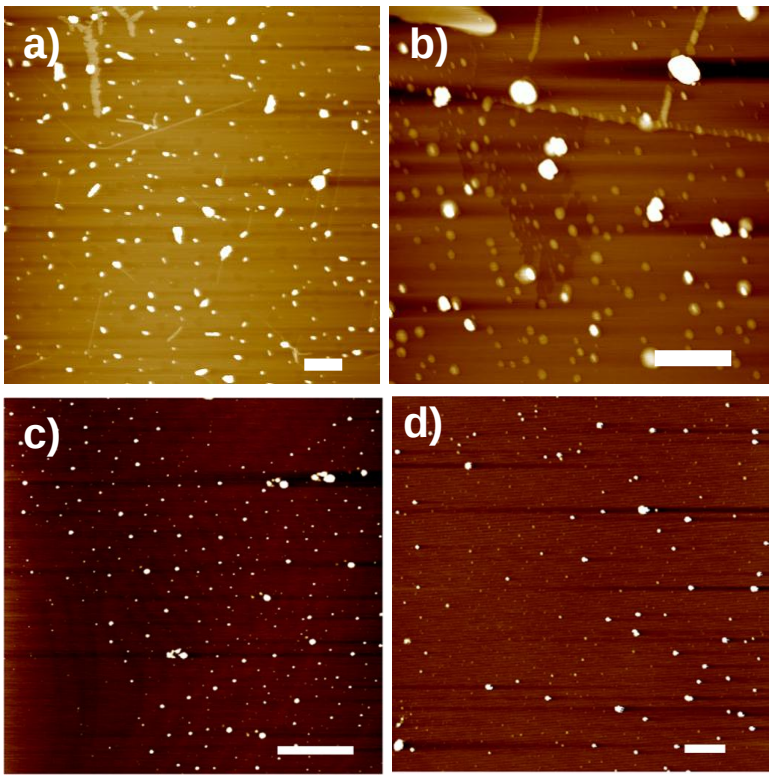


**Figure 3.2** Atomic force microscopy images showing the formation of spherical aggregates of a) Fmoc-FY*p* and b) Fmoc-S c) Fmoc-T and d) Fmoc-RGD in solution. (Scale bar = 2 μm).

The driving force behind the self-assembly of aromatic peptide amphiphiles is known to be weak hydrophobic interactions leading to π-π stacking between fluorenyl groups themselves, and hydrogen bonding between peptide components.[19] The supramolecular self-assembly was studied by monitoring the fluorescence emission of Fmoc-moieties **(see Figure 3.3)**. The spectra of Fmoc-FY/X pre-gelation mixtures comprised of two emitting species: the first at 320 nm which representing the Fmoc-peptide monomer while the second, a shoulder peak at 380 nm corresponding to the spherical aggregates.[18] After the completion of gelation, the peak attributed to the Fmoc group experienced a slight red shift, whereas the signal from the shoulder (i.e.

peak at 380 nm) reduced in intensity. The intensity reduction of the shoulder peak suggests the reorganization of fluorenyl group from spherical aggregates [18] to fibres with extended π stacked fluorenyl groups which is further represented by peak appearance at 420-460 nm.[14]

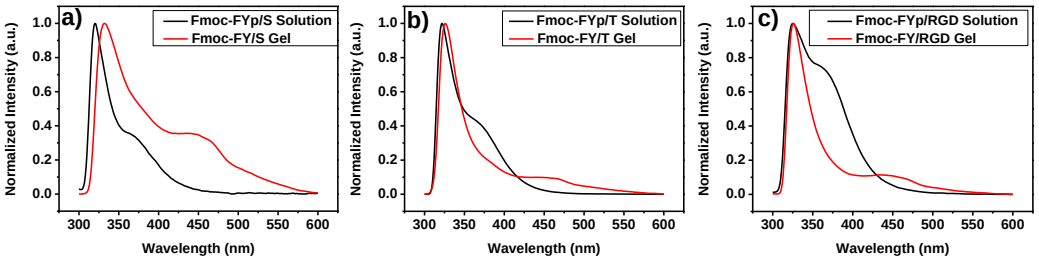


**Figure 3.3** Fluorescence emission of a) Fmoc-FY/S, b) Fmoc-FY/T and c) Fmoc-FY/RGD before and after gelation.

In order to provide evidence of structure co-assembly with the S, T or RGD functionality presented at the fibre surface, we studied the surface charge of the formed fibres. Zeta (**ζ**) potential analysis, as previously used on gel fibres by Rexeisen *et al.*,[20] was applied for micellar aggregates and fibres (**see Table 3.1**). All samples were prepared in low concentration (2.5 mM for Fmoc-FY*p* and 5 mM for Fmoc-FY/X). Concentrations were chosen where fibres form without giving rise to gelation (as confirmed by TEM in **Figure 3.4)**.

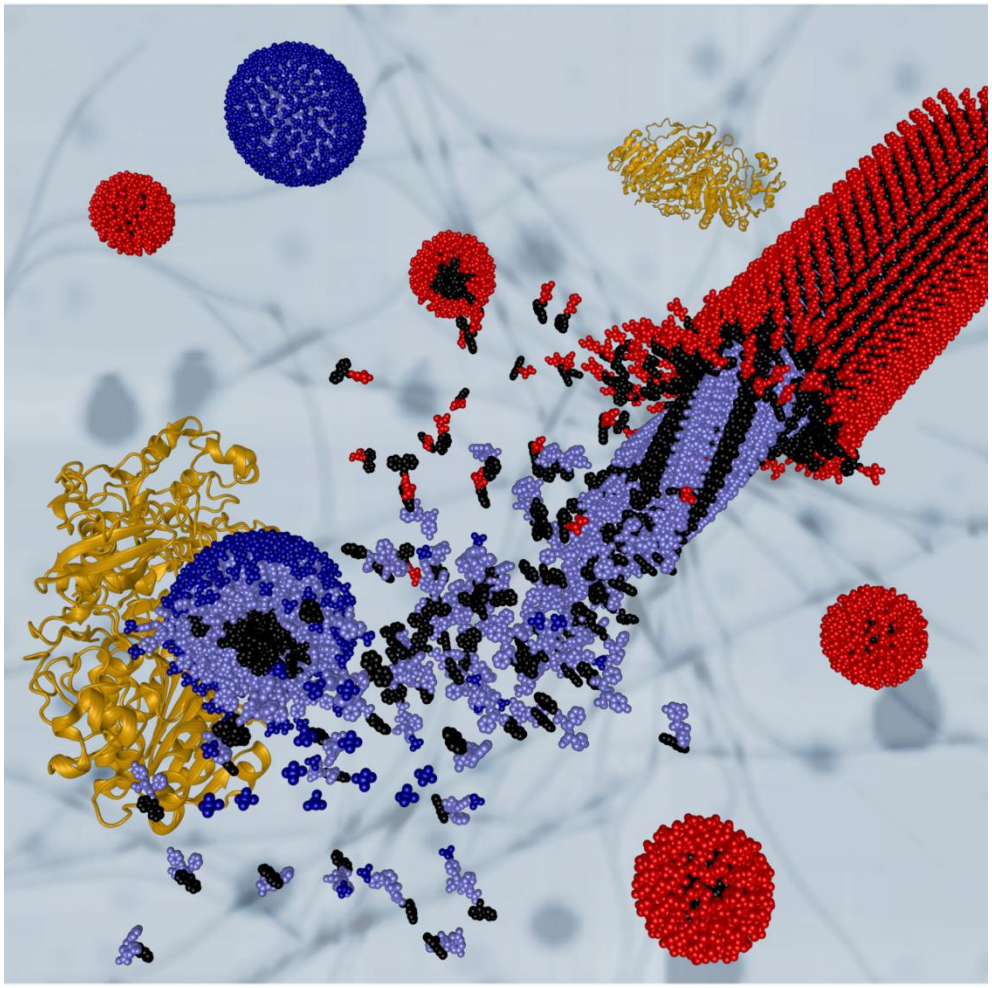

**Scheme 3.2** Schematic illustration of biocatalytic co-assembly at the molecular level. Spherical aggregates of surfactant-like amino acids (red spheres) and peptide-based hydrogelator (blue spheres) co-assemble under the action of the enzyme.

As expected, Fmoc-FY*p* and Fmoc-X had negative zeta potentials, indicating that the deprotonated carboxylic groups of X (S, T or RGD) are displayed on the surface (**see Scheme 3.2**). After fibre formation (24 hours), all two-component systems (i.e. Fmoc-FY/X) showed a negative charge which is in agreement with the presentation of surfactant-like components in a core/shell type morphology. Bare Fmoc-FY showed a smaller negative value (-0.49 mV) compared to the co-assembled systems.

This is in agreement with previous work by Tang *et al.* [9a] showing that the apparent pKa of the terminal carboxylic acid on Fmoc-FF is substantially shifted due to the favoured self-assembly of the uncharged form. For Fmoc-T and Fmoc-RGD, the negative charge was further enhanced upon co-assembly with Fmoc-FY, which may suggest that the ionization is more pronounced when presented on the fibre surface, compared to within the micellar aggregates. These observations suggest that Fmoc-X molecules are decorating the Fmoc-FY fibres displaying $COO^-$ on the surface. As a control experiment the co-assembly of Fmoc-FY and Ac-S was studied (Ac, N-acetyl). The Ac-protected amino acid is expected to have a lower propensity to bind to the Fmoc-FY fibrous core due to its less hydrophobic, non-aromatic protection group. Ac-S alone showed a slightly negative charge, which suggests a level of aggregation. The co-assembled system showed a similar charge as Fmoc-FY alone. Although Ac-S assembly at the surface cannot be excluded completely (indeed, FTIR data discussed further down suggests there may be some interaction), it is clear that, unlike for Fmoc-S, the fibre surface charge of Fmoc-FY remains largely unchanged, which is in stark contrast to the co-assembled structures for Fmoc-S, T and RGD (**Table 3.1**).

**Table 3.1** ζ-potential values for all components in micellar aggregates state and in fibres state. Each value represents the mean±SD (n=3).

| Sample | ζ-Potential mV±SD |
|---|---|
| Micellar aggregates/ precursors | |
| Fmoc-FY*p* (solution) | -9.8±1.5 |
| Fmoc-S (solution) | -6.5±1.6 |

| | |
|---|---|
| Fmoc-T (solution) | -1.2±0.3 |
| Fmoc- RGD (solution) | -13.2±1.9 |
| Ac-S (solution) | -4.03 ± 1.2 |
| Fibers | |
| Fmoc-FY (bare fibres) | -0.5±0.1 |
| Fmoc-FY/S (co-assembled) | -6.2±1.0 |
| Fmoc-FY/T (co-assembled) | -9.7±0.5 |
| Fmoc-FY/RGD (co-assembled) | -37.6±3.0 |
| Fmoc-FY/Ac-S (co-assembled) | -0.7±0.2 |

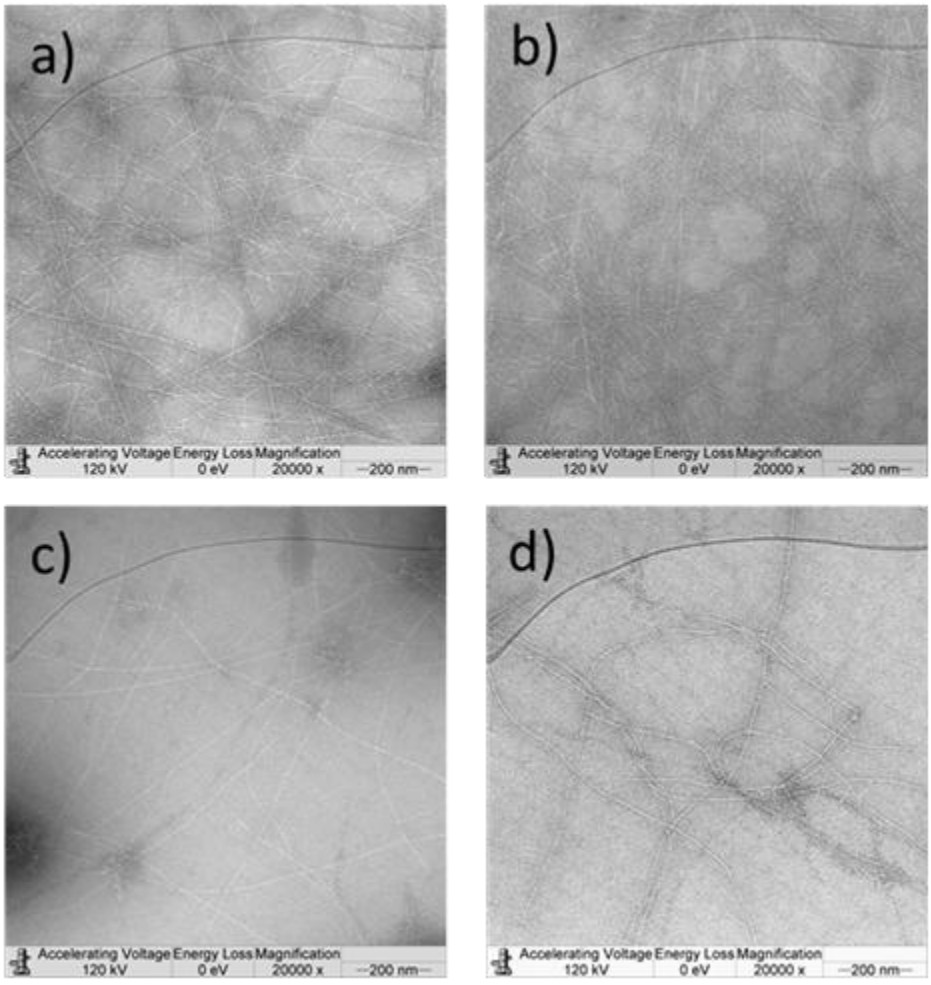

**Figure 3.4** TEM images of a) 2.5 mM Fmoc-FY, b) 5 mM Fmoc-FY/S, c) 5 mM Fmoc-FY/T and d) Fmoc-FY/RGD.

The co-assembly mode and β-sheet formation was further supported by FTIR spectroscopy in $D_2O$ of pre-gelator/surfactant mixture before and after gelation **(see Figure 3.5/a-c)**. The FTIR spectrum of Fmoc-FY gels shows typical amide I peaks at 1630 $cm^{-1}$ and 1681 $cm^{-1}$ which are associated with the presence of Fmoc-peptide amide and carbamate groups in a β-sheet conformation.[21] Spectra of pre-gelator solutions are not showing these peaks, implying a lack of secondary structure formation for these pre-gelators. For all samples, the detection of a broad vibrational absorption around 1595 $cm^{-1}$ resulting from the asymmetric stretching of the C-terminal $COO^-$ group,[22] indicates that a proportion of $COO^-$ groups are deprotonated. In RGD-containing samples, there is a contribution to this peak at around 1585 $cm^{-1}$ from $COO^-$ group in the Asp side chain. Moreover, in all RGD-containing samples, there is a fixed contribution at 1673 $cm^{-1}$, which can be attributed to asymmetric vibrational absorption of $CN_3H_5^+$ in Arg side chains.[23]

The fact that the amide I peaks remain unaffected upon the introduction of Fmoc-S, shows that the presence of Fmoc-S does not significantly disrupt the β-sheet structure. However, for Fmoc-T and Fmoc-RGD it was noted that the 1681 $cm^{-1}$ carbamate peak increases in intensity with respect to the 1630 $cm^{-1}$ amide peak. This observation suggests the partial incorporation of the surfactant-like Fmoc-T, presumably through its carbamate group, into the hydrogen bonding pattern of the Fmoc-FY structure. Additionally, Fmoc-S, -T and -RGD show faint, broad absorptions around 1678 $cm^{-1}$ in the solution phase. After gelation, these shift to 1666 $cm^{-1}$, with the band being most intense in Fmoc-RGD, followed by Fmoc-T,

but not positively discernible in Fmoc-S. Moreover, there is a peak present at 1611 $cm^{-1}$ in the Fmoc-FY/X gels with similar behaviour (i.e. more intense in RGD > T > S). Although the physical origin of these peaks is yet unclear, we have tentatively assigned these to partial inclusion of the Fmoc-T and -RGD into the fibrous core. From IR data shown here and in comparison with a previous closely related non-enzymatic co-assembly system (Fmoc-FF/RGD)[24], we conclude that Fmoc-FY/T and Fmoc-FY/RGD gels are consistent with a more disruptive type of packing (i.e. Fmoc-T and Fmoc-RGD partly intercalate the Fmoc-FY β-sheet structure), while Fmoc-S shows orthogonal (non-intrusive) packing. In our previous work, non-enzymatically prepared Fmoc-FF/RGD, we proposed that the two peptide sequences of FF and RGD could be self-assembled through intermolecular hydrogen bonds forming anti-parallel β-sheet structures where it was proposed that the Fmoc-groups on both peptides interacted with one another and formed π–π stacks to interlock the β-sheets.[24] The main bands of the Fmoc-FY/Ac-S co-assembly exhibit a similar absorption profile to the non-disrupted Fmoc-FY and Fmoc-FY/S stacks, but weak additional bands at 1611 and 1666 $cm^{-1}$ as discussed above, indicating a level of binding of Ac-S and partial inclusion into the fibrous stack **(Figure 3.5/d)**. Finally, we note that that Fmoc-FY/T and Fmoc-FY/RGD did not form gel in $D_2O$.

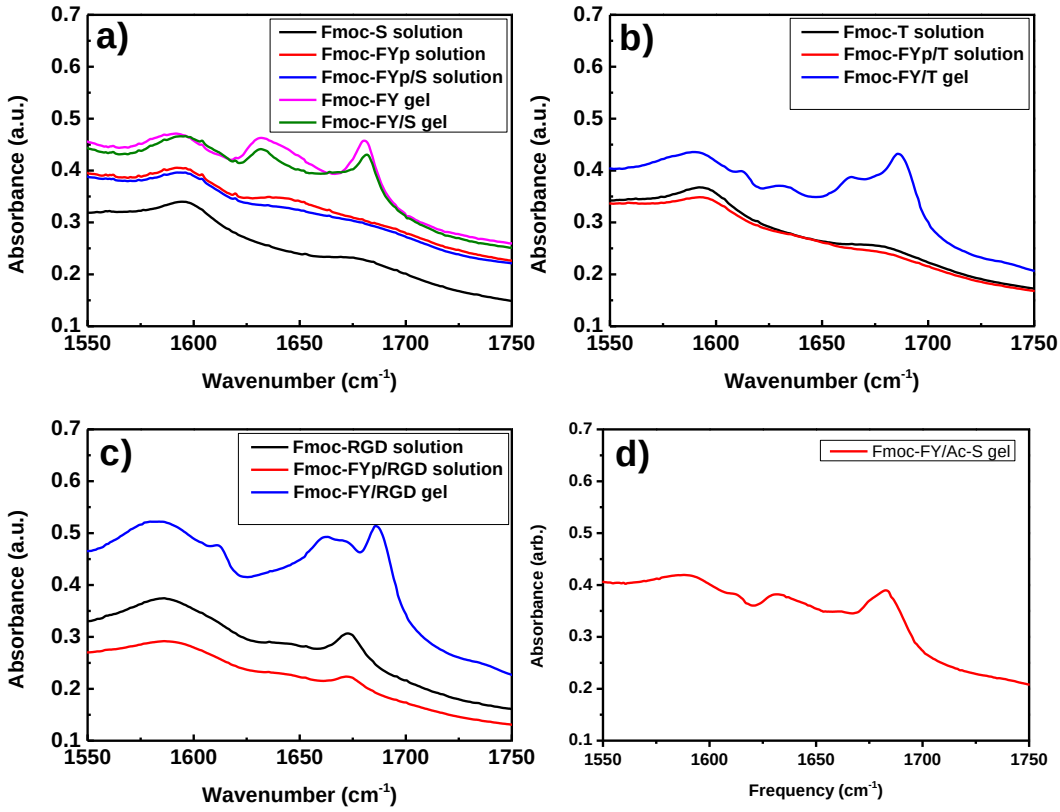


**Figure 3.5** a-c**)** FTIR absorbance spectra of pre-gelators (Fmoc-FY*p*, Fmoc-X and a mixture of both) and gelators (gels of Fmoc-FY and Fmoc-FY/X). d) FTIR absorbance spectrum of Fmoc-FY/Ac-S gel.

In order to study the effect of enzymatic reaction rate on supramolecular structure[25], gels were prepared with different enzyme concentrations **(see Figure 3.6)**. Enzyme concentrations are reported in units where one enzyme unit corresponds to the amount of enzyme that hydrolyses 1 μmol of 4-nitrophenyl phosphate per min at pH 9.8 and 37°C. Enzyme concentrations were chosen as the lowest concentration which led to gelation for each system (5U for Fmoc-FY/S; 10U for Fmoc-FY/T; 15U for Fmoc-FY/RGD) followed by two higher concentrations (25U and 50U). The pre-gelation solution was composed of a total concentration of 20 mM of 1:1 molar ratio for Fmoc-FY*p*/S and Fmoc-FY*p*/T. 20 mM Fmoc-FY*p*/RGD of the same molar ratio

(1:1) did not form gels at the same conditions for other gels and was therefore decreased to a 3:1 ratio, which led to gel formation. The conversion of Fmoc-FY*p* pre-gelator to the Fmoc-FY gel was monitored by HPLC using different enzyme concentrations in the presence of Fmoc-X during 24 hours. Different enzyme concentrations led to control the rate of conversion as illustrated in **Figure 3.8**. As expected, there was a clear trend, with high enzyme concentrations giving rise to faster conversions.

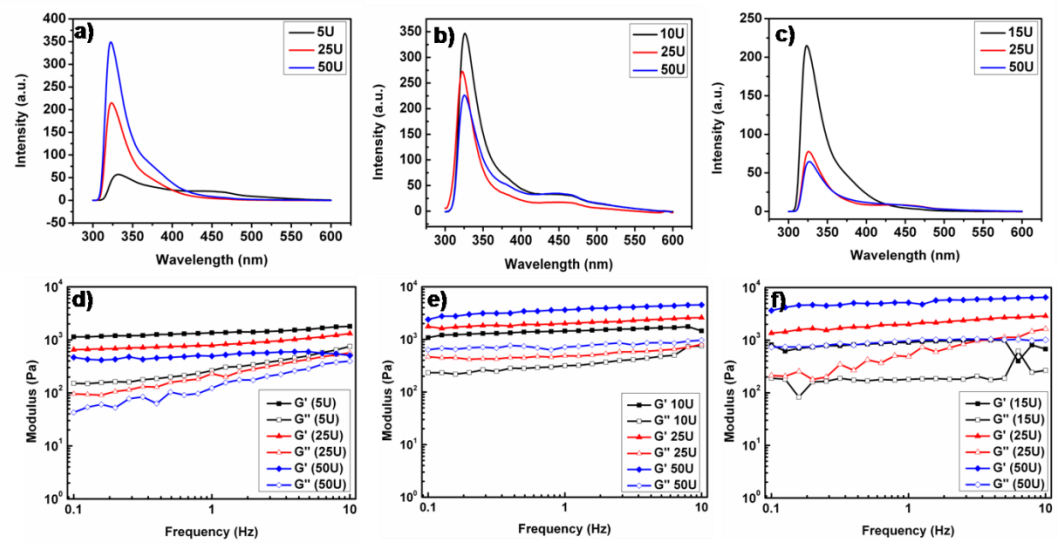


**Figure 3.6 a-c)** Fluorescence spectra showing the effect of varying enzyme concentration on the order of the fibrous nanostructure for Fmoc-FY/S, Fmoc-FY/T and Fmoc-FY/RGD respectively. **d-f)** Rheology data illustrating the effect of enzyme concentration on gel stiffness for Fmoc-FY/S, Fmoc-FY/T and Fmoc-FY/RGD respectively.

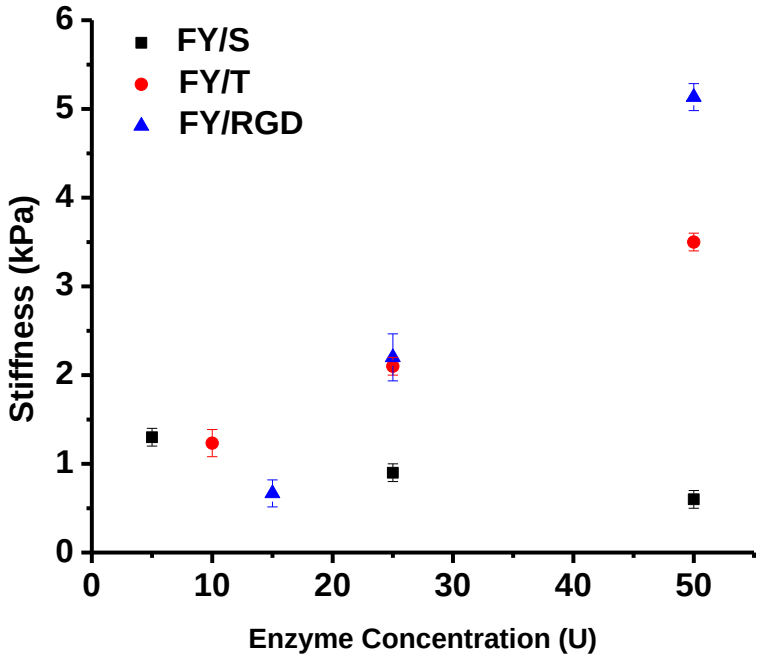


**Figure 3.7** Summary of rheology data illustrating the effect of enzyme concentration on the stiffness of different hydrogel combinations.

The enzyme kinetics dictate the gelation properties, with faster conversion rates giving rise to stiffer gels. Similar behaviour was previously observed for enzymatic dephosphorylation of Fmoc-Y [24] and a beta peptide based system.[26] In addition, Ozbas *et al.*[27] observed that in a ionic strength triggered gelation system higher salt concentrations gave rise to faster gelation and higher gel stiffness. The reason for this correlation between gel strength and self-assembly rate is complex, with possible factors recently reviewed by Adams and co-workers.[28] In general, it is believed to be linked to the formation of kinetic aggregates that are less organized compared to thermodynamic assembly products, giving rise to more extensive crosslinking at fibre defect sites. However, in biocatalytic systems there are further contributions from enzyme structuring (templating) and localized catalytic action, giving rise to a

positive correlation between gel strength and fluorescence quenching, implying increased stiffness linked to increased supramolecular order, as previously demonstrated for a related system.[14] A similar trend is observed in **Figure 3.6/a-f** and **Figure 3.7** for Fmoc-FY/T and Fmoc-FY/RGD systems with higher enzyme concentration leading to faster dephosphorylation kinetics resulting in more ordered structures and stiffer gels. Remarkably, the opposite effect, both for fluorescence and gel stiffness, was observed for the Fmoc-FY/S system (**Figure 3.6/a,d).** In addition to reduced stiffness at higher enzyme concentrations, less ordered fluorenyl groups were obtained as evident from the reduced peak at 420-460 nm and decreased quenching. This observation is perhaps more in line with expectation, in that slow kinetics give rise to higher order and fewer defects, as previously observed for a non-enzymatic catalytic self-assembly process.[29] The reason behind the different behaviour for Fmoc-FY/S system is not known yet and warrants further investigation.

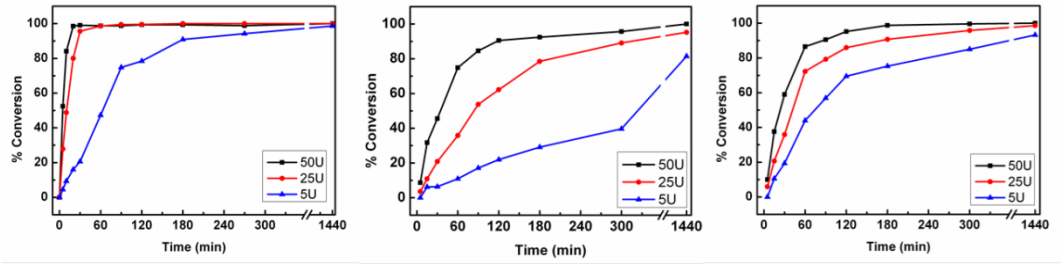


**Figure 3.8.** HPLC monitoring of Fmoc-FY*p* to Fmoc-FY conversion in the presence of **a)** Fmoc-S, **b)** Fmoc-T and **c)** Fmoc-RGD using different alkaline phosphatase concentration.

Having established our system, the suitability of the formed functionalised nanofibres for 2D cell culture was evaluated using human dermal fibroblasts cell line.

The cells were cultured for 24 hours on gels of either bare fibres (Fmoc-FY*p*) or functionalised fibres (Fmoc-FY/X). Live/dead staining was used to evaluate the mortality of cells in culture. **Figure 3.9** clearly shows that cells cultured on bare fibres Fmoc-FY*p* were dead after 24 hours (red staining for dead cells). However, most cells cultured on functionalised fibres (Fmoc-FY/X) were alive (green staining for alive cells). When the culture time was extended (*i.e.* after 48 hours), most of the cells on both bare and functionalised cells were dead. This might be attributed tentatively to intracellular self-assembly (**see also section 2.3.1**) or the high concentration of alkaline phosphatase used to trigger the self-assembly process. This is in line with previous results by Kate Thornton when similar systems (Fmoc-*p*Y and Fmoc-FY*p*) failed to culture embryonic stem cells.[31]

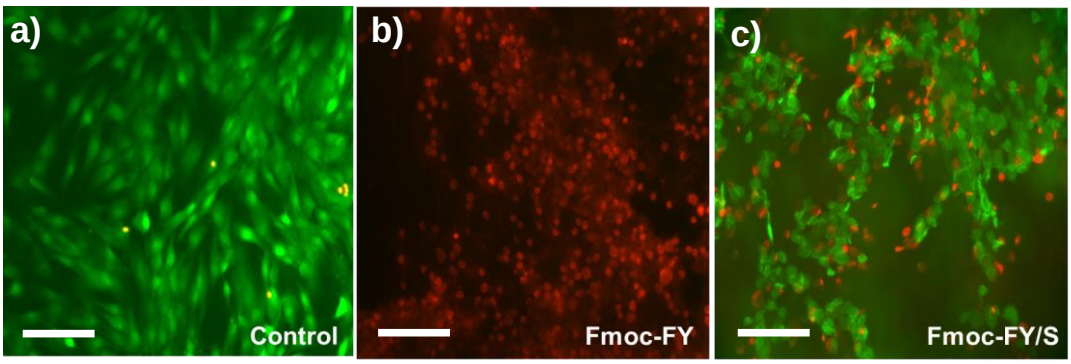


**Figure 3.9** Live/dead staining for human dermal fibroblasts cultured two-dimensionally for 24 hours on a) glass coverslip (control), b) bare fibres (Fmoc-FY) and c) functionalised fibres (Fmoc-FY/S). Scale bare = 50 µm.

## 3.4Conclusion

We have demonstrated that the combination of short peptide-based gelators and surfactants can co-assemble when triggered biocatalytically and under physiological conditions. The systems showed on-demand transformation from micellar structure into co-assembled nanofibres that, depending on the surfactant molecular architecture, display the surfactant head group functionality at the surface of the fibre. Different enzyme concentrations showed a significant effect on mechanical properties (i.e. gel stiffness), self-assembly time, and molecular arrangements. Controlling hydrogel chemical composition, as well as stiffness [30] is known to be of importance in cell culture applications.

While the data presented here clearly suggest that two component structures can co-assemble into fibrous architectures that present varying surface functionality, the co-assembly clearly depends on the chemical nature of the building blocks. A core-shell co-assembly is one possible mode of supramolecular organization, which we believe to be the case for Fmoc-FY/S. Other examples (Fmoc-FY/T and Fmoc-FY/RGD) represent a more complex co-organization, with evidence of intercalation of the surfactants into the self-assembling fibre stacks. In all these three cases, co-assembly gives rise to substantially enhanced negative surface charged as demonstrated by zeta-potential measurements. Preliminary cell culture results of human dermal fibroblasts shows that functionalised nanofibres were more suitable than bare fibres after 24 hours. However, cells cultured for 48 hours were mostly dead on both scaffolds of bare and functionalised fibres. The reason behind this observation was tentatively attributed to the intracellular self-assembly and the possible cytotoxicity of the hydrogelators. Future work will focus on the use of a wider range of gelators to elucidate the design rules of these systems. Certainly, presentation of bioactive

groups and subsequent demonstration of their activity will be required to assess the utility of this co-assembly approach in biomedical and nanotechnological applications.

## 3.5References


1. a) J.-M. Lehn, *Science*, 2002, **295**, 2400-2403; b) G. M. Whitesides, B. Grzybowski, *Science*, 2002, **295**, 2418-2421.

2. a) S. Zhang, *Nature Matererials*, 2004, **3**, 7-8; b) S. Mann, *Angewandte Chemie International Edition*, 2008, **47**, 5306-5320.

3. D. N. Woolfson and Z. N. Mahmoud, *Chemical Society Review*, 2010, **39**, 3464-3479.

4. J. D. Hartgerink, E. Beniash and S. I. Stupp, *Science*, 2001, **294**, 1684-1688.

5. a) A. Horii, X. M. Wang, F. Gelain and S. G. Zhang, *PLoS One*, 2007, **2**, e190, DOI: 10.1371/journal.pone.0000190; b) Y. Kumada and S. G. Zhang, *PLoS One*, 2010, **5**, e10305, DOI: 10.1371/journal.pone.0010305.

6. C. A. DeForest, B. D. Polizzotti and K. S. Anseth, *Nature Matererials*, 2009, **8**, 659-664.

7. A. Y. Wang, X. Mo, C. S. Chen and S. M. Yu, *Journal of the American Chemical Society*, 2005, **127**, 4130-4131.

8. A. Miyachi, T. Takahashi, S. Matsumura and H. Mihara, *Chemistry–A European Journal*, 2010, **16**, 6644-6650.

9. (a) C. Tang, A. M. Smith, R. F. Collins, R. V. Ulijn, A. Saiani, *Langmuir* 2009, **25**, 9447-9453; (b) D. J. Adams, L.M. Mullen, M. Berta, L. Chen and W. J. Frith. *Soft Matter*, 2010, **6**, 1971-1980.

10. H. Hong, Y. Mai, Y. Zhou, D. Yan, Y. Chen, *Journal of Polymer Science, Part A: Polymer Chemestry*, 2007, **46**, 668-681.

11. M. Reches, E. Gazit, *Science*, 2003, **300**, 625-627.

12. B. Ozbas, J. Kretsinger, K. Rajagopal, J. P. Schneider, D. J. Pochan, *Macromolecules*, 2004, **37**, 7331-7337.

13. a) Z. Yang, H. Gu, D. Fu, P. Gao, J. K. Lam, B. Xu, *Advanced Materials*, 2004, **16**, 1440-1444; b) Z. Yang, G. Liang, B. Xu, *Accounts of Chemical Research*, 2008, **41**, 315-326; c) J. H. Collier, P. B. Messersmith, *Bioconjugate Chemistry*, 2003, **14**, 748-755; d) S. Winkler, D. Wilson, D. Kaplan, *Biochemistry*, 2000, **39**, 12739-12746; e) S. Toledano, R. J. Williams, V. Jayawarna, R. V. Ulijn, *Journal of the American Chemical Society*, 2006, **128**, 1070-1071; f) M. Zelzer, S. J. Todd, A. R. Hirst, T. O. McDonald, R. V. Ulijn, *Biomaterials Science*, 2013, **1**, 11-39; g) Y. Gao, J. Shi, D. Yuan, B. Xu, *Nature Communications*, 2012, **3**, 1033.

14. A. R. Hirst, S. Roy, M. Arora, A. K. Das, N. Hodson, P. Murray, S. Marshall, N. Javid, J. Sefcik, J. Boekhoven, J. H. van Esch, S. Santabarbara, N. T. Hunt, R. V. Ulijn, *Nature Chemistry*, 2010, **2**, 1089-1094.

15. W. Wang, Z. Yang, S. Patanavanich, B. Xu, Y. Chau, *Soft Matter*, 2008, **4**, 1617-1620.

16. W. Wang, Y. Chau, *Chemical Communications*, 2011, **47**, 10224-10226.

17. B. G. Cousins, A. K. Das, R. Sharma, Y. Li, J. P. McNamara, I. H. Hillier, I. A. Kinloch, R. V. Ulijn, *Small*, 2009, **5**, 587-590.

18. J. W. Sadownik, J. Leckie, R. V. Ulijn, *Chemical Communications*, 2011, **47**, 728-730.

19. a) A. M. Smith, R. J. Williams, C. Tang, P. Coppo, R. F. Collins, M. L. Turner, A. Saiani, R. V. Ulijn, *Advanced Materials*, 2008, **20**, 37-41; b) L. Chen, K. Morris, A. Laybourn, D. Elias, M. R. Hicks, A. Rodger, L. Serpell, D. J. Adams, *Langmuir*, 2009, **26**, 5232-5242. c) D. M. Ryan, B. L. Nilsson, *Polymer Chemistry*, 2012, **3**, 18-33; d) D. J. Adams, P. D. Topham, *Soft Matter*, 2010, **6**, 3707-3721.

20. E. L. Rexeisen, W. Fan, T. O. Pangburn, R. R. Taribagil, F. S. Bates, T. P. Lodge, M. Tsapatsis and E. Kokkoli, *Langmuir*, 2010, **26**, 1953-1959.

21. S. Fleming, P. W. J. M. Frederix, I. Ramos Sasselli, N. T. Hunt, R. V. Ulijn, and T. Tuttle, *Langmuir*, 2013, **29** , 9510-9515.

22. P. Hellwig, U. Pfitzner, J. Behr, B. Rost, R. P. Pesavento, W. v. Donk, R. B. Gennis, H. Michel, B. Ludwig, W. Mäntele, *Biochemistry*, 2002, **41**, 9116-9125.

23. A. Barth, *Progress in Biophysics and Molecular Biology*, 2000, **74**, 141-173.

24. M. Zhou, A.M. Smith, A.K. Das, N.W. Hodson, R.F. Collins, R.V. Ulijn, J.E. Gough, *Biomaterials*, 2009, **30**, 2523-2530.

25. K. Thornton, A. M. Smith, C. L. R. Merry, R. V. Ulijn, *Biochemical Society Transactions*, 2009, **37**, 660-664.

26. Z. Yang, G. Liang, M. Ma, Y. Gao, B. Xu, *Small*, 2007, **3**, 558-562.

27. B. Ozbas, J. Kretsinger, Karthikan Rajagopal, J.P. Schneider, D.J. Pochan, *Macromolecules*, 2004, **37**, 7331-7337.

28. J. Raeburn, A.Z. Cardoso, D.J. Adams, *Chemical Society Review*, 2013, **42**, 5143-5156.

29. J. Boekhoven, J.M. Poolman, C. Maity, F. Li, L.Van der Mee, C.B. Minkenberg, E. Mendes, J.H. van Esch, R. Eelkema, *Nature Chemistry*, 2013, **5**, 433-437.

30. A. J. Engler, S. Sen, H. L. Sweeney, D. E. Discher, *Cell*, 2006, **126**, 677-689.

31. Kate Thornton **2010**, *Enzyme Triggered Self-Assembled Peptide Derivative Hydrogels for Embryonic Stem Cell Culture*, PhD Thesis, University of Strathclyde.

# 4. Using Two-Component Co-Assembly to Assess the Effect of Chemical Functionality on Adipose Stem Cell Differentiation

## Objectives

The key research objectives of this chapter are to:

i. Develop various peptide-based nanofibres functionalised with simple sugar or amino acid derivatives using two-component co-assembly.

ii. Investigate the possibility of tuning the physical and mechanical (*i.e.* stiffness) properties by changing components concentration.

iii. Study the effect of chemical functionality on adipose stem cell culture and differentiation.

## 4.1Introduction

Human adipose stem cells (ASC) are considered to be an important cell source for tissue engineering and regenerative medicine due to a number of advantages, such as ease of access and availability in large quantities.[1-5] In general, human cells are anchorage-dependent cells as they need a supportive surface to bind to and to be metabolically active. The extracellular matrix (ECM), the complex yet dynamic environment surrounding cells, provides this type of support, where cell-matrix interactions start signalling cascades involved in key cell functions (e.g. regeneration).[6-8] It is known that cell behaviour depends on three main ECM properties, namely (i) its biochemistry presented by the chemical functionality exposed to the cells, (ii) its (nanoscale) topography and (iii) its mechanical properties (*i.e.* stiffness).[9-11] By gaining control over one or more of the above mentioned properties, cell behaviour can be directed and controlled. The complexity of natural ECM and cell-matrix interactions makes design of materials for regenerative medicine applications challenging because of the variety of factors that influence cell fate.[12]

One approach to study the ECM microenvironment is by using two-dimensional (2D) materials. These materials have been successfully used to study the embryonic stem cells differentiation to hepatocytes based on ECM protein arrangement[13] and epithelial cells based on charge, hydrophilicity and branching.[14] Human mesenchymal stem cells (hMSCs) attachment and growth,[15] neural stem cell differentiation have also been studied.[16]

Another approach is through incorporating functionality using three-dimensional (3D) materials. In general, 2D cell cultures do not perfectly mimic *in vivo* cell

growth which limits the ability to study cell-cell, cell-material interactions and therapeutics delivery to cells (especially in case of cancer cells that grow three dimensionally). Therefore, 3D materials potentially open up the way to mimic *in vivo* cell culture more reliably. Benoit and co-workers reported the first example on the effect of remarkably simple functional groups on the differentiation of MSCs when encapsulated three dimensionally in polymeric (PEG-based) hydrogels. The encapsulated cells could be induced to differentiate to osteoblasts or adipocytes by having control over the chemical functionality (*i.e.* in the presence of phosphate or t-butyl functionality respectively).[17] Despite significant efforts to mimic and understand the cell-ECM interactions and the effect on cell behaviour, the fundamental understanding is still limited. Therefore, there is a need for further simple molecular systems to study the (bio)chemical functionality effects in a 3D context.

Supramolecular self-assembly approach has been utilised to make biomaterials in this context.[18] Peptides and their derivatives are of particular interest for a number of reasons mentioned in s**ection 2.2.1**. Functional cues have been introduced using different routes.[19] One route is by designing building blocks that able to self-assemble and have functionality (bioactive sequence) expressed at their surface. The Stupp research group successfully developed biomaterials based on peptide-amphiphiles for this purpose[20] typically formed by a long aliphatic tail, allowing hydrophilic and bioactive cues to be presented on the fibres surface. Zhang's group designed self-assembled scaffolds based on RADA functionality.[32] An alternative route to incorporation of functional groups is through post-assembly where

functionality can be added to a previously formed scaffold through non-covalent and hydrophobic interactions,[21] which will be utilised in this work.

In a previous study, our group reported on the co-assembly of Fmoc-FF and Fmoc-RGD (FF/RGD). It has been suggested that the bioactive peptide (RGD) is presented on the surface of the formed fibres which led to successful *in vitro* 3D culture of dermal fibroblasts.[22] The effect of chemical functionality, such as $NH_2$, COOH and OH, through introducing Fmoc protected amino acids (K, E or S, respectively) on the response of different cell types (chondrocytes, 3T3 and human dermal fibroblasts) was also studied.[23] Fmoc-FF/S hydrogel was the most compatible with all the three tested cell types although at that stage it was not yet clear how the functional groups were incorporated.[25] As shown in **Chapter 3**, we have successfully demonstrated on-demand formation of functionalised nanofibres by combining the advantages of biocatalytic self-assembly and surfactant/gelator co-assembly.[24] We concluded that although the supramolecular organization depends on the building blocks chemistry, the surfactant head group functionality found to be displayed at the surface of the fibres.

We are interested in the development of functional three-dimensional hydrogels using simple amino acids and simple sugars amphiphiles. So, building on our previous knowledge, in the current work, we aim to study the effect of chemical functionality on the ASCs differentiation using peptide-based and sugar-based simple building blocks. First, we studied the co-assembly of Fmoc-FF hydrogelator with functional surfactant-like (i) amino acid amphiphiles: [Fmoc-S, (displaying OH functionality) and Fmoc-Cysteic Acid (CA) (displaying $SO_3H$)] and (ii) sugar amphiphiles [Fmoc-Glucosamine-6-phosphate (GluP) (displaying $OPO_3H_2$) and

Fmoc-Glucosamine-6-Sulfate (GluS) (displaying $OSO_3H$)] **(Figure 4.1)**. The formed co-assembled structures were first characterized by fluorescence spectroscopy, FTIR, rheology and transmission electron microscopy. Then, in collaboration with the 3B's research group, University of Minho, Portugal, the effect of different chemical functionality on ASCs differentiation has been studied.

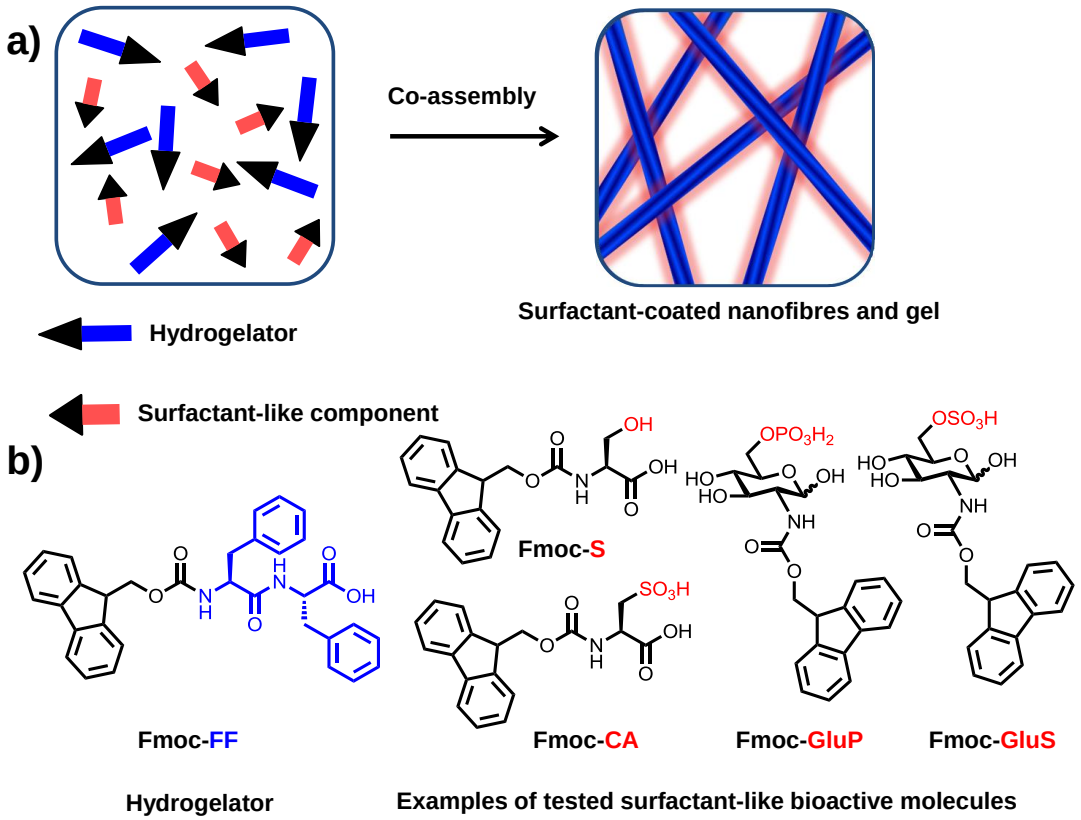


**Figure 4.1** a) Illustration of two-component co-assembly to form functionalised nanofibres. b) Chemical structures of components under investigation.

## 4.2Materials and Methods

Fmoc-FF was purchased from BiogelX, UK. Fmoc-S and Fmoc-Cysteic Acid were purchased from Bachem, UK. Fmoc-Glucosamine-6-Phosphate and Fmoc-Glucosamine-6-Sulfate were kindly supplied by the 3B's research group, University of Minho/Portugal. Cell culture inserts for 12-well plates with 1.0 µm pore size were

purchased from Greiner bio-one, UK. All other reagents were purchased from Sigma-Aldrich, UK and used as supplied.

### 4.2.1 Gel preparation

Samples were prepared by mixing Fmoc-FF and Fmoc-X [X= S, CA, GluS or GluP] in 14 ml glass vials by suspending the powders in water to obtain the required final concentration. NaOH solution (0.5 M) was added drop wise accompanied with vortex and sonication till full dissolution and a clear solution was formed (pH ~10). 0.5 M HCl was then added to adjust the pH value of the mixture (pH 7.5-8.0). Solutions were filtered through 0.8 µm filters, sterilised under UV light for one hour and left to stand in fridge for at least 24 hours before making the gels or making any characterization. Before gel making, mixtures solutions were kept for 30 minutes in a cell incubator (in addition to cell media), until the solution reach 37 °C. 300 µl of each solution were transferred to cell culture inserts in 12-well plates. A volume of 1400 µl of culture medium (αMEM) was added to each well (outside the insert) and incubated for 90 min at 37 °C in a humidified atmosphere with 5% $CO_2$ to allow gelation. Following gelation, the medium surrounding the inserts was replaced and 300 µl of medium gently added to the surface of the gels. Following overnight culture the pH of the gel stabilized at around pH 7.5 (±0.5). Medium was removed from hydrogels that were used for spectroscopic, microscopic and mechanical characterization.

### 4.2.2 Transmission electron microscopy (TEM)

Images were taken for the pre-gelation mixtures prepared according to the procedure mentioned above. For instrument details refer to section 3.2.3 above.

### 4.2.3 Fluorescence spectroscopy

1 ml samples were prepared in a 1 $cm^2$ quartz cuvette. Fluorescence emission spectra were measured on a Jasco FP-6500 spectrofluorometer at a scanning speed of 500 $nm.min^{-1}$. The emission spectra were recorded between 300 and 600 nm resulting from excitation at 280 nm, using a bandwidth of 3 nm with a medium response and a 1 nm data pitch.

### 4.2.4 Circular Dichroism

Samples were pipetted into a 0.1 mm cell and spectra were measured on a Jasco J600 spectropolarimeter with 1 s integrations, a step size of 1 nm and a single acquisition with a slit width of 1 nm.

### 4.2.5 FTIR spectroscopy

FTIR samples were prepared according the procedure mentioned above but in $D_2O$ instead of water and measured for the pre-gelation mixtures (Refer to section 3.2.7 for instrument details).

### 4.2.6 Rheology

(Refer to section 3.2.8).

### 4.2.7 Zeta Potential

(Refer to section 3.2.5).

### 4.2.8 Biological methods

Gels were prepared according to the method described in section 4.2.1. After overnight incubation of the prepared hydrogels, the cell media on the surface and around the insert was removed. The media in the well were replaced with fresh media. The media on the surface of the gel was refilled with 100 µl cell suspension (l x $10^5$ cells) along with 200 µl of new media. Upon addition of fresh media, this was mixed with the cell suspension using the pipette to even out the cell distribution on

the surface. For longer term use, the old media was removed after every 24 hours (in the first 2 days) and subsequently after every 48 hours.

After seeding cells on the gel substrate, the cells were rinsed three times in PBS (Invitrogen Gibco) and fixed in solution containing 10% Formalin (Sigma) for 30 min at 4 ºC. Upon fixing the cells, they were washed three times with PBS before the cells were permeabilized using 0.2% Triton x-100 (Sigma) in PBS for 5 minutes at 4 ºC. After being washed with the buffer, the cells were incubated in a fresh blocking solution prepared with 3% Bovine Serum Albumin (BSA) (Sigma) in PBS for 30 min at room temperature. The samples were then incubated with TRITC-conjugated Phalloidin (1:200 dilution in PBS, 50 µg/ml) for 30 minutes at 4 ºC, which was followed by rinsing and staining with DAPI (1:1000 dilution in PBS) for 30 minutes at 4 ºC. The samples were then mounted onto glass slides with Prolong Gold anti-fade reagent (obtained from Molecular Probes Invitrogen, UK) and imaged with the Nikon Eclipse E600 fluorescence microscope.

## 4.3Results and Discussion

FTIR spectroscopy was previously performed to assess the mode of co-assembly and formation of β-sheet-like structures in the Fmoc-FF core.[24, 25] FTIR was measured for the pre-gelation components (individual components and co-assembled solutions), **see Figure 4.2.** Absorptions at 1625 and 1687 $cm^{-1}$ are consistent with Fmoc-peptide amide and carbamate groups arranged in a β-sheet conformation.[26] Spectra of the surfactant-like (Fmoc-X) solutions are not showing these peaks, implying a lack of formation of an organized H-bonded network of the carbonyl carbamates. The fact that the amide I peaks remain present upon the introduction of Fmoc-X (*i.e.* in the Fmoc-FF/X co-assembly), shows that the presence of Fmoc-X does not significantly

disrupt the β-sheet structure. However, the decrease in intensity in these peaks might suggest that a low propensity of intercalation have occurred. The broad peak around 1590 $cm^{-1}$ ($COO^-$ stretch) indicates that at least part of the present C-termini is deprotonated for Fmoc-FF, Fmoc-S and Fmoc-CA containing pre-gelation mixtures. The absence of 1590 $cm^{-1}$ peak in Fmoc-GluS and Fmoc-GluP is due to the absence of $COO^-$ group in their structures.

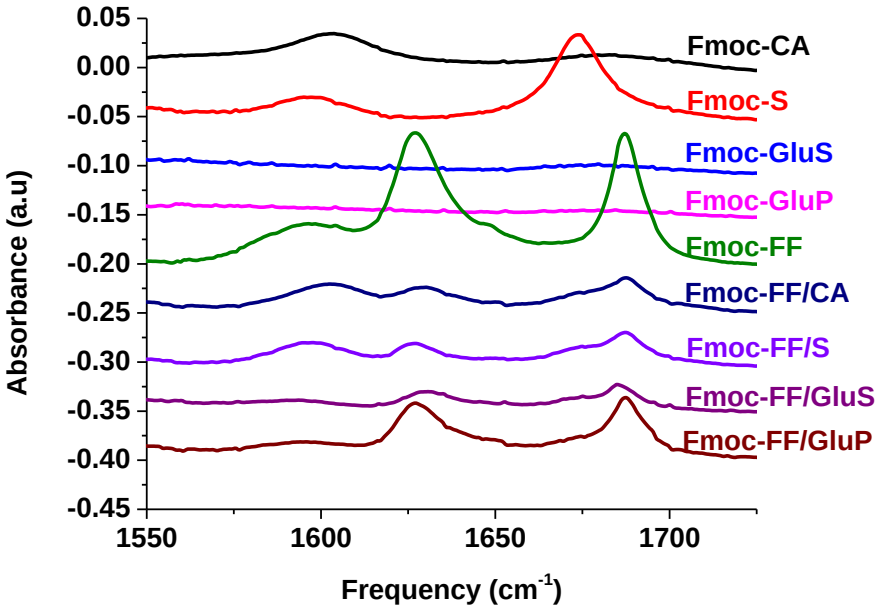


**Figure 4.2** FTIR absorbance spectra of precursors [Fmoc-FF, Fmoc-X (X=CA, S, GluS or GluP)] and the co-assembled mixtures of both.

The supramolecular organization was studied by monitoring the fluorescence emission of Fmoc-moieties **(see Figure 4.3)**. As expected, Fmoc-FF spectrum showed two emission peaks, one at ~320 nm reflecting the monomeric fluorenyl group and another at 420-440 nm reflecting excimeric fluorenyl emission owing to the π-stacking interactions between the fluorenyl groups.[27] The spectra of Fmoc-X before co-assembly comprised of two emitting species: the monomeric peak at 320

nm peak and a shoulder peak at 380 nm corresponding to presumed fluorenyl groups arrangements to spherical (micellar) aggregates.[24, 28] The shoulder peak is more pronounced for (Fmoc-S>Fmoc-CA>Fmoc-GluS and Fmoc-GluP). After co-assembly, the signal from the shoulder (*i.e.* peak at 380 nm) reduced in intensity. The spectrum of the Fmoc-FF/X systems closely resemble that of Fmoc-FF, with the 380 nm peak reduction suggesting that the Fmoc-FF structure is not disrupted by the presence of Fmoc-X but also the disappearance of the spherical aggregates. These findings further support the FTIR results.

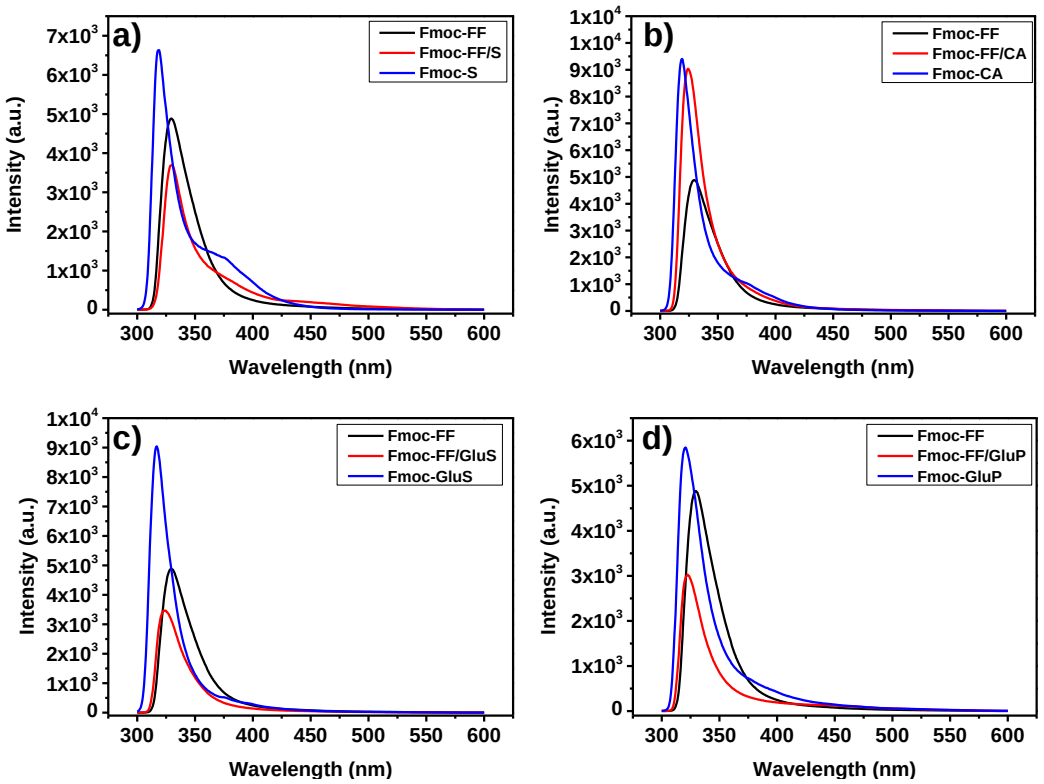


**Figure 4.3** Fluorescence emission of Fmoc-FF and Fmoc-X (before co-assembly) and Fmoc-FF/X (after co-assembly).

Circular Dichroism (CD) was used to study the effect of co-assembly on supramolecular chirality associated with the formation of Fmoc-FF nanofibres

**(Figure 4.4)**. Fmoc-FF demonstrated a positive peak at ~305 nm in addition to another peak at around ~278 nm which believed to be due to phenylalanine contribution.[29, 30] All individual surfactant-like moieties (Fmoc-X) showed no CD signals which suggest that no chirality is associated with the aggregation of the individual components.[25] When co-assembled with Fmoc-FF (Fmoc-FF/X systems), the first peak at ~305 nm did not display any change in location for all co-assembled systems and was further enhanced (most obvious for Fmoc-FF/S system) which suggests that the presence of Fmoc-X is stabilising the formed fibres through enhancing their supramolecular chiral organisation.[25]

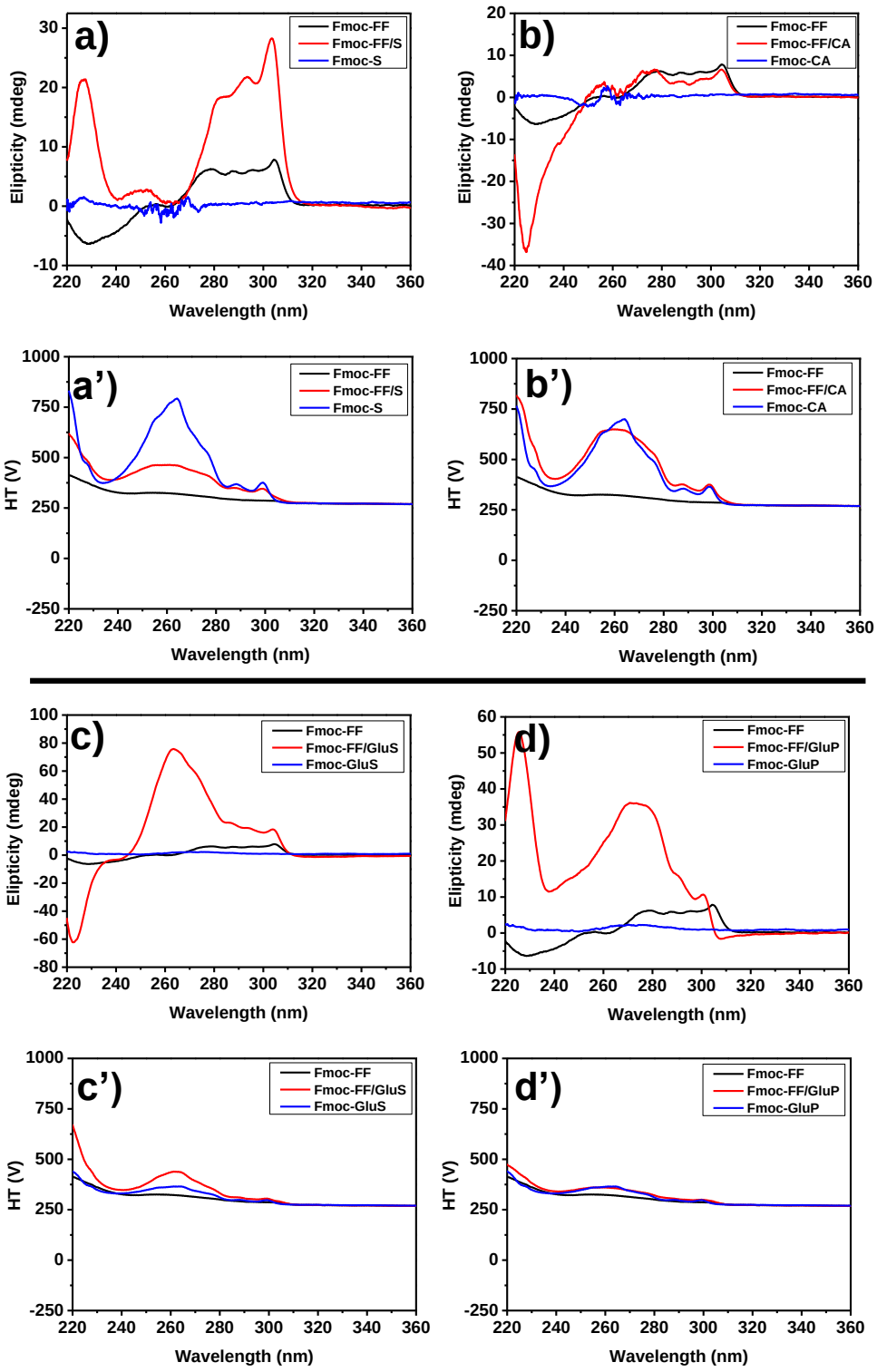


**Figure 4.4** CD spectra (a-d) and the corresponding high tension (HT) spectra (a'-d'). Each graph shows the CD spectra form the gelator (Fmoc-FF), the surfactant (Fmoc-X) and the surfactant coated nanofibres (Fmoc-FF/X).

The organisation of the individual components in isolation is evident from TEM images **(Figure 4.5)**, with Fmoc-FF forming nanofibres and Fmoc-X forming spherical aggregates. Upon co-assembly only fibres were observed with the disappearance of any aggregates. This suggests that Fmoc-FF fibres have become incorporated with the surfactant-like components as we previously suggested for similar systems.[24, 25] To further verify the mode of assembly, Zeta potential measurements were performed (see below).

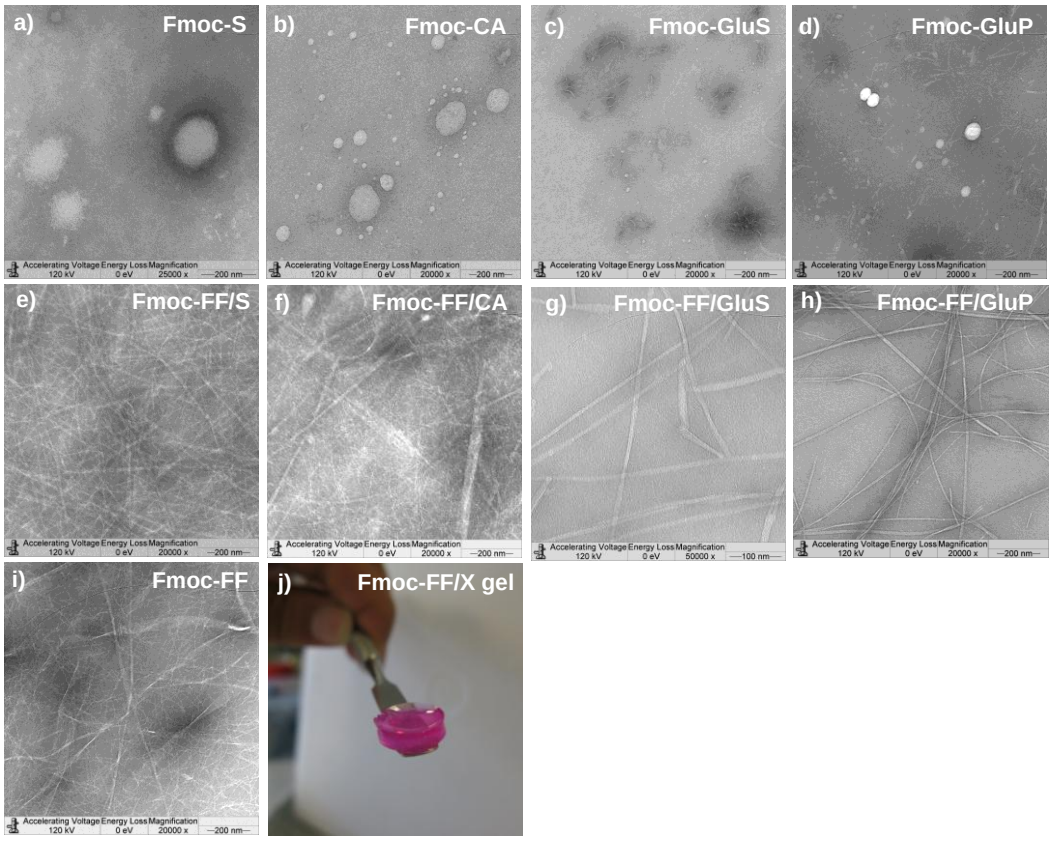


**Figure 4.5** TEM images shows the formation of **a-d)** spherical aggregates of the precursors (Fmoc-S, Fmoc-CA, Fmoc-GluS, Fmoc-GluP) and **e-i)** nanofibres formation of (Fmoc-FF, Fmoc-FF/S, Fmoc-CA, Fmoc-GluS and Fmoc-GluP) **j)** optical image of Fmoc-FF/GluS gels as an example (all Fmoc-FF/X optically look the same).

In order to provide evidence of structure co-assembly with S, CA, GluS or GluP functionality presented at the nanofibres surface, we studied the surface charge of the formed nanofibres. Zeta (ζ) potential analysis, as previously used on gel fibres, was applied for micellar aggregates and nanofibres (see **Table** 4.**1**). All samples were prepared in low concentration (2.5 mM for Fmoc-FF and 2.5 mM for Fmoc-FF/X). Concentrations were chosen where fibres form without giving rise to gelation. As expected, Fmoc-X had negative zeta potential, indicating that the deprotonated carboxylic groups of (S and CA), sulphate group of (GluS) or phosphate group of (GluP) are displayed on the surface. After fibre formation (24 h), all two-component systems (*i.e.*, Fmoc-FF/X) showed a negative charge which is in agreement with the presentation of surfactant-like components on the surface of self-assemble nanofibres. Bare Fmoc-FF showed a smaller negative value (-0.04 mV) compared to the co-assembled systems. This is in agreement with findings in **Chapter 3** and previous work by our group showing that the apparent pKa of the terminal carboxylic acid on Fmoc-FF is substantially shifted due to the favoured self-assembly of the uncharged form.[33] For Fmoc-S, the negative charge was further enhanced upon co-assembly with Fmoc-FF, which may suggest that the ionization is more pronounced when presented on the fibre surface, compared to within the micellar aggregates. Co-assembled Fmoc-CA and Fmoc-GluS showed lower surface charge compared to precursors (spherical aggregated) which might suggest that some functionality head groups are embedded within the co-assembled structure towards the core (Fmoc-FF). The surface charge of Fmoc-GluP was not significantly changed after co-assembly. These observations suggest that Fmoc-X molecules are decorating the Fmoc-FF fibres displaying functionality on the surface.

**Table 4.1** ζ-potential values for all components in micellar aggregates state and in fibres state. Each value represents the mean±SD (n=3).

| Sample | ζ-Potential mV±SD |
|---|---|
| Micellar aggregates/ precursors | |
| Fmoc-S (solution) | -6.5±1.6 |
| Fmoc-CA (solution) | -109.0±1.0 |
| Fmoc-GluS (solution) | -112.0±23.7 |
| Fmoc-GluP (Solution) | -74.4±5.3 |
| Fibres | |
| Fmoc-FF (bare fibres) | -0.0±0.0 |
| Fmoc-FF/S (co-assembled) | -46.4±1.6 |
| Fmoc-FF/CA (co-assembled) | -70.9±10.5 |
| Fmoc-FF/GluS (co-assembled) | -56.0±1.5 |
| Fmoc-FF/GluP (co-assembled) | -55.4±6.1 |

Controlling hydrogel mechanical properties (*i.e.* stiffness)[9] is known to be of importance in cell culture applications. Rheology was measured to evaluate the stiffness for the co-assembled gels in the presence and absence of fetal bovine serum (FBS), a widely used serum-supplement for the *in vitro* cell culture applications. For the pre-gelation mixtures composed of the same chemical components, varying the total concentration led to form gels with different stiffness values. It is clear that by increasing the total concentration, the stiffness increases **(See Figures 4.6 and 4.7)**.

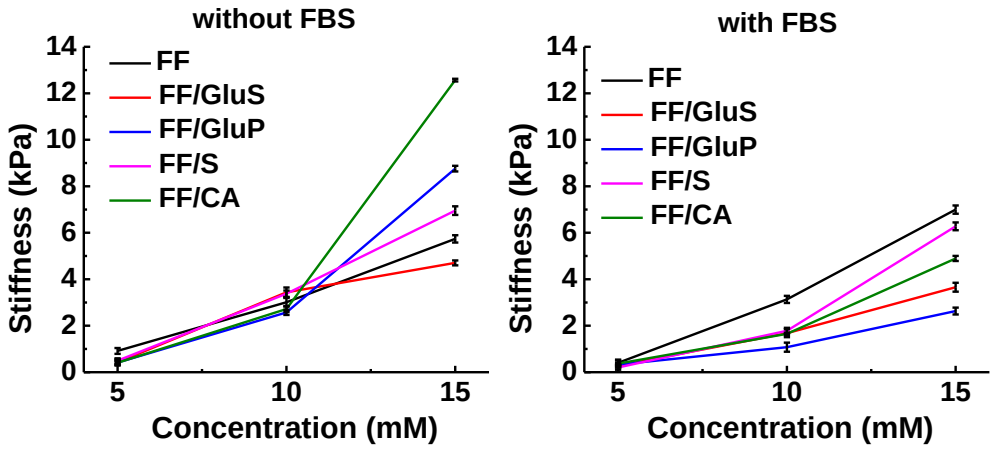


**Figure 4.6** Summary of rheology data illustrating the effect of mixtures concentration on the stiffness of different hydrogel combinations in the presence and absence of FBS.

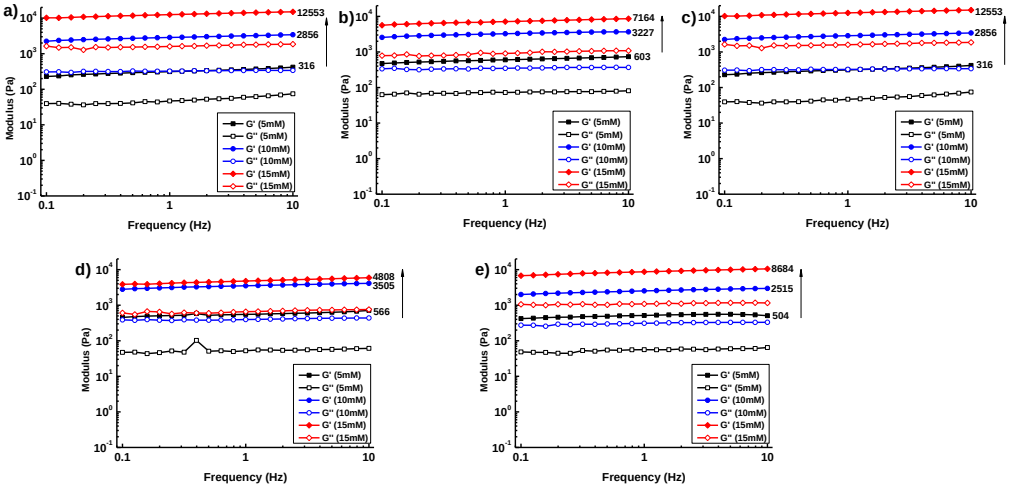


**Figure 4.7** Rheology data illustrating the effect of concentration on the stiffness of hydrogels with different combinations in FBS free medium. **a)** Fmoc-FF, **b)** Fmoc-FF/S, **c)** Fmoc-FF/CA, **d)** Fmoc-FF/GluS and **e)** Fmoc-FF/GluP.

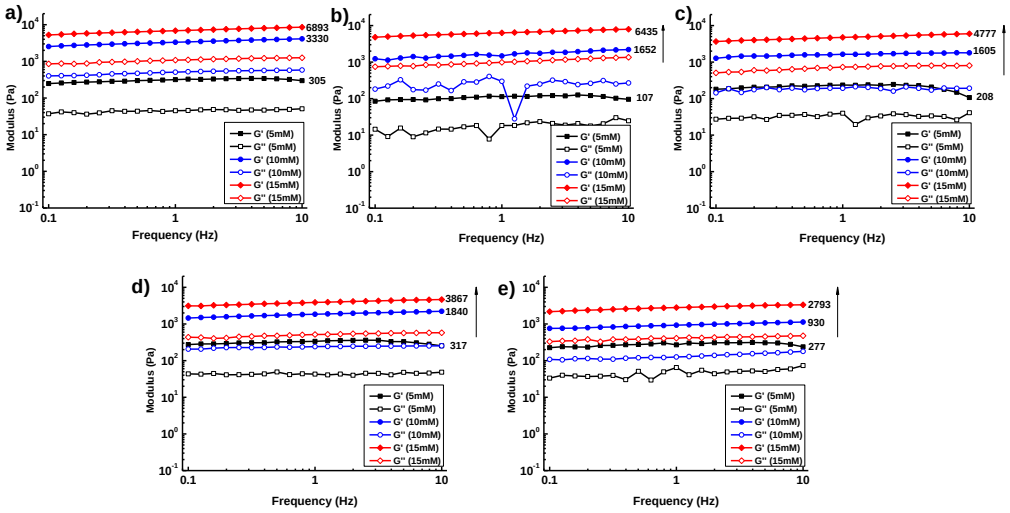


**Figure 4.8** Rheology data illustrating the effect of concentration on the stiffness of hydrogels with different combinations in medium containing FBS. **a)** Fmoc-FF, **b)** Fmoc-FF/S, **c)** Fmoc-FF/CA, **d)** Fmoc-FF/GluS and **e)** Fmoc-FF/GluP.

## Adipose stem cell culture

### 2D culture without additional proteins (FBS)

The viscoelasticity of adipocyte tissues is known to be around 0.61 kPa;[31] therefore, ASCs were cultured using gels with a similar stiffness value as determined by rheology (as discussed above). To assess the suitability of the prepared hydrogels as scaffolds for ASCs culture, cells were cultured for two days on Fmoc-FF gels (bare nanofibres, as a control experiment) and functionalized nanofibres (Fmoc-FF/X). The experiment was conducted in the presence and in the absence of FBS. A control experiment was performed on normal TCPS (Tissue Culture Polystyrene).

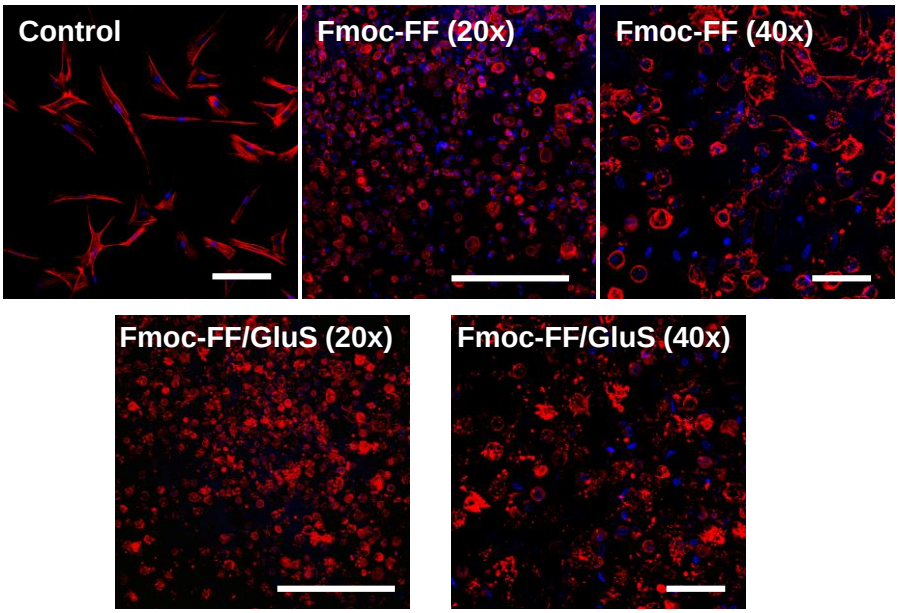


**Figure 4.9** Fluorescence microscopy images of ASCs cultured for two days two dimensionally on scaffolds of bare fibers (Fmoc-FF) and functionalized fibers (Fmoc-FF/GluS) without additional proteins, red color for actin (Phalloidin staining) and blue for nuclei (DAPI staining). Scale bare = 50 µm.

**Figure 4.9 and Figure 4.10** show 2D cultured ASCs for two days. Cells cultured on gels without added proteins (i.e. FBS) are found to be homogeneously distributed within the gel matrix and found to be migrated inside the gels to about 30 μm (for Fmoc-FF scaffold) and to about 65 μm (for Fmoc-FF/GluS scaffold) **(see Figure 4.9)**.

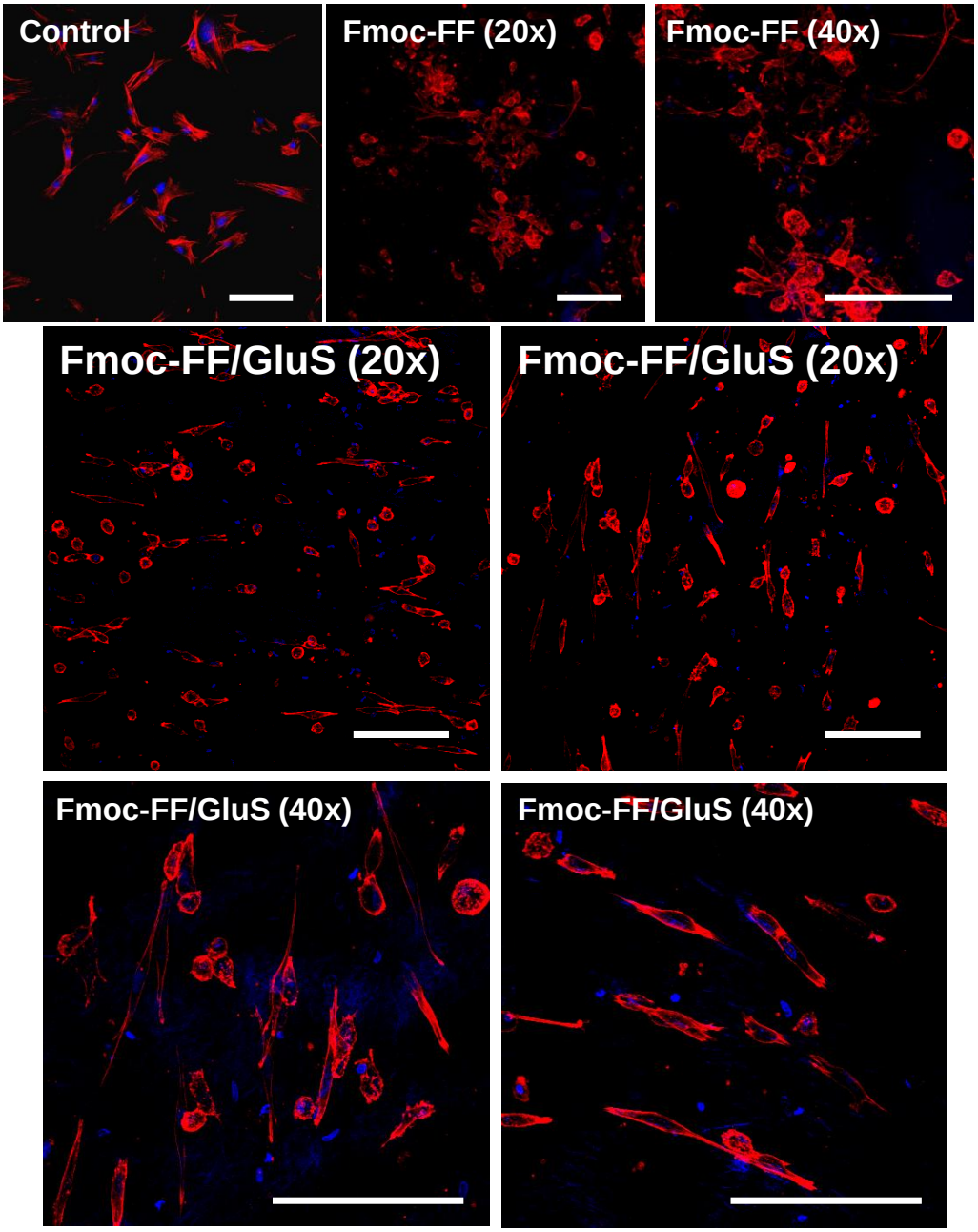

**Figure 4.10** Fluorescence microscopy images of ASCs cultured for two days two dimensionally on scaffolds of bare fibers (Fmoc-FF) and functionalized fibers (Fmoc-FF/GluS) with the addition of FBS, red color for actin (Phalloidin staining) and blue for nuclei (DAPI staining). Scale bare = 50 µm.

When the cells were cultured under the same conditions but in the presence of FBS, cells cultured on Fmoc-FF scaffolds were found to form clusters with more spread cells migrated to about 55 µm inside the gel matrix. Cells cultured on Fmoc-FF/GluS scaffolds changed their shape to be spindle-like and migrated inside the gel matrix to about 50 µm. **(see Figure 4.10)**.

The change of the cells shape would suggest that the gels (Fmoc-FF/GluS) are biocompatible and the cells are possibly differentiating. This will be confirmed in the ongoing experiments (by the 3 B's research group) where cell culture will be performed for a longer period of time and PCR experiments will be conducted to check the cells differentiation.

## 4.4Conclusions and Future Work

In this chapter, we aimed to study the effect of chemical functionality of co-assembled two-components on the differentiation of adipose stem cells. Different surfactant-based functionalities (simple amino acid and sugar derivatives) were co-assembled with Fmoc-FF, a well-established hydrogelator. The co-assembled structures were characterised by various techniques including FTIR, fluorescence spectroscopy, circular dichroism, zeta potential, TEM and rheology. Based on obtained results we can conclude that depending on the components chemistry, co-assembly mode can be affected with the chemical functionality presented on the surface of the nanofibres. Moreover, scaffolds produced *via* co-assembly showed

biocompatibility with possible differentiation. Longer cell culture studies are under the way which will be accompanied by PCR measurements to confirm differentiation.

## 4.5References


1. P. C. Baer, *Stem cells and development*, 2011, **20**, 1805-1816.
2. W. Gao, X. Qiao, S. Ma and L. Cui, *Journal of cellular and molecular medicine*, 2011, **15**, 2575-2585.
3. C. Gardin, V. Vindigni, E. Bressan, L. Ferroni, E. Nalesso, A. D. Puppa, D. D'Avella, D. Lops, P. Pinton and B. Zavan, *International Journal of Molecular Sciences*, 2011, **12**, 6749-6764.
4. L. Tirkkonen, H. Halonen, J. Hyttinen, H. Kuokkanen, H. Sievänen, A.-M. Koivisto, B. Mannerström, G. K. Sándor, R. Suuronen and S. Miettinen, *Journal of The Royal Society Interface*, 2011, **8**, 1736-1747.
5. S. Haimi, G. Gorianc, L. Moimas, B. Lindroos, H. Huhtala, S. Räty, H. Kuokkanen, G. K. Sándor, C. Schmid and S. Miettinen, *Acta Biomaterialia*, 2009, **5**, 3122-3131.
6. E. J. Amis, *Nature Materials*, 2004, **3**, 83-85.
7. P. Bianco, M. Riminucci, S. Gronthos and P. G. Robey, *Stem cells*, 2001, **19**, 180-192.
8. J. C. Meredith, J. L. Sormana, B. G. Keselowsky, A. J. García, A. Tona, A. Karim and E. J. Amis, *Journal of Biomedical Materials Research Part A*, 2003, **66**, 483-490.
9. A. J. Engler, S. Sen, H. L. Sweeney and D. E. Discher, *Cell*, 2006, **126**, 677-689.

10. R. McBeath, D. M. Pirone, C. M. Nelson, K. Bhadriraju and C. S. Chen, *Developmental Cell*, 2004, **6**, 483-495.

11. W. L. Murphy, T. C. McDevitt and A. J. Engler, *Nature Materials*, 2014, **13**, 547-557.

12. R. A. Marklein and J. A. Burdick, *Advanced Materials*, 2010, **22**, 175-189.

13. C. J. Flaim, S. Chien and S. N. Bhatia, *Nature Methods*, 2005, **2**, 119-125.

14. D. G. Anderson, S. Levenberg and R. Langer, *Nature Biotechnology*, 2004, **22**, 863-866.

15. D. S. da Costa, R. A. Pires, A. M. Frias, R. L. Reis and I. Pashkuleva, *Journal of Materials Chemistry*, 2012, **22**, 7172-7178.

16. D. G. Anderson, D. Putnam, E. B. Lavik, T. A. Mahmood and R. Langer, *Biomaterials*, 2005, **26**, 4892-4897.

17. D. S. Benoit, M. P. Schwartz, A. R. Durney and K. S. Anseth, *Nature Materials*, 2008, **7**, 816-823.

18. R. J. Williams, R. J. Mart and R. V. Ulijn, *Peptide Science*, 2010, **94**, 107-117.

19. D. N. Woolfson and Z. N. Mahmoud, *Chemical Society Reviews*, 2010, **39**, 3464-3479.

20. H. Cui, M. J. Webber and S. I. Stupp, *Peptide Science*, 2010, **94**, 1-18.

21. A. Miyachi, T. Takahashi, S. Matsumura and H. Mihara, *Chemistry-A European Journal*, 2010, **16**, 6644-6650.

22. M. Zhou, A. M. Smith, A. K. Das, N. W. Hodson, R. F. Collins, R. V. Ulijn and J. E. Gough, *Biomaterials*, 2009, **30**, 2523-2530.

23. V. Jayawarna, S. M. Richardson, A. R. Hirst, N. W. Hodson, A. Saiani, J. E. Gough and R. V. Ulijn, *Acta Biomaterialia*, 2009, **5**, 934-943.

24. Y. M. Abul-Haija, S. Roy, P. W. J. M. Frederix, N. Javid, V. Jayawarna and R. V. Ulijn, *Small*, 2014, **10**, 973-979.

25. S. Fleming, S. Debnath, P. W. J. M. Frederix, N. T. Hunt and R. V. Ulijn, *Biomacromolecules*, 2014, **15**, 1171-1184.

26. S. Fleming, P. W. Frederix, I. n. Ramos Sasselli, N. T. Hunt, R. V. Ulijn and T. Tuttle, *Langmuir*, 2013, **29**, 9510-9515.

27. A. M. Smith, R. J. Williams, C. Tang, P. Coppo, R. F. Collins, M. L. Turner, A. Saiani and R. V. Ulijn, *Advanced Materials*, 2008, **20**, 37-41.

28. J. W. Sadownik, J. Leckie and R. V. Ulijn, *Chemical Communications*, 2011, **47**, 728-730.

29. R. W. Woody, *Biopolymers*, 1978, **17**, 1451-1467.

30. E. H. Strickland and S. Beychok, *Critical Reviews in Biochemistry and Molecular Biology*, 1974, **2**, 113-175.

31. E. M. Darling, M. Topel, S. Zauscher, T. P. Vail and F. Guilak, *Journal of Biomechanics*, 2008, **41**, 454-464.

32. T. C. Holmes, S. de Lacalle, X. Su, G. Liu, A. Rich and S. Zhang, *Proceedings of the National Academy of Sciences of the United States of America*, 2000, **97**, 6728–6733.

33. C. Tang, A. M. Smith, R. F. Collins, R. V. Ulijn, A. Saiani, *Langmuir* **2009**, *25*, 9447.

# 5. Controlling Cancer Cell Fate using Localized Biocatalytic Self-Assembly of an Aromatic Carbohydrate Amphiphile*

## Objectives:

The key research objectives of this chapter are to:

i. Develop an enzyme responsive sugar based hydrogelator.

ii. Investigate the possibility of tuning the physical and mechanical (*i.e.* stiffness) properties by changing the enzyme concentration.

iii. Study the effect of this hydrogel on phosphatase secreting cells (*e.g.* Osteosarcoma cell line, SaOS2).

* This work was published in part as: R. A. Pires, Y. M. Abul-Haija, D. S. Costa, R. Novoa-Carballal, R. L. Reis, R. V. Ulijn, I. Pashkuleva. *Journal of the American Chemical Society* 2015**, 137**, 576-579.

Declaration of contribution to published article: Any reproduced work from the aforementioned published article I was solely responsible for, including the written article itself, unless otherwise stated. The cell work was performed by the 3B's research group from University of Minho in Portugal.

## 5.1Introduction

Molecular self-assembly[1, 2] of peptide amphiphiles, short peptides appended with aromatic[3] or aliphatic moieties[4], has been a hot topic in the biomedical field for the last two decades.[5, 6] Designed peptide amphiphiles can be used in the 'bottom-up approach' to create structures that resemble the extracellular matrix (ECM) at both structural and functional levels but are much simpler in composition.[7-10] In addition to peptides, other self-assembling amphiphilic molecules, including carbohydrate and nucleotide moieties have emerged: for example, carbohydrate derivatives or mixed nucleobase/amino acid/carbohydrate conjugates self-assemble into nanofibres and gel under specific conditions (*e.g.* presence of certain cations, manipulation of temperature, pH, *etc.*).[11, 12] Because the self-assembly process is orchestrated by different types of intermolecular interactions (e.g. electrostatic, aromatic stacking, hydrophobic effects, hydrogen bonding),[13] subtle changes in the chemical structure of the amphiphile can affect the assembly structure and process.

One approach to control and direct molecular self-assembly uses the selective catalytic activity of enzymes. Typically, enzymes remove steric or electrostatic blocking groups from non-assembling amphiphile precursors and generate building blocks at the site of catalysis, in a process known as enzymatically-triggered or biocatalytic self-assembly (see also **Chapter 3**).[14-16] Such systems have been studied for several years because of their selectivity, ability to trigger the assembly under physiological conditions and localized action.[17, 18] Usually, the procedure involves recombinant enzymes *in vitro* by direct addition to the precursor solution,[15, 19] with recent examples of *in situ* biocatalytic self-assembly that use enzymes present in the intracellular/pericellular environment.[14, 15, 18, 20-24] Phosphatases have attracted attention because of the abundance of phosphorylation and dephosphorylation

reactions that take place *in vivo*. Especially alkaline phosphatase (ALP) is widely used as a diagnostic and prognostic marker in different pathologies.[25] ALP is present in highly mineralized tissues and is usually expressed on the basement membrane of osteoblasts.[26] It is overexpressed in some osteosarcomas[26, 27] making it a valid target for localized anti-cancer therapies. Recently, Xu *et al*[18] reported that enzymatic formation of nanofibers of self-assembled aromatic tripeptide amphiphiles in the pericellular space of cancer cells leads to selective inhibition of the cellular metabolic activity, which depends on the concentration of phosphatases in the biological medium.

Herein, we present an aromatic carbohydrate amphiphile, namely, *N*-(fluorenylmethoxycarbonyl)-glucosamine-6-phosphate (**1**), as alternative substrate in this approach (**1** was also used for nanofibres functionalisation in **Chapter 4**). Carbohydrates are the most abundant biomolecules and represent one of the four building elements of life.[28, 29] In particular, glucose is the main player in the carbohydrate metabolism because it can be converted into all other monosaccharides needed for the glycan biosynthesis. Once internalized by the cell, glucose is activated to the nucleotide glucose-6-phosphate (importantly not permeable to cell membrane) and transported to the Golgi where cell surface and ECM glycans are assembled.[28] The generated glycans are involved in a plethora of biological events through specific pathways but also by providing mechanical cues to the cells: because carbohydrates are rich in hydroxyl groups they generate highly hydrated gels. The physiological importance of this ability of carbohydrates is highlighted in different tissues and organs, *e.g.* cartilage tissue is abundant in glycosaminoglycans and as a result 70 to 85% of the weight of the whole tissue is water.[30] We therefore

hypothesize that carbohydrate amphiphiles open up completely new possibilities as therapeutic platforms complementing the more established peptide-based systems, due to their rich chemistry, gelation ability and roles in biological recognition. The introduction of a carbohydrate moiety will result in the formation of supramolecular hydrogels that share some of the glycan properties, but are much simpler.

## 5.2Materials and Methods

### 5.2.1 Transmission electron microscopy (TEM)

Carbon-coated copper grids (200 mesh) were glow discharged in air for 30 s. The grid was touched onto the gel surface for 3 s and blotted down using filter paper. Negative stain (20 μL, 1% aqueous methylamine vanadate obtained from Nanovan; Nanoprobes) was applied and the excess was removed using filter paper. The dried specimens were then imaged using a LEO 912 energy filtering transmission electron microscope operating at 120kV fitted with 14 bit/2 K Proscan CCD camera.

### 5.2.2 Fluorescence spectroscopy

1 mL samples were prepared in a 1 $cm^2$ quartz cuvette. Fluorescence emission spectra were measured on a Jasco FP-6500 spectrofluorometer at a scanning speed of 500 $nm.min^{-1}$. The emission spectra (resulting from excitation at 280 nm) were recorded between 300 and 600 nm, using a bandwidth of 3 nm with a medium response and a 3 nm data pitch.

### 5.2.3 Rheology

To assess the mechanical properties of the hydrogels, dynamic frequency sweep experiments were carried out on a strain-controlled rheometer (Kinexus rotation rheometer) using a parallel-plate geometry (20 mm) with a 0.50 cm gap. An integrated temperature controller was used to maintain the temperature of the sample

stage at 25 °C. Precautions were taken to minimize solvent evaporation and to keep the sample hydrated: a solvent trap was used and the atmosphere within was kept saturated. To ensure the measurements were made in the linear viscoelastic regime, an amplitude sweep was performed and the results showed no variation in elastic modulus (G') and viscous modulus (G'') up to a strain of 1%. The dynamic modulus of the hydrogel was measured as a frequency function, where the frequency sweeps were carried out between 0.1 and 10 Hz. Stiffness values were reported as the modulus average between 0.1-10 Hz ± standard deviation. The measurements were repeated at least three times to ensure reproducibility.

### 5.2.4 High resolution scanning electron microscopy (SEM)

Images were acquired in a FEI Nova 2000, under an acceleration voltage of 15.0 kV, a working distance of 5.1 mm and a magnification of 10,000 times.

### 5.2.5 In vitro gel preparation

Samples were prepared by dissolving predetermined amounts of **1** in 1 mL of PBS (at pH 7.4) followed by vortex and sonication until full dissolution. Then, a predetermined volume of ALP was added (Sigma, ALP concentrations are reported in units where one enzyme unit corresponds to the amount of enzyme that hydrolyses 1 μmol of 4-nitrophenyl phosphate per min at pH 9.8 at 37°C). Immediately after that, solution was allowed to gel in an incubator at 37°C in 5% $CO_2$ atmosphere. All characterizations were performed after 24 hours unless otherwise mentioned.

### 5.2.6 Biological methods

SaOs2 cancer cell line from human osteosarcoma and ATDC5 pre-chondrocyte cell line derived from mouse teratocarcinoma (ECACC, UK) were used because of their different levels of ALP expression. Cells were cultured at 37 °C in a humidified 95/5% air/$CO_2$ atmosphere using DMEM (Sigma, in the case of SaOs2) or DMEM-

F12 (Gibco, UK, for the ATDC5 culture) supplemented with 10% FBS (Gibco, UK), and 1% A/B (Gibco, UK) solution. Cells were used in suspension or as monolayers (50k cells/mL), in contact with **1** at different initial concentrations (0 - 20 mM) during different time periods. After each time point, culture medium was collected for ALP quantification, HPLC and SEM characterization. Metabolic activity was assessed by MTS (CellTiter 96® AQueous One Solution Cell Proliferation Assay, Promega) according to the supplier's instructions. The relative metabolic activity (%) of the SaOs2 and ATDC5 cells was determined for each condition and was compared with the values obtained in the absence of **1**. The optical density (OD) was read at 490 nm on a multiwell microplate reader (Synergy HT, Bio-Tek Instruments). After the MTS test, cells were thoroughly washed with PBS and used for ALP quantification. Both membrane-bound and extracellular ALP was quantified according to the p-nitrophenol method. Gels were dehydrated in a graded series of ethanol and imaged by placing them on a silicon wafer (i.e. no coating was applied). Cell monolayers on Au supports were imaged after washing with ultrapure water (2-3 s), immersing in liquid nitrogen and freeze-dried. For brightfield microscopy, after each time point, cells were fixated with 10% buffered formalin, washed with PBS and incubated at 37°C during 30 min with Congo Red (0.1 mg/mL, Sigma). Cells were washed with PBS and imaged using an Axio Imager Z1 m (Zeiss). For the ALP inhibition experiments we used the Pierce phosphatase inhibitor (Thermo Scientific) that was prepared following the manufacturer instruction (1 tablet per 10 mL of culture medium with FBS). The cell monolayers (ATDC5 and SaOS2) were incubated with the inhibitor during 24 h under standard culture conditions (37°C, 5% $CO_2$). Afterwards, the cells were washed with PBS and incubated with different

concentrations of **1** under the same conditions as previously described for the non-inhibition experiments.

## 5.3Results and Discussion

We report on the use of **1** as a selective ALP substrate for osteosarcoma cells (SaOs2). We provide data about the specificity of this system by comparative tests using cells with a lower ALP expression profile, namely pre-chondrocytes (ATDC5). Our results demonstrate that the system can be used in an anti-osteosarcoma strategy, with limited impact on the surrounding healthy cells/tissues as illustrated in **Scheme 5.1**.

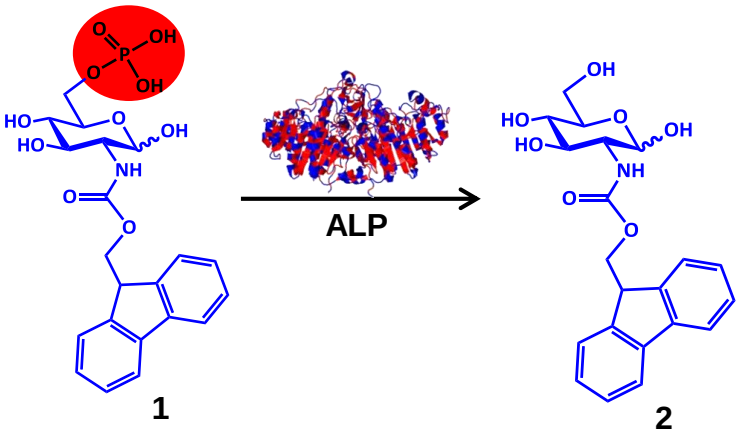


**Scheme 5.1.** Illustration of enzymatic transformation of **1** to **2** upon enzymatic activity of phosphatases (*e.g.* ALP).

Self-assembly and gelation of the precursor **1** and the dephosphorylated analogue (*i.e.* **2**) were evaluated using three different concentrations of **1** (*i.e.* 10, 15 and 20 mM) and different ALP concentrations (*i.e.* 25, 50 and 75 U) in PBS at pH 7.4 (**Figure 5.1**). Concentrations of **1** were chosen to be >5 mM, the critical gelation concentration of **2**.[11] Before ALP addition, a transparent solution was observed which was transformed to a transparent gel phase upon ALP addition (**Figure 5.1C**

**insets**). Gelation time varied from 1 h to 5 h depending on precursor and enzyme concentrations; gels formed faster when higher precursor and enzyme concentrations were used (gels tested by inverted vial method).

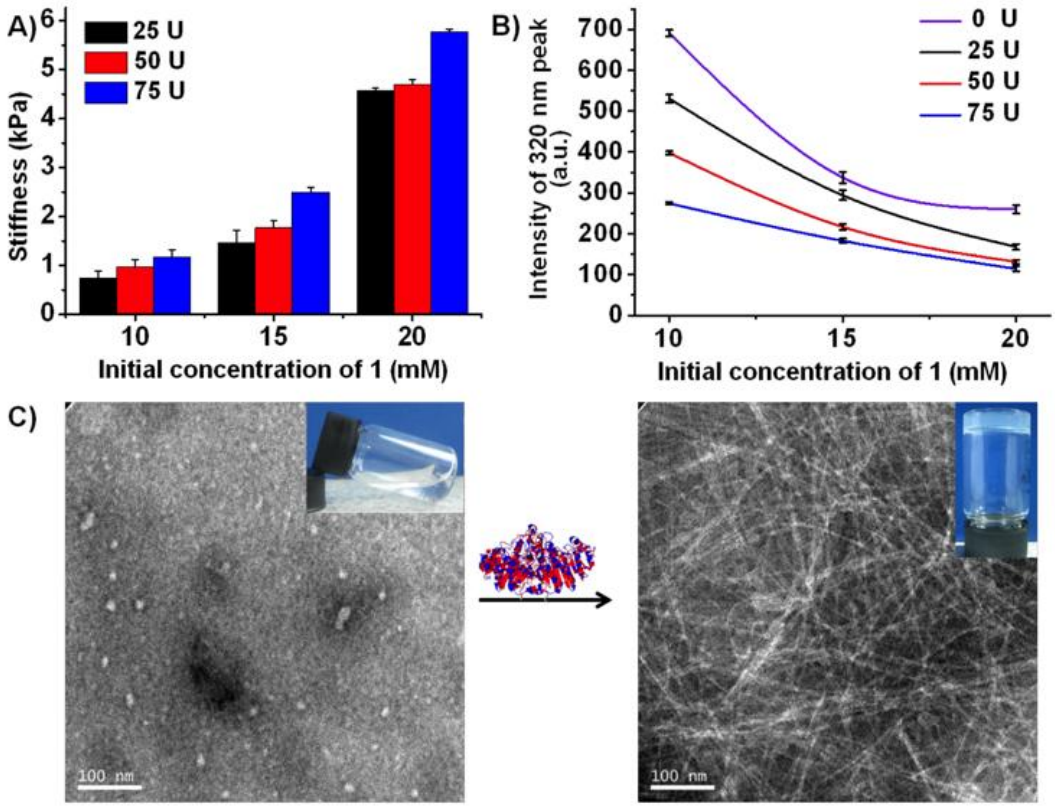


**Figure 5.1** Effect of the concentration of ALP and **1** on the (A) mechanical properties (rheology) of the formed hydrogels; (B) supramolecular arrangement of fluorenyl groups observed by monitoring fluorescence intensity of fluorenyl main peak at 320 nm, and C) enzymatic transformation of **1** (clear solution of spherical aggregates) to **2** (gel of nanofibrous networks) observed by TEM.

HPLC was used to assess the ability of ALP to dephosphorylate **1** and to study the dephosphorylation rate during 24 h (**Figure 5.2**). The conversion rate could be controlled by the enzyme concentration: faster conversion was observed when higher

enzyme concentration was used. Similar behaviour was previously reported for phosphorylated Fmoc-dipeptide systems.[14, 31]

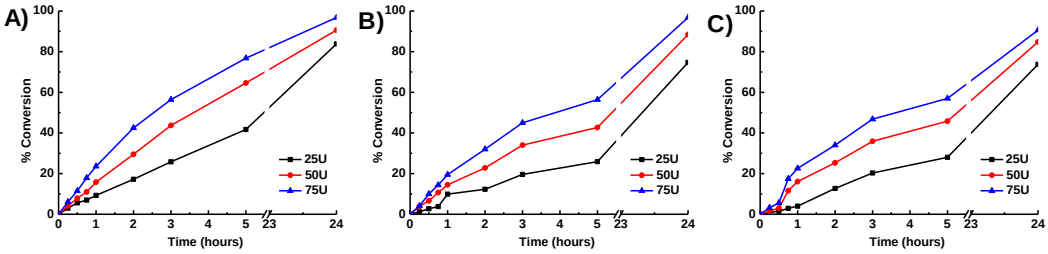


**Figure 5.2** HPLC monitoring of **1** [(A) 10 mM, (B) 15 mM, (C) 20 mM] to **2** conversion during 24 h in the presence of different ALP concentrations (25, 50 and 75 U).

In biocatalytic self-assembly, enzyme kinetics (*i.e.*, the rate of production of self-assembly building blocks) dictate gelation properties, such as supramolecular arrangement and the subsequent gel stiffness.[32] Therefore, the mechanical properties of the formed hydrogels were evaluated by rheology after 24 h of ALP addition (**Figure 5.1A and 5.3**). As expected, higher ALP concentrations led to formation of stiffer gels. These observations were directly correlated with fluorescence emission intensities of fluorenyl main peak at 320 nm (**Figure 5.1B and 5.4**). A clear trend was observed, as **1** and/or ALP concentrations increase, the peak at 320 nm quenches, which suggest more efficient supramolecular stacking within the gel fibres. The morphology of the generated assemblies, involving a supramolecular transformation from spherical aggregates for **1** to nanofibers of **2** was further characterized by transmission electron microscopy (TEM) (**Figure 5.1C and Figure 5.5**). We observed nanofibrous structures whose network density and resulting gel stiffness can be controlled by either **1** or ALP concentrations.

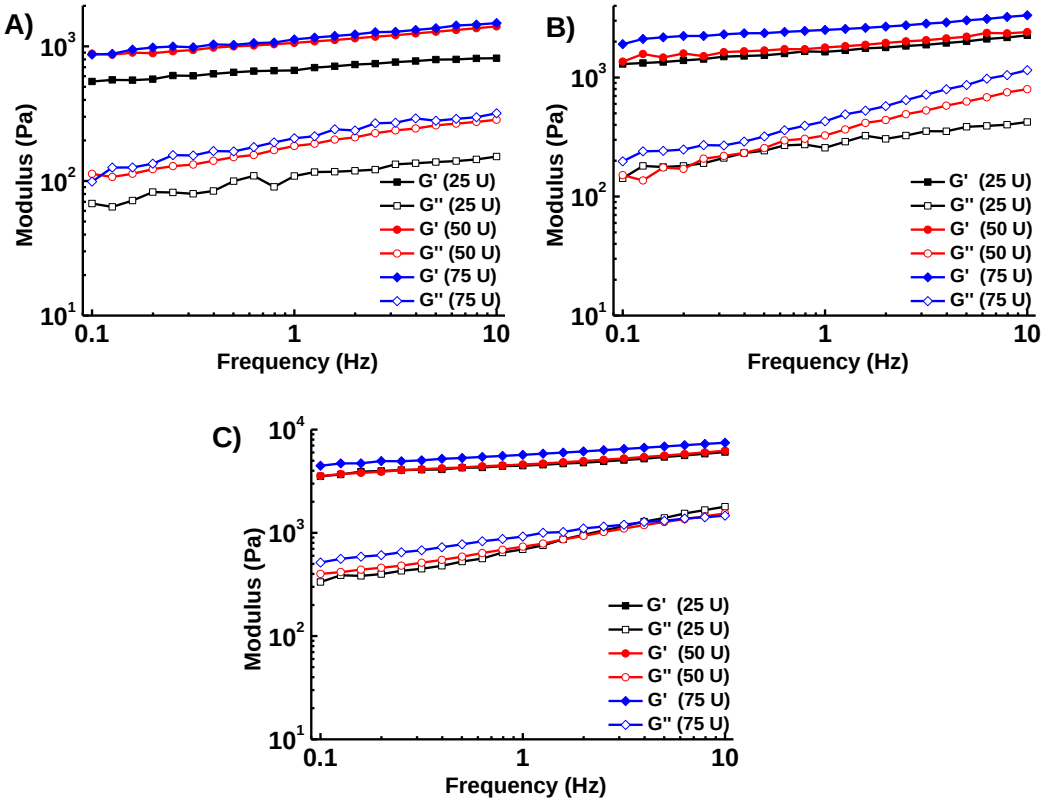


**Figure 5.3** Rheology data illustrating the effect of the concentrations of ALP (25, 50 and 75 U) and **1** ((A) 10 mM, (B) 15 mM and (C) 20 mM) on gel stiffness.

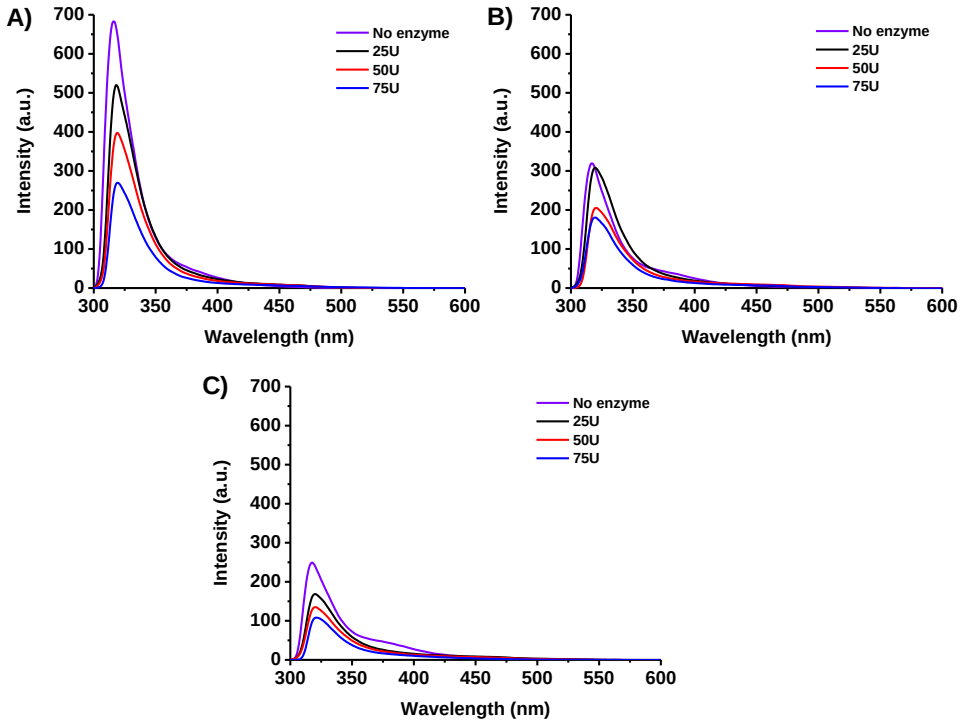

**Figure 5.4** Fluorescence emission spectra showing the effect of the concentrations of ALP (25, 50 and 75 U) and **1** ((A) 10 mM, (B) 15 mM and (C) 20 mM) on the supramolecular organization of the formed nanostructures.

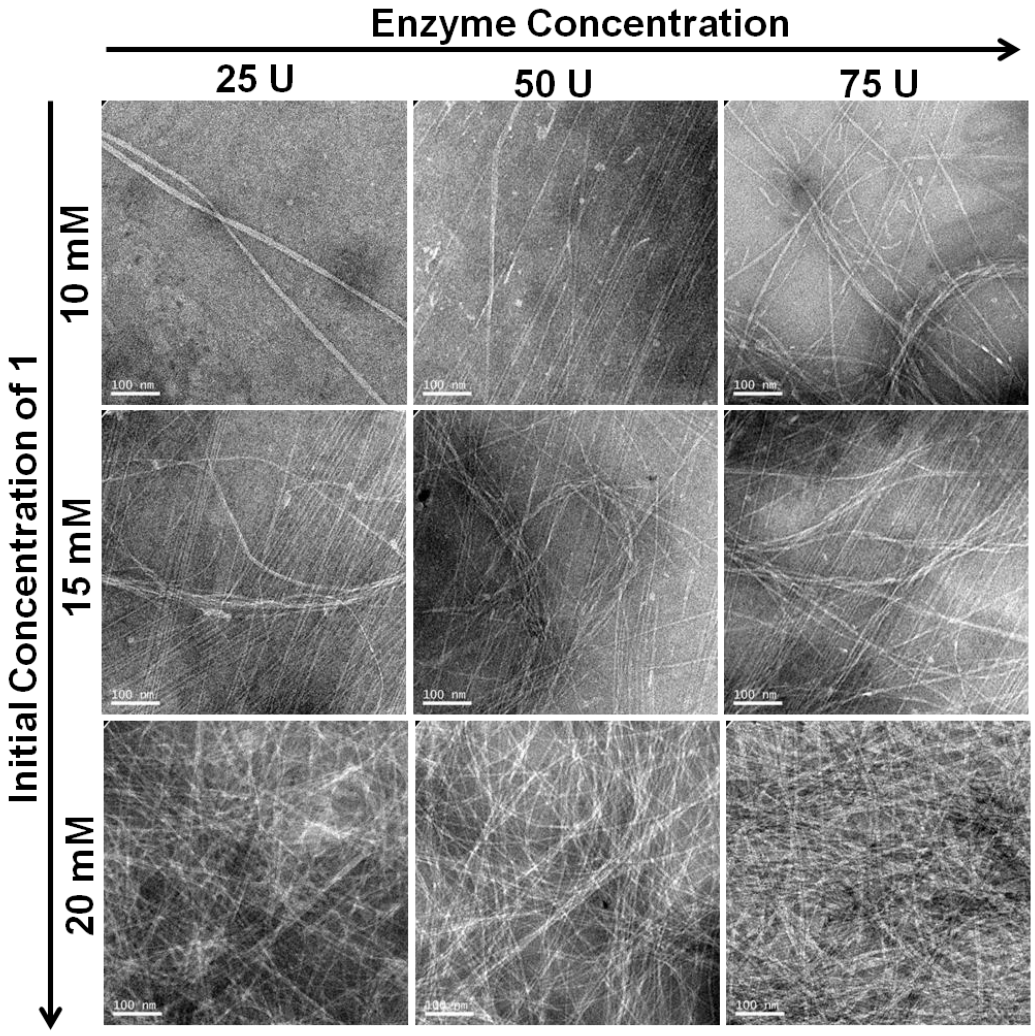


**Figure 5.5** TEM images showing the effect of the concentrations of ALP and **1** on the morphology of the *in vitro* produced **2** (nanofibres density), scale bar = 100 nm.

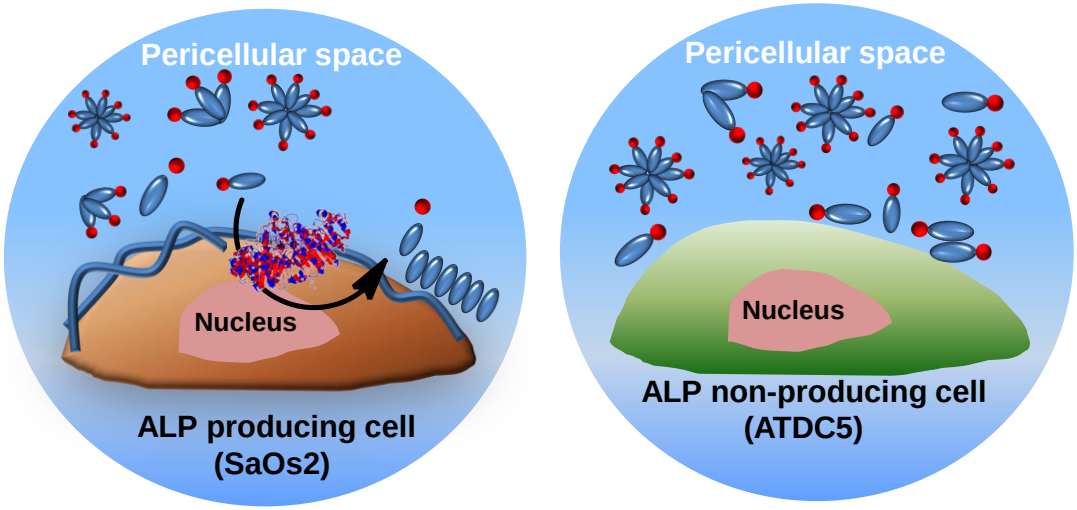


**Scheme 5.2** Illustration of *in situ* biocatalytic self-assembly in the presence of membrane bound ALP. This process found to be specific for ALP overexpressing cells (e.g. SaOS2) resulting in the formation of nanofibres surrounding cells and cell death while leaving less expressing cells (ATDC5) unaffected.

In collaboration with the 3B's research group, we studied the conversion of **1** to **2** *in situ* in the presence of membrane-bound ALP, which is overexpressed in osteosarcoma cells (SaOs2 cells). Upon dephosphorylation, **2** formed nanofibres (hydrogel) that surrounded cells leading to cell death. This process was found to be cell specific as cells producing less amount of membrane-bound ALP (*i.e.* ATDC5) were not significantly affected (**Scheme 5.2**).

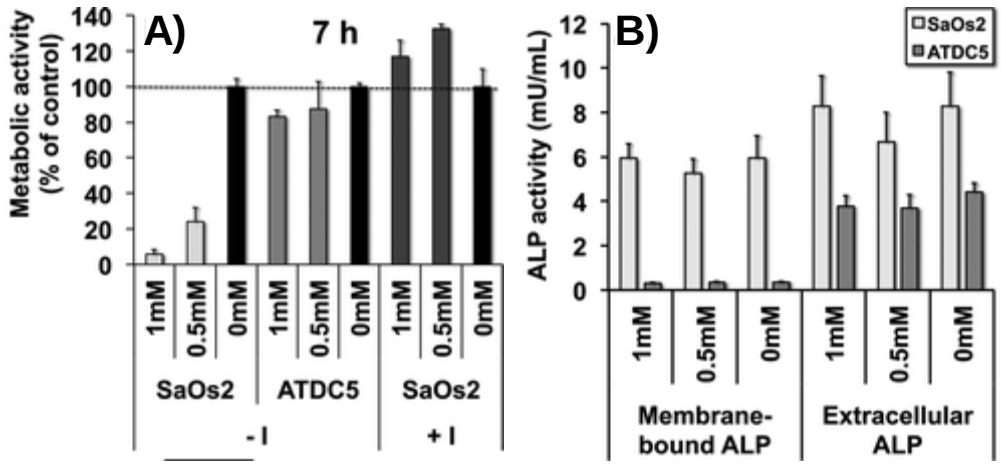


**Figure 5.6** A) Metabolic activity of SaOs2 and ATDC5 monolayer cultures in the presence of different concentrations of **1** for 7 hours (control 0 mM, 0.5 mM, and 1 mM), without (−I) and with (+I) phosphatase inhibitor. (B) Activity of the membrane bound and extracellular ALP in the SaOs2 and ATDC5 cell cultures as a function of the concentration of **1**.

While the presence of **1** hardly affects the metabolic activity of ATDC5 cell, it drastically decreases the metabolic activity of SaOs2 cells (**Figure 5.6A**). By quantifying both membrane-bound and extracellular ALP in SaOs2 and ATDC5 cells cultures, membrane bound ALP was found to have 15-20 times higher value and extracellular ALP has 1.5-2 higher value for SaOs2 compared to those of ATCD5, indicating that membrane bound ALP is mainly responsible for the cytotoxicity of **1** (**Figure 5.6B**).

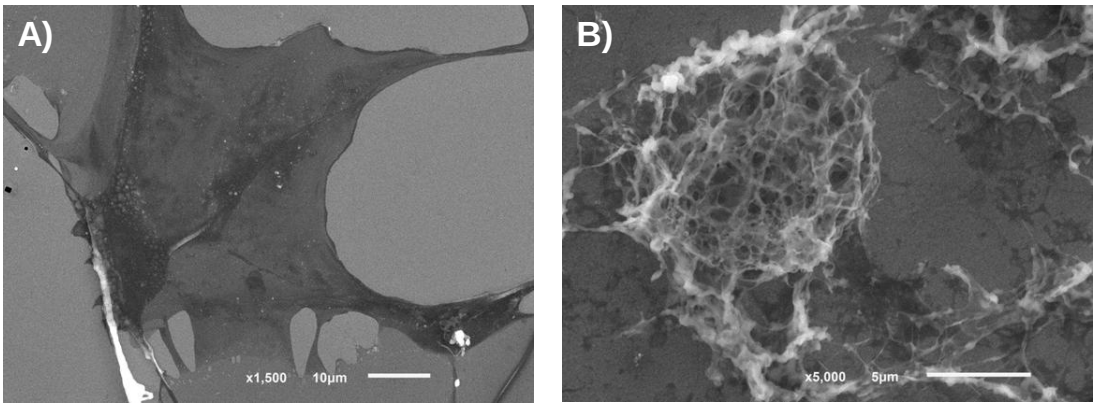


**Figure 5.7** SEM images of SaOs2 cells, cultured for 7 h, in the (A) absence and (B) presence of **1** (0.5 mM).

Moreover, it was confirmed that the conversion of **1** to **2** by SaOs2 cells results in pericellular nanofibres (**Figure 5.7B**), while these nanofibres are absent without the addition of **1** (**Figure 5.7A**). The successful use of carbohydrate derivatives on osteosarcoma cells opens up new possibilities for developing new cancer therapeutics based on biocatalytically triggered self-assembly.

These results are consistent with the recently reported nanonets of peptide amphiphiles, whose formation is triggered upon dephosphorylation of its derivative by surface and secretory phosphatases in the pericellular environment.[18] As in the case of peptides, the transformation of **1** to **2** by the membrane bound ALP leads to the formation of self-assembled "cage-like" hydrogels around SaOs2 cells. These assemblies may reduce/block metabolite exchange between the cells and thus, they have profound effect on critical cellular activities (e.g. adhesion, motility, proliferation) that ultimately lead to cell apoptosis.[34]

## 5.4Conclusions

In summary, we demonstrated that a simple carbohydrate phosphate derivative (**1**) is converted into the self-assembling hydrogelator **2** *in situ* by the SaOs2 membrane-bound ALP. Upon conversion, **2** generates a cytotoxic nanonet/hydrogel "cage" surrounding the cells. We proved that this process is cell-specific, as other cell types, e.g. ATDC5, with lower membrane-bound ALP expression profiles are not affected by **1** at the same concentrations as the ones tested for the SaOs2 cells. The reported system can be exploited in the development of anti-osteosarcoma strategies. Our data can be further exploited in the design of similar systems sensitive to other types of enzymes that are overexpressed at the pericellular environment of other cancer cells and use them as therapeutic targets. Moreover, the larger diversity of the carbohydrate regio- and stereochemistry, in comparison to the peptide-based systems, opens additional possibilities for the design of amphiphiles with improved gelation and kinetics.

## 5.5References


1. J.-M. Lehn, *Science*, 2002, **295**, 2400-2403.
2. G. M. Whitesides and B. Grzybowski, *Science*, 2002, **295**, 2418-2421.
3. S. Fleming and R. V. Ulijn, *Chemical Society Reviews*, 2014, **43**, 8150-8177.
4. A. Dehsorkhi, V. Castelletto and I. W. Hamley, *Journal of Peptide Science*, 2014, **20**, 453-467.
5. J. Boekhoven and S. I. Stupp, *Advanced Matererials*, 2014, **26**, 1642-1659.
6. Y. M. Abul-Haija and R. V. Ulijn, in *Hydrogels in Cell-Based Therapies*, Eds. C. J. Connon and I. W. Hamley, The Royal Society of Chemistry, Cambridge, 2014, pp. 112-134.
7. J. Kisiday, M. Jin, B. Kurz, H. Hung, C. Semino, S. Zhang and A. J. Grodzinsky, *Proceedings of the National Academy of Sciences of the United States of America*, 2002, **99**, 9996-10001.
8. R. N. Shah, N. A. Shah, M. M. D. Lim, C. Hsieh, G. Nuber and S. I. Stupp, *Proceedings of the National Academy of Sciences of the United States of America*, 2010, **107**, 3293-3298.
9. V. Jayawarna, M. Ali, T. A. Jowitt, A. E. Miller, A. Saiani, J. E. Gough and R. V. Ulijn, *Advanced Matererials*, 2006, **18**, 611.
10. A. Mahler, M. Reches, M. Rechter, S. Cohen and E. Gazit, *Advanced Materials*, 2006, **18**, 1365-1370.
11. L. S. Birchall, S. Roy, V. Jayawarna, M. Hughes, E. Irvine, G. T. Okorogheye, N. Saudi, E. De Santis, T. Tuttle, A. A. Edwards and R. V. Ulijn, *Chemical Science*, 2011, **2**, 1349-1355.
12. X. Du, J. Zhou, O. Guvench, F. O. Sangiorgi, X. Li, N. Zhou and B. Xu, *Bioconjugate Chemistry*, 2014, **25**, 1031-1035.

13. A. C. Mendes, E. T. Baran, R. L. Reis and H. S. Azevedo, *Wiley Interdisciplinary Reviews: Nanomedicine and Nanobiotechnology*, 2013, **5**, 582-612.

14. Y. M. Abul-Haija, S. Roy, P. W. J. M. Frederix, N. Javid, V. Jayawarna and R. V. Ulijn, *Small*, 2014, **10**, 973-979.

15. Z. M. Yang, H. W. Gu, D. G. Fu, P. Gao, J. K. Lam and B. Xu, *Advanced Materials*, 2004, **16**, 1440-1444.

16. R. V. Ulijn, *Journal of Materials Chemistry*, 2006, **16**, 2217-2225.

17. R. J. Williams, T. E. Hall, V. Glattauer, J. White, P. J. Pasic, A. B. Sorensen, L. Waddington, K. M. McLean, P. D. Currie and P. G. Hartley, *Biomaterials*, 2011, **32**, 5304-5310.

18. Y. Kuang, J. Shi, J. Li, D. Yuan, K. A. Alberti, Q. Xu and B. Xu, *Angewandte Chemie International Edition*, 2014, **53**, 8104-8107.

19. S. Toledano, R. J. Williams, V. Jayawarna and R. V. Ulijn, *Journal of the American Chemical Society*, 2006, **128**, 1070-1071.

20. Y. Kuang and B. Xu, *Angewandte Chemie International Edition*, 2013, **52**, 6944-6948.

21. Z. M. Yang, K. M. Xu, Z. F. Guo, Z. H. Guo and B. Xu, *Advanced Materials*, 2007, **19**, 3152.

22. J. W. Sadownik, J. Leckie and R. V. Ulijn, *Chemical Communications*, 2011, **47**, 728-730.

23. W. P. Wang, Z. M. Yang, S. Patanavanich, B. Xu and Y. Chau, *Soft Matter*, 2008, **4**, 1617-1620.

24. Z. Yang, G. Liang, Z. Guo, Z. Guo and B. Xu, *Angewandte Chemie International Edition*, 2007, **46**, 8216-8219.

25. P. P. L. Liu, K. S. Leung, S. M. Kumta, K. M. Lee and K. P. Fung, *Oncology*, 1996, **53**, 275-280.

26. C. Pautke, M. Schieker, T. Tischer, A. Kolk, P. Neth, W. Mutschler and S. Milz, *Anticancer Research*, 2004, **24**, 3743-3748.

27. J. C. Randall, D. C. Morris, S. Zeiger, K. Masuhara, T. Tsuda and H. C. Anderson, *Journal of Histochemistry and Cytochemistry*, 1989, **37**, 1069-1074.

28. A. Varki, R. D. Cummings, J. D. Esko, H. H. Freeze, P. Stanley, C. R. Bertozzi, G. W. Hart and M. E. Etzler, eds., *Essentials of Glycobiology*, CSH Press, New York, 2009.

29. I. Pashkuleva and R. L. Reis, *Journal of Materials Chemistry*, 2010, **20**, 8803-8818.

30. J. M. Mansour, in *Kinesiology: the Mechanics and Pathomechanics of Human Movement*, ed. C. A. Oatis, Lippincott Williams and Wilkins, Philadelphia, 2003, pp. 66-79.

31. Z. Yang, G. Liang, M. Ma, Y. Gao and B. Xu, *Small*, 2007, **3**, 558-562.

32. K. Thornton, A. M. Smith, C. L. R. Merry and R. V. Ulijn, *Biochemical Society Transactions*, 2009, **37**, 660-664.

33. J. F. Shi, X. W. Du, D. Yuan, J. Zhou, N. Zhou, Y. B. Huang and B. Xu, *Biomacromolecules*, 2014, **15**, 3559-3568.

34. J. A. Zorn, H. Wille, D. W. Wolan and J. A. Wells, *Journal of the American Chemical Society*, 2011, **133**, 19630-19633.

# 6. Sequence-Adaptive Peptide/Biopolymer Co-Assembly*

## Objectives:

The main objective of this chapter is to develop a new class of adaptive materials which are able to change their molecular composition and nanoscale structure by combining biocatalytic peptide exchange (using peptide dynamic combinatorial chemistry, DCC), sequence selective peptide self-assembly (forming nanotubes versus nanosheets) and peptide/polymer co-assembly.

* This work has been submitted for publication to Biomacromolecules.

Declaration of contribution to submitted article: Any reproduced work from the aforementioned submitted article I was solely responsible for, including the written article itself, unless otherwise stated.

## 6.1Introduction

Self-assembly[1-3] coupled with biocatalysis[4-6] provides a useful approach for fabrication of adaptive nanostructures, inspired by dynamic processes in living systems. In biology, components interact, assemble, compete and selectively decompose when they are no longer required.[7] To date, few synthetic mimics have focused on dynamic features of the final structures– which would be key to forming truly adaptive structures. Some examples now exist of reconfigurable materials[8] that are able to respond to changes in their environment by readjusting their morphology and/or function cooperatively.[2, 9] In addition, selective enzymatic degradation of polymer bioconjugates, by taking advantage of electrostatics to enhance or reduce degradation has been described recently.[10]

A potentially useful approach to achieving molecular adaption of soft biomaterials would involve changing molecular composition through reversible reactions, using the tools of dynamic combinatorial chemistry (DCC).[11-14] In this approach, building blocks with exchangeable components are formed through reversible interactions to create a dynamic mixture.[15-17] Molecular recognition and assembly between these building blocks (or with externally added templates) then give rise to autonomous optimization of the noncovalent interactions, *i.e.* the most thermodynamically stable product is amplified selectively.[18]

Peptides are particularly useful as building blocks in DCC in a biomaterials context, due to the rich chemistry and functionality available from primary sequences of twenty amino acids, as well as their biological relevance. We have previously developed enzymatically driven peptide libraries that operate through peptide

sequence exchange to identify self-assembling peptide derivatives in a library through continuous formation and hydrolysis of the amide bond.[19,20]

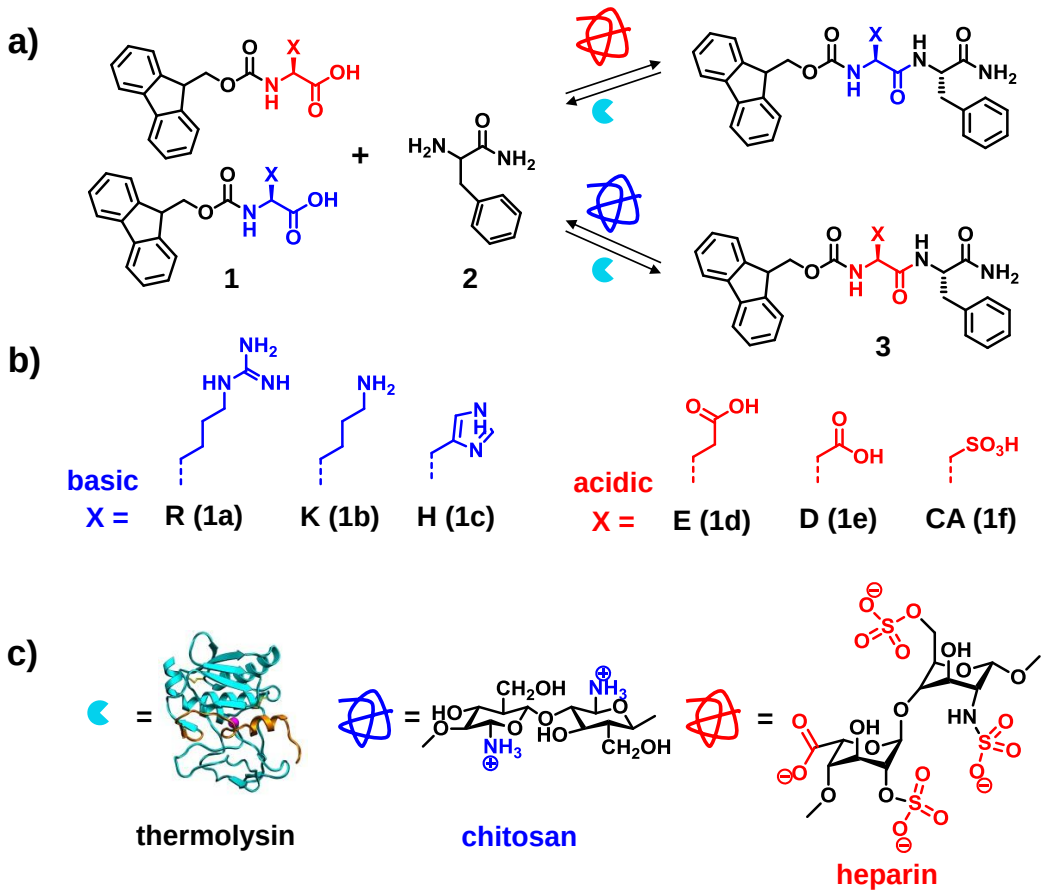


**Figure 6.1** a) Enzymatically triggered *in situ* condensation reaction in which dipeptide derivatives **3** were formed from Fmoc-amino acid **1** (b) (with variable $pK_a$ values on the side chain) and phenylalanine amide **2**. **3** formation and assembly to form nanostructures was evaluated biocatalytically in the presence and absence of biopolymers (c).

Enhancement of the properties of supramolecular (peptide based) systems may be achieved by co-assembly[21, 22] with macromolecules where specific interactions (*e.g.* electrostatic, aromatic stacking) and templating[23] might be utilized to direct the assembly process. Recently, Ni and Chau designed a viral mimic through the

electrostatic co-assembly of an oligo peptide with DNA.[24] Stupp demonstrated the co-assembly of cationic short peptide amphiphiles and anionic biopolymers (hyaluronic acid, HA), resulting in the formation of hierarchically structured macroscopic sacs and membranes.[25-27] Adams reported on controlling the mechanical properties of dipeptide derivatives through polymer co-assembly.[28] Mata recently described hybrid multifunctional nanofibrous membranes based on electrostatic interactions between the co-assembled cationic peptide and anionic biopolymer (HA).[29] It is clear from these examples that co-assembly between biopolymers and self-assembling peptides can have dramatic effects of materials properties and consequent function.

Here, we show that, by combining biocatalytic peptide exchange (using peptide DCC), sequence selective peptide self-assembly (forming nanotubes versus nanosheets) and peptide/polymer co-assembly, a new class of adaptive materials may be developed which change their molecular composition and nanoscale structure depending on the biopolymer present by readjusting molecular composition. These systems may have implications for design and discovery of future responsive, multi-component nanostructures.

To develop such a system, three main requirements were considered: (i) peptide components should undergo a fully reversible sequence exchange, giving low yields in the absence of the biopolymer template; (ii) charge complementary peptide sequences should be selected and amplified by electrostatic templating between peptide and polymer; (iii) system components should display differential co-assembly and express different morphologies depending on composition. The components of the system are given in **Figure 6.1**.

Building on previous enzymatic peptide libraries, we used fluorenylmethoxycarbonyl (Fmoc) capped dipeptide amides as a model system to demonstrate our concept. These aromatic peptide amphiphiles[30, 31] are known to self-assemble through the combination of π-stacking interactions (among the fluorenyl components) and hydrogen bonding interactions (between the peptides). We previously demonstrated fully reversible enzymatic sequence exchange of Fmoc-amino acid with amino acid esters and amides[32, 33] producing Fmoc-dipeptides which are efficient in assembly and gelation. In this work, we focus on selection for co-assembly with charged biopolymers reliant on templating and electrostatics; hence charged amino acids were introduced.

## 6.2Materials and Methods

All chemicals were commercially available and were used without further purification. Fmoc protected (R, K, H, D, C.A) and F-$NH_2$ were purchased from Bachem. Fmoc protected E was purchased from Fluorochem. Thermolysin, PBS tablets and chitosan were purchased from Sigma. Heparin sodium salt from porcine intestinal mucosa was purchased from Millipore.

### 6.2.1 High-performance liquid chromatography (HPLC)

A Dionex P680 HPLC pump was used to quantify conversions of the enzymatic reaction. A 50 µl sample was injected onto a Macherey-Nagel C18 column with a length of 250 mm and an internal diameter of 4.6 mm and 5-mm fused silica particles at a flow rate of 1 ml.min-1. The eluting solvent system had a linear gradient of 20% (v/v) acetonitrile in water for 4 min, gradually rising to 80% (v/v) acetonitrile in water at 35 min. This concentration was kept constant until 40 min when the gradient was decreased to 20% (v/v) acetonitrile in water at 42 min. Sample preparation

involved mixing 30 µl of sample with acetonitrile–water (1 ml, 70:30 mixture) containing 0.1% trifluoroacetic acid. The purity of each identified peak was determined by UV detection at 280 nm.

### 6.2.2 Transmission electron microscopy (TEM)

Carbon-coated copper grids (200 mesh) were glow discharged in air for 30 s. The grid was touched onto the mixture surface and blotted down using a filter paper. Negative stain (20 µL, 1% aqueous methylamine vanadate obtained from Nanovan; Nanoprobes) was applied and the excess was removed using filter paper. The dried samples were then imaged using a LEO 912 energy filtering TEM operating at 120 kV fitted with 14 bit/2 K Proscan CCD camera.

## 6.3Results and Discussion

To satisfy requirement (i) charged Fmoc-amino acids (**1a-1f**) with different side chain $pK_a$ values (**Table 6.1**) were reacted individually with four-fold excess of the hydrophobic amino acid amide,[19, 33] phenylalanine-$NH_2$ (F-$NH_2$, **2**) using different concentrations (**Table 6.2**), *i.e.* +ve: Arginine R (**1a**); Lysine K (**1b**); Histidine H (**1c**) or -ve: Glutamic Acid E (**1d**); Aspartic Acid D (**1e**); Cysteic Acid CA (**1f**) with **2** in PBS (pH 7.4), **Figure 6.1**.

**Table 6.1** Yields of *in situ* condensation reaction in the absence and presence of biopolymers (heparin or chitosan) in isolation by HPLC.

| entry | $pK_a$ | %Yield | | |
|---|---|---|---|---|
| | | None | Heparin | Chitosan |
| **1a** | 12.48 | 0 | 0 | 0 |
| **1b** | 10.54 | 9 | 72 | 9 |
| **1c** | 6.04 | 98 | 98 | 98 |
| **1d** | 4.07 | Excluded; 3 products (**Figure 6.7a**) | | |
| **1e** | 3.9 | 92 | 91 | 91 |
| **1f** | 1.3 | 10 | 9 | 92 |

**Table 6.2** Optimization of dipeptide derivatives with basic side chains by measuring yield% of *in situ* condensation reaction in the absence and presence of biopolymers (heparin and chitosan) by HPLC.

| entry | Concentration (mM/mM) | Yield% | | |
|---|---|---|---|---|
| | | None | w/ Heparin | w/ Chitosan |
| **1a** | 1:4 | 0 | 0 | 0 |
| | 5:20 | 0 | 0 | 0 |
| | 10:40 | 0 | 0 | 0 |
| | 20:80 | 0 | 0 | 0 |
| **1b** | 1:4 | 0 | 0 | 0 |
| | 5:20 | 0 | 21.9 | 0 |
| | 10:40 | 4.4 | 37.4 | 4.5 |
| | 20:80 | 9.4 | 71.7 | 8.9 |
| **1c** | 1:4 | 0 | 0 | 0 |
| | 5:20 | 63.5 | 63.3 | 63.2 |
| | 10:40 | 93.8 | 94.0 | 93.6 |
| | 20:80 | 98.1 | 98.1 | 98.0 |

Thermolysin was used (1 $mg.ml^{-1}$) to catalyse the reversible hydrolysis/condensation reaction. Mixtures were vortexed and sonicated to allow dissolution. % yields of products **3a-3f** were evaluated by HPLC after 24 and 48 hours (to ensure equilibrium has been reached), **Table 6.1**. **Table 6.2** provides the HPLC results obtained for amino acids with basic side chains with varying $pK_a$ values (**1a-1c**) using different

concentrations and after 48 hours. As results suggested, 20:80 molar ratio of **1**:**2** is the best concentration ratio. Concentration of amino acids with acidic side chains (**1d-1f**) was then also fixed (*i.e.* 20:80) for consistency.

To produce a sequence adaptive system,[34] we require low yielding amide formation to provide opportunities for electrostatic co-assembly driving the reaction to higher yields. In the absence of biopolymers, **1a** did not show tendency to form the dipeptide derivative (**3a**) while **3b** was produced in a low yield (9%). **3c** formed in a high yield (98%), in the absence of an external template. **1d** formed three products which included the side chain condensation and was therefore disregarded (as demonstrated by LC/MS, **Figure 6.7 (appendix**). **3e** was formed in a high yield (92%) and **3f** was formed in a low yield (10%). From these results, it is clear that the $pK_a$ value has a substantial effect on the condensation reaction where amino acid derivatives with either high or low $pK_a$ values (**1a**, **1b** and **1f**) showed limited yields. The formation of **3c** and **3e** in high yields is most likely due to suppression of ionization of the side chain[35] upon self-assembly, giving rise to high yielding nanostructures. Thus, it is expected that **1b** and **1f** are the best candidates for amplification by peptide/polymer electrostatic co-assembly.

We then studied the templating effect of oppositely charged biopolymers on assembly and the subsequent formation of nanostructures. For this purpose, we chose polyanionic heparin and polycationic chitosan. Biopolymer concentrations were calculated on the basis of 1:1 charge equivalents with the charged amino acids used, as follows. Heparin was considered as the sodiated analogue structure shown in **Figure 6.1c**, with molecular weight of 665.4 $g.mol^{-1}$ and 4 negative charges per repeating unit.[36] The appropriate masses of dry polymer were added directly to the

mixtures. Chitosan concentrations were based on average molecular weight of the repeating units of 171.5 (calculated based on 75% degree of deacetylation) and one positive charge per repeating unit.[37] Chitosan was dissolved in 0.5% acetic acid first then added to the mixture with the pH value adjusted to 7.4 with 0.5 M HCl/NaOH as required.

Gratifyingly, enzymatic condensation yields were increased substantially upon the addition of the oppositely charged biopolymer to 72% and 92% for **3b** and **3f** respectively, while it was not significantly affected in the case of **1a**, **1c** and **1e**. Therefore, only **1b** and **1f** were taken further in this study.

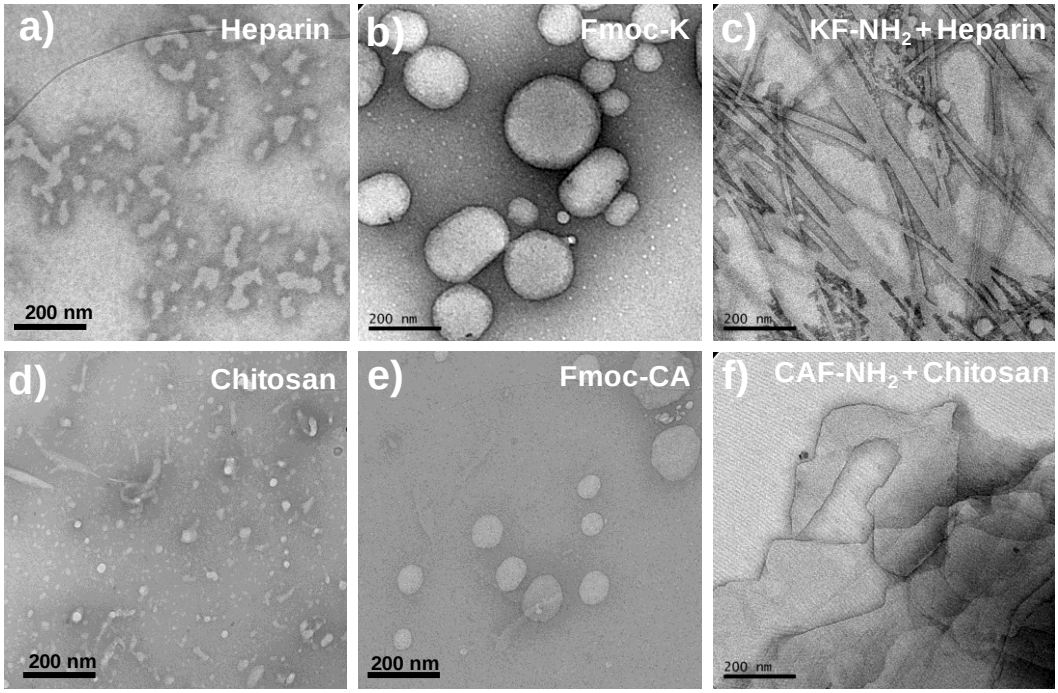


**Figure 6.2** TEM images showing random aggregates of biopolymers (a,d) and spherical aggregates of precursors (**1b** and **1f**/ b, e) and differential co-assembly into nanotubes and nanosheets depending on complimentary biopolymer. Scale bar = 200 nm.

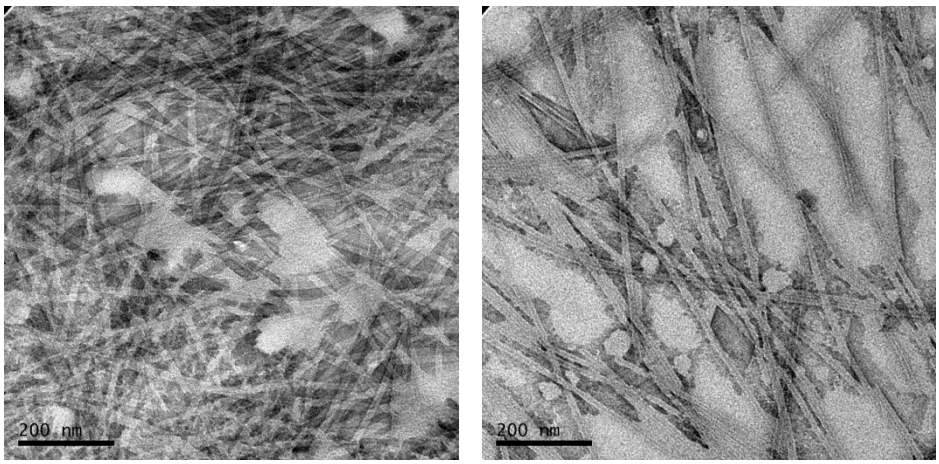


**Figure 6.3** Additional TEM images showing the formation of nanotubes of **3b** (yield=72%).

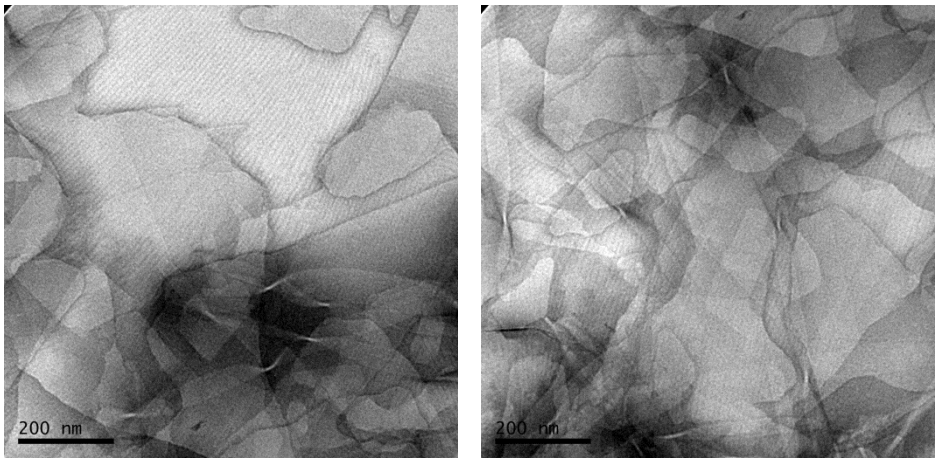


**Figure 6.4** Additional TEM images showing the formation of nanosheets of **3f** (yield=92%).

To gain insights into the morphology of the co-assembled nanostructures formed, precursors and products of selected candidates were examined by transmission electron microscope (TEM), **Figure 6.2**. TEM images show random aggregations of biopolymers, spherical aggregations of precursors (**1b** and **1f**) and differential co-assembly leading to the formation of **3b** nanotubes[38] and **3f** nanosheets depending on

complimentary biopolymer (additional TEM images are included in **Figure 6.3** and **Figure 6.4**).

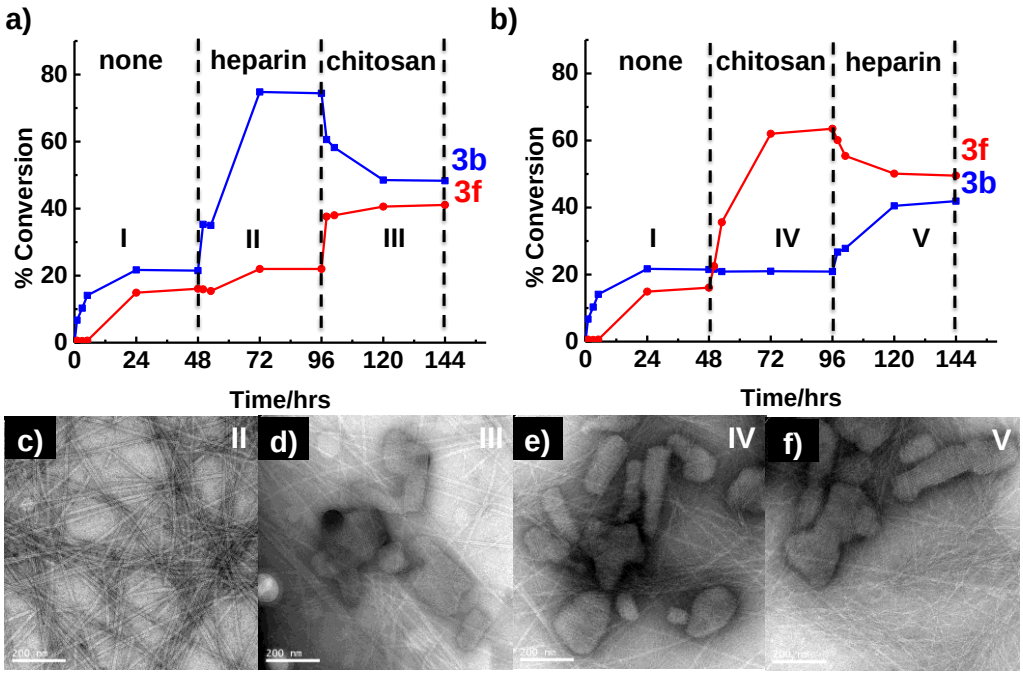


**Figure 6.5** (a-b) HPLC data showing % peptide conversion for mixtures in one-pot a) 1b, 1f, 2 and thermolysin was mixed for 48 hours (Stage I) followed by heparin until equilibrium was reached (Stage II) followed by chitosan for another 48 hours (Stage III). b) Stage I was followed by chitosan (Stage IV) until equilibrium was reached followed by heparin for another 48 hours (Stage V). (c-f) TEM images of nanostructures competing in one pot. c) Nanotubes dominating after Stage II. d) Nanosheets were mainly formed after Stage III (with some tubes/fibres). e) Nanotubes, nanosheets and aggregates mixture formed after Stage IV. f) A mixture of nanostructures was formed after Stage V. Scale bar = 200 nm.

Having established a system that shows sequence selective amplification driven by peptide/polymer co-assembly, we then tested the adaptive potential of a mixed system that could express different morphologies, depending on the polymer added.

Thus, selected components (*i.e.* **1b**, **1f**, **2** and thermolysin) were mixed in one-pot and allowed to compete for 48 hours to make sure that the system has reached equilibrium (**Figure 6.5/a-b**); yield% was evaluated by HPLC. Low yield (21% and 16%) was produced for **3b** and **3f** respectively showing that having both charged species **1b** and **1f** present simultaneously increases the yields of both peptides, most likely through co-assembly of the charge complementary peptides **3b** and **3f**.[39] As discussed, templates might stabilize certain products which lead to a shift in equilibrium towards these products. So, heparin biopolymer was added to the mixture forming **3b** selectively (74% after 48 hours). This was attributed to the electrostatic interaction of positively charged **3b** and polyanionic heparin. Then, chitosan was added to the same mixture which led for **3b** hydrolyse while **3f** was amplified. At 144 hours, **3b** formed at 48% and **3f** 41%. Similarly, adding polycationic chitosan to the amino acids mixture selectively forms **3f** (63% after 48 hours). Adding heparin to the same mixture led to decompose part of **3f** (49%) and form **3b** in 42%. This clearly shows that the designed system is dynamic and adaptive as it can exchange peptide sequence depending on the templating effect of chosen biopolymers.

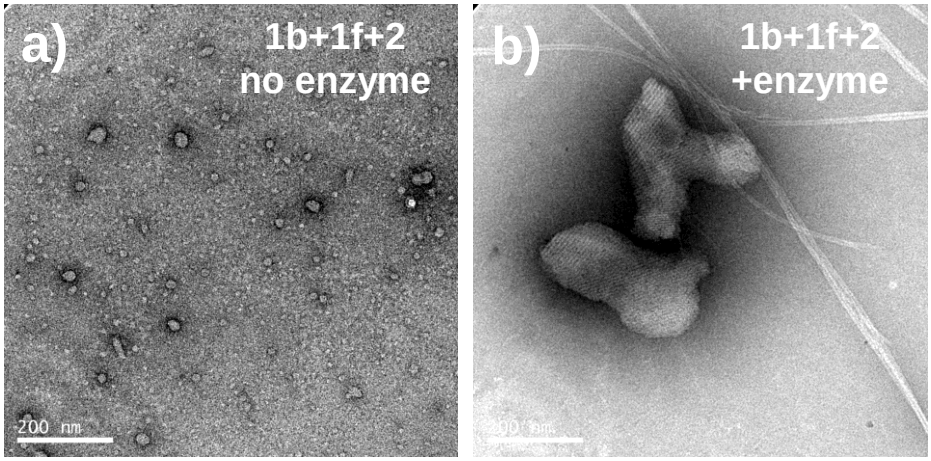


**Figure 6.6** TEM images showing spherical aggregates of one pot system components before thermolysin addition (a) and the formation of two different structures (nanotubes of **3b** and nanosheets of **3f**). Scale bar = 200 nm.

The morphology change of amino acid/dipeptide derivatives in one pot was evaluated using TEM, **Figure 6.5/c-f**. Before the enzyme addition, amino acid derivatives formed spherical aggregates (**Figure 6.6a**). After the addition of enzyme and after 48 hours, few nanotubes and nanosheets of **3b** and **3f** respectively were observed (**Figure 6.6b**). Adding heparin selectively enhances the formation of **3b** nanotubes (**Figure 6.7c**) while the addition of chitosan amplifies the formation of **3f,** few tubes/fibres can be observed as well. **Figure 6.7e-f** shows the formation of a mixture of nanostructures after 144 hours.

## 6.4Conclusion

In summary, we successfully designed adaptive nanostructures through the combination of enzymatically triggered *in situ* condensation reaction, dynamic combinatorial chemistry and co-assembly with biopolymers holding opposite charge (which acted as templates). Amide bond formation could be enhanced substantially

due to the template presence (*i.e.* electrostatic interactions between amino acids and biopolymer macromolecules), which in turn led to form reconfigurable structures; from spherical aggregates to nanotubes or nanosheets depending on the template. Overall, we present a new class of adaptive biomaterials that display sequence and structure adaption by competing catalytic amplification and decomposition that may be of use in future dynamic biomaterials design.

## 6.5Appendix

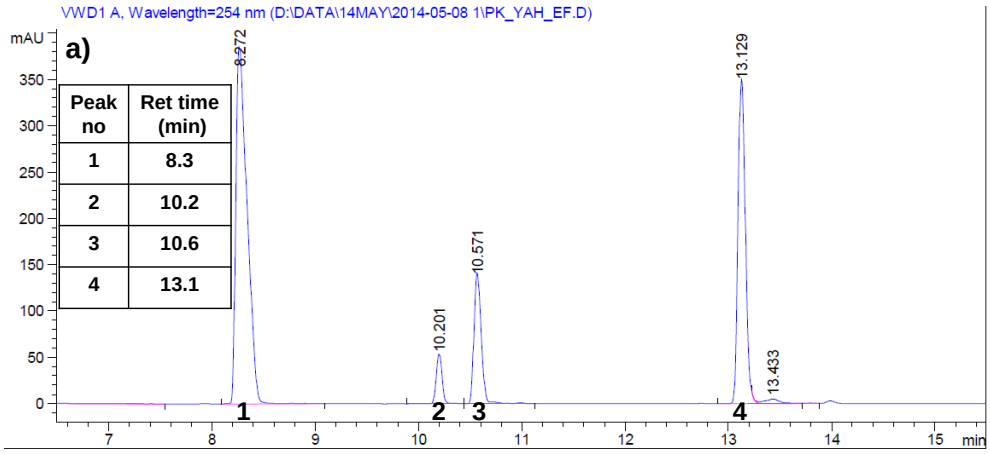


**Figure 6.7/a.** LC evidence of the formation of three different products (peaks 2-3) when **1d** was coupled enzymatically with **2**. For MS fragments corresponding to each peak see below (**Figure 6.7/b-e**).

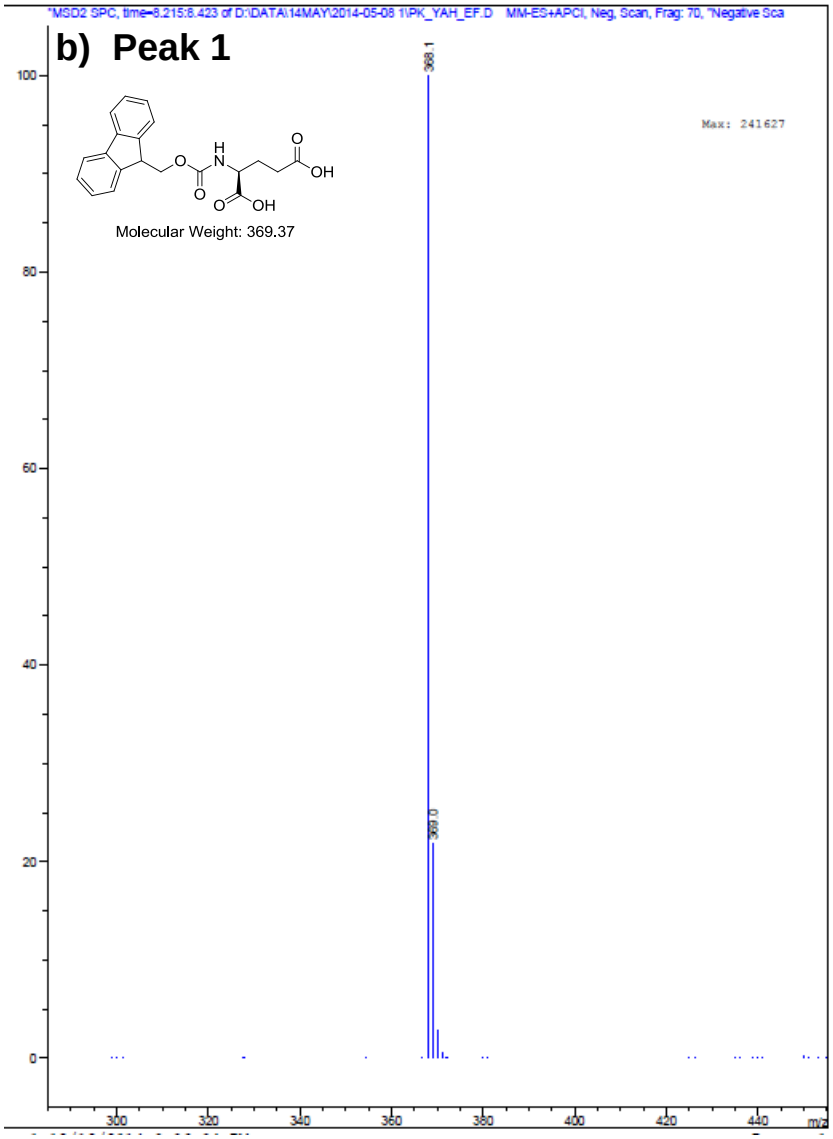


**Figure 6.7/b.** MS fragments corresponding to the first LC peak with the expected formed product.

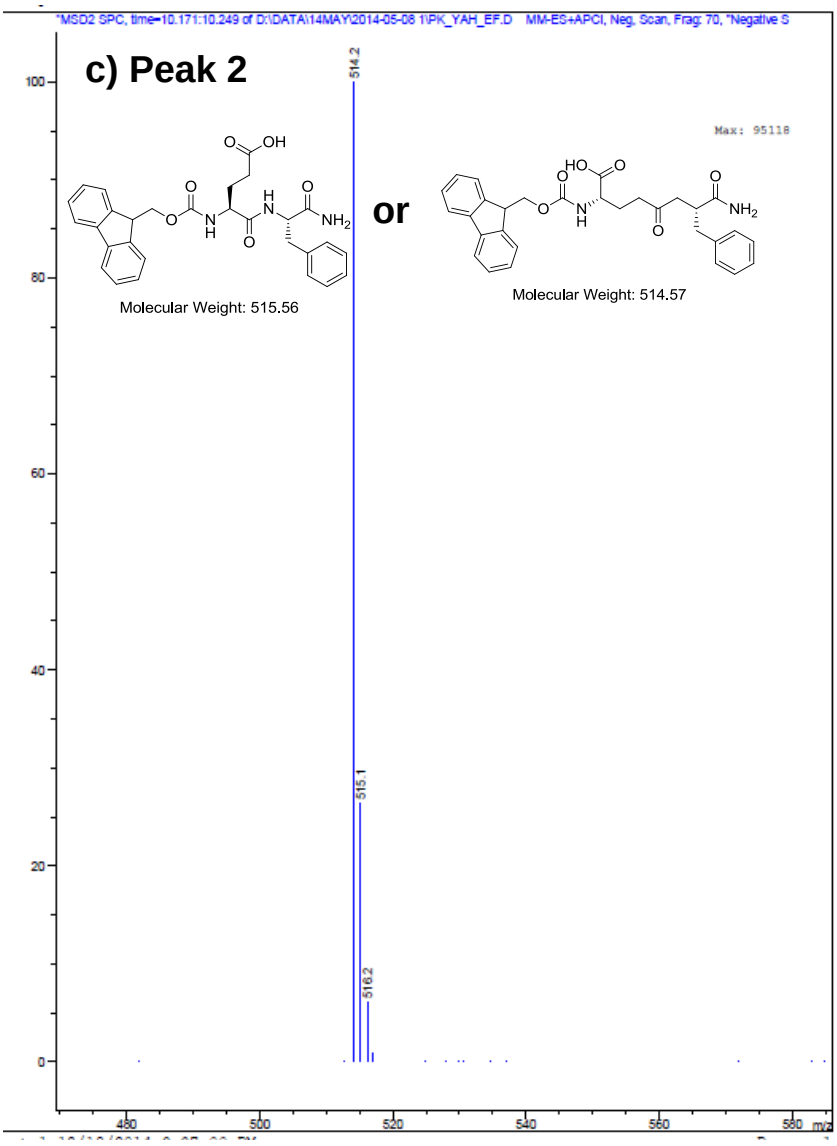


**Figure 6.7/c.** MS fragments corresponding to the second LC peak with the expected formed product.

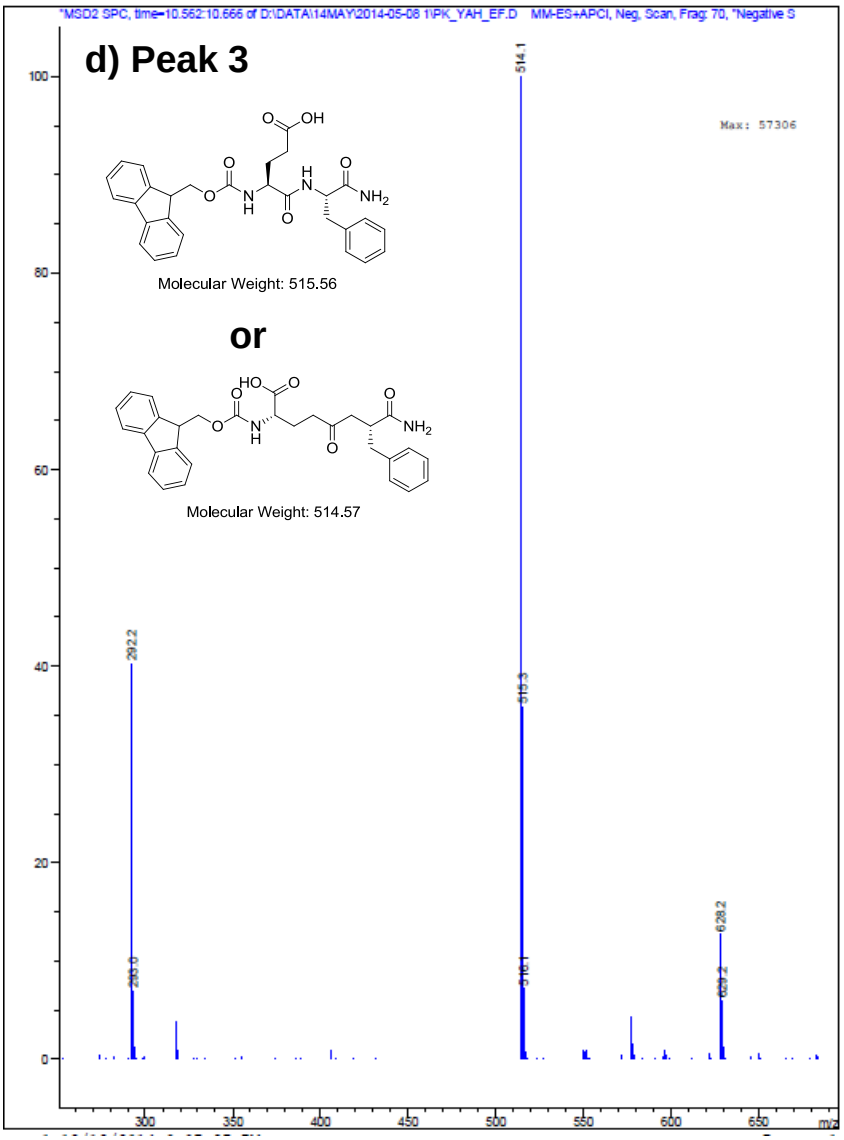


**Figure 6.7/d.** MS fragments corresponding to the third LC peak with the expected formed product.

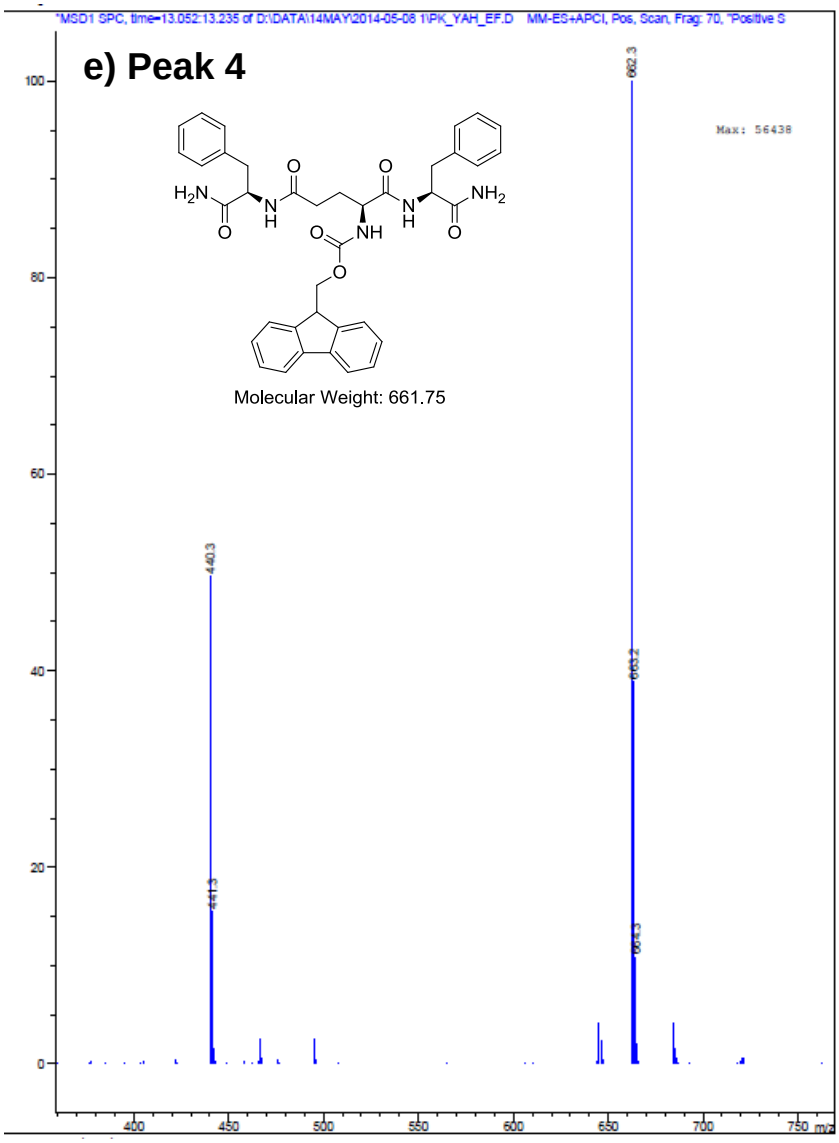


**Figure 6.7/e.** MS fragments corresponding to the forth LC peak with the expected formed product.

## 6.6References


1. G. M. Whitesides and B. Grzybowski, *Science*, 2002, **295**, 2418-2421.
2. T. Aida, E. Meijer and S. Stupp, *Science*, 2012, **335**, 813-817.
3. J.-M. Lehn, *Angewandte Chemie International Edition*, 2015, **54**, 3276-3289.
4. Z. Yang, H. Gu, D. Fu, P. Gao, J. K. Lam and B. Xu, *Advanced Materials*, 2004, **16**, 1440-1444.
5. J. Zhou, X. Du, Y. Gao, J. Shi and B. Xu, *Journal of the American Chemical Society*, 2014, **136**, 2970-2973.
6. T.-H. Ku, S. Sahu, N. M. Kosa, K. M. Pham, M. D. Burkart and N. C. Gianneschi, *Journal of the American Chemical Society*, 2014, **136**, 17378-17381.
7. A. Desai and T. J. Mitchison, *Annual Review of Cell and Developmental Biology*, 1997, **13**, 83-117.
8. Y. Wang, Z. Huang, Y. Kim, Y. He and M. Lee, *Journal of the American Chemical Society*, 2014, **136**, 16152-16155.
9. J. D. Badjić, A. Nelson, S. J. Cantrill, W. B. Turnbull and J. F. Stoddart, *Accounts of Chemical Research*, 2005, **38**, 723-732.
10. S. Samarajeewa, R. P. Zentay, N. D. Jhurry, A. Li, K. Seetho, J. Zou and K. L. Wooley, *Chemical Communications*, 2014, **50**, 968-970.
11. J.-M. Lehn and A. V. Eliseev, *Science*, 2001, **291**, 2331-2332.
12. S. Otto, R. L. E. Furlan and J. K. M. Sanders, *Drug Discovery Today*, 2002, **7**, 117-125.
13. S. Maiti and L. J. Prins, *Chemical Communications*, 2015, **51**, 5714-5716.
14. J. Li, P. Nowak and S. Otto, *Journal of the American Chemical Society*, 2013, **135**, 9222-9239.

15. Y. Ruff, V. Garavini and N. Giuseppone, *Journal of the American Chemical Society*, 2014, **136**, 6333-6339.

16. D. Janeliunas, P. van Rijn, J. Boekhoven, C. B. Minkenberg, J. H. van Esch and R. Eelkema, *Angewandte Chemie International Edition*, 2013, **52**, 1998-2001.

17. Y. Kang, K. Liu and X. Zhang, *Langmuir*, 2014, **30**, 5989-6001.

18. E. Mattia and S. Otto, *Nature Nanotechnology*, 2015, **10**, 111-119.

19. R. J. Williams, A. M. Smith, R. Collins, N. Hodson, A. K. Das and R. V. Ulijn, *Nature Nanotechnology*, 2008, **4**, 19-24.

20. S. K. M. Nalluri and R. V. Ulijn, *Chemical Science*, 2013, **4**, 3699-3705.

21. D. J. Cornwell and D. K. Smith, *Materials Horizons*, 2015, 10.1039/C1034MH00245H.

22. L. Chen, S. Revel, K. Morris, D. G. Spiller, L. C. Serpell and D. J. Adams, *Chemical Communications*, 2010, **46**, 6738-6740.

23. N. Javid, S. Roy, M. Zelzer, Z. Yang, J. Sefcik and R. V. Ulijn, *Biomacromolecules*, 2013, **14**, 4368-4376.

24. R. Ni and Y. Chau, *Journal of the American Chemical Society*, 2014, **136**, 17902-17905.

25. D. Carvajal, R. Bitton, J. R. Mantei, Y. S. Velichko, S. I. Stupp and K. R. Shull, *Soft Matter*, 2010, **6**, 1816-1823.

26. R. M. Capito, H. S. Azevedo, Y. S. Velichko, A. Mata and S. I. Stupp, *Science*, 2008, **319**, 1812-1816.

27. L. W. Chow, R. Bitton, M. J. Webber, D. Carvajal, K. R. Shull, A. K. Sharma and S. I. Stupp, *Biomaterials*, 2011, **32**, 1574-1582.

28. G. Pont, L. Chen, D. G. Spiller and D. J. Adams, *Soft Matter*, 2012, **8**, 7797-7802.

29. A. C. Mendes, K. H. Smith, E. Tejeda-Montes, E. Engel, R. L. Reis, H. S. Azevedo and A. Mata, *Advanced Functional Materials*, 2013, **23**, 430-438.

30. S. Fleming and R. V. Ulijn, *Chemical Society Reviews*, 2014, **43**, 8150-8177.

31. Y. Zhang, H. Gu, Z. Yang and B. Xu, *Journal of the American Chemical Society*, 2003, **125**, 13680-13681.

32. C. G. Pappas, Y. M. Abul-Haija, A. Flack, P. W. J. M. Frederix and R. V. Ulijn, *Chemical Communications*, 2014, **50**, 10630-10633.

33. S. Toledano, R. J. Williams, V. Jayawarna and R. V. Ulijn, *Journal of the American Chemical Society*, 2006, **128**, 1070-1071.

34. Y. Ura, J. M. Beierle, L. J. Leman, L. E. Orgel and M. R. Ghadiri, *Science*, 2009, **325**, 73-77.

35. C. Tang, A. M. Smith, R. F. Collins, R. V. Ulijn and A. Saiani, *Langmuir*, 2009, **25**, 9447-9453.

36. S. M. Bromfield, A. Barnard, P. Posocco, M. Fermeglia, S. Pricl and D. K. Smith, *Journal of the American Chemical Society*, 2013, **135**, 2911-2914.

37. S.-P. Tsai, C.-Y. Hsieh, C.-Y. Hsieh, D.-M. Wang, L. L.-H. Huang, J.-Y. Lai and H.-J. Hsieh, *Journal of Applied Polymer Science*, 2007, **105**, 1774-1785.

38. H. Xu, A. K. Das, M. Horie, M. S. Shaik, A. M. Smith, Y. Luo, X. Lu, R. Collins, S. Y. Liem, A. Song, P. L. A. Popelier, M. L. Turner, P. Xiao, I. A. Kinloch and R. V. Ulijn, *Nanoscale*, 2010, **2**, 960-966.

39. B. Adhikari, J. Nanda and A. Banerjee, *Soft Matter*, 2011, **7**, 8913-8922.

# 7. Conclusion and Future Research

## 7.1Conclusion

While peptide based hydrogels were suggested as potential scaffolds to maintain cell culture and ultimately control cell fate, further investigation into the effect of nanostructures properties and materials fabrication still critical in understanding cell behaviour. The aim of this research was to design and fabricate adaptive peptide and/or sugar based functional bio(materials) with tuneable and well defined mechanical properties. Particularly, it focused on the fabrication of gel scaffolds of functionalised peptide based nanofibres triggered enzymatically (**Chapter 3**) or chemically by pH switch (**Chapter 4**). This was achieved by hydrogelator/surfactant co-assembly. Despite the method used to trigger assembly and functionalisation, the mode of assembly and supramolecular organisation were found to be dependent on the chemistry of components under investigation. Furthermore, the mechanical properties (stiffness) were able to be tuned by changing the enzyme concentration (**Chapter 3**) or total components concentration (**Chapter 4**). While the enzymatic approach failed to maintain fibroblast cell culture, preliminary cell studied showed ability to maintain adipose stem cells (ASCs) and showed change cell shape, which might be an indication for possible differentiation.

The first example of enzymatically triggered self-assembly of aromatic sugar amphiphile was reported in **Chapter 5**. Both mechanical properties and supramolecular organization were found to be tuneable by varying the enzyme concentration and/or initial sugar derivative concentration. This material was then used to control cell fate.

Finally, a new class of adaptive materials were designed and reported in **Chapter 6**. This material showed ability to change its molecular composition and nanoscale structure by combining biocatalytic peptide exchange (using peptide dynamic combinatorial chemistry), sequence selective peptide self-assembly (forming nanotubes versus nanosheets) and peptide/polymer co-assembly.

## 7.2Future Work

The conclusions drawn from this thesis have opened up the opportunity for further work and developments. This section acknowledges the required improvements and set up a research agenda for future research. Having established the fabricated scaffolds *via* two component co-assembly, the next obvious step is to correlate between the optimum stiffness value and the type of chemical functionality in order to control cell fate. Different types of sugar residues could be used with probably multiple units (*i.e.* di and tri sugar derivatives). Another part that might be taken a step further is to design new sugar based gelators to be used as therapeutic agents to control cancer cell fate. Cells that overexpress certain enzymes as markers of diseased status are particularly interesting.

It is clear that the stem cell microenvironment (i.e. ECM) acts to control stem cell growth (self-renewal) and differentiation in a dynamic manner (continuous ECM formation and deformation associated with functional and morphological changes). Current developed biomaterials can achieve either of these functions; these materials are designed either for growth or differentiation and lack the flexibility to support both stem cell functions. Therefore, there is a need to design dynamic materials that can support cell growth (self-renewal) followed by on demand cell differentiation. It

would be interesting to fabricate materials that completely natural (without the presence of aromatic capping group) with minimum complexity (*Nature Chemistry 2015, 7, 30-37*). Using the design rules reported in the previously mentioned paper, charged tri- or tetra-peptide based hydrogelators might be discovered. This can be achieved by designing 3D (charged) hydrogels with defined stiffness (with stiffness value similar to stem cell tissues) and chemistry that can support cell self-renewal (undifferentiated cells). For example, hydrogels composed of the positively charged KYF and the negatively charged FYD. Peptide components could be co-assembled in different molar ratios to allow for one type of charges being in excess in the hydrogel composition. Then, the stiffness can be tuned (increased) by introducing a new oppositely charged component: (i) biopolymers; such as the positively charged chitosan. Chitosan is soluble at slightly acidic conditions and well known for gelability at physiological conditions. Pectin as negatively charged biopolymer could be added as well. Pectin is soluble at physiological conditions and can gel in the presence of metal ions (e.g. $Ca^{+2}$) due to crosslinking with carboxyl group within its backbone. The choice of biopolymers depends on the selected excess peptide (ii) metal ions can be also used to enhance crosslinking within the negatively charged peptides. This allows stiffening the gel on demand by enhancing building blocks assembly and/or formation of second, interpenetrating network for the combatable stiffness value that match with the required phenotype (*i.e.* resulting in chondrogenesis on a stiff gel or osteogenesis on a rigid gel). Hence the fabrication of 3D gels that allow cells to grow to large numbers and then change to functional cells in a controllable manner mimicking stem cell microenvironment dynamics.

Furthermore, the work should result in new fundamental insights in multicomponent assembly, dynamics of nanostructures and control of cell/surface interactions.